DISSERTATION

submitted to the
Combined Faculty of Natural Sciences and Mathematics of the Ruperto Carola University Heidelberg, Germany

for the degree of
Doctor of Natural Sciences

Presented by
Xiyan Zhao (M.Sc, Biomedical Engineering)
born in Shenyang, China
Oral examination: 15.07.2021

Role of COPI paralogous proteins during pluripotent cells differentiation into neurons

Referees: Prof. Dr. Felix Wieland
Prof. Dr. Julien Béthune

This work has been carried out at the Biochemistry Center of the University of Heidelberg from November 2017 to November 2020 under the supervision of Professor Dr. Julien Béthune.

Acknowledgement

First and foremost I wish to extend my sincerest thanks to my director, my mentor Prof. Dr. Julien Béthune for giving me the opportunity to work in his lab, for supervising me throughout my PhD. I appreciate that all the academical discussions we have, not only about the project but also about what is important in scientific thinking. I really do appreciate how he has challenged me to think and to integrate new ideas

Next, I would like to thank my TAC members Prof. Dr. Felix Wieland and Dr. Sebastian Schuck for giving nice suggestions for my work. I also have the pleasure to thank Prof. Dr. Felix Wieland for providing me antibodies and equipments for my experiments.

I would like to thank my examiner Prof Dr. Michael Brunner for considering it.

I would like to thank all my team members and special thanks to Lea Kubitz always supporting and helping me.

Additionally, I would like to thank Dr. Monika Langlotz and Dr. Christian Ackermann for helping me with my experiments.

I would like to thank Barbara for helping me with the administration.

Last, but very importantly, I would like to thank my Mother. From Primary School to my post graduate University, I have traveled to a lot of different places within China. My only motivation in life is to fulfill the dreams she didn't achieve when she was young. I can't remember how many times I felt like I could no longer carry on because of the pressure of reality. After 5 years of working as an animal experiment tutor, in the thirtieth year of my life, I am determined to start my new journey and come to beautiful Heidelberg to study as a Ph.D. student. Thanks again to my mother for dedicating her whole life to me, and fully supporting my development. However, due to my poor English and older age, I am full of anxiety and disbelief that I can complete my Ph.D. studies in Germany. In the meantime, I am very grateful to Prof. Dr. Julien Béthune for his help and patient guidance. Because of these factors, I have been gifted with the courage and patience to face any difficulties and challenges.

Abstract

Coat protein complex I (COPI) vesicles coated with the heptameric complex coatomer mediate retrograde cargo trafficking from Golgi to endoplasmic reticulum as well as intra-Golgi transport. Whether paralogous subunits of coatomer have different functions is currently unclear. In this thesis, we reveal distinct roles of paralogous coatomer subunits γ1-COP and γ2-COP during the neuronal differentiation of mouse pluripotent cells. Following genome editing experiments, our work shows that γ1-COP specifically facilitates neurite extension and underlines a paralogue-specific function of the COPI pathway and offers evidence for the role of COPI coated vesicles in neuronal polarization. Furthermore, to explore the mechanism of γ1-COP specific functions during pluripotent cells differentiation into neurons, the combination proximity-dependent biotinylation with affinity purification and mass spectrometry (AP-MS) was applied to analyze whether the interactome of γ-COPs reveals paralogue-specific cargos or regulators. In the light of label free quantification (LFQ) analysis, various neurogenesis-related proteins were significantly enriched in the γ1-COP interactome indicating that γ1-COP may preferentially traffic such proteins during the process of pluripotent cells neuronal differentiation.

Zusammenfassung

Mit dem heptameren Komplex-Coatomer beschichtete Coat Protein Complex I (COPI) - Vesikel vermitteln den retrograden Frachthandel von Golgi zum endoplasmatischen Retikulum sowie den Intra-Golgi-Transport. Ob paraloge Untereinheiten des Coatomers unterschiedliche Funktionen haben, ist derzeit unklar. In dieser Arbeit zeigen wir unterschiedliche Rollen der paralogen Coatomer-Untereinheiten γ1-COP und γ2-COP während der neuronalen Differenzierung pluripotenter Mauszellen. Nach Experimenten zur Bearbeitung des Genoms zeigen unsere Arbeiten, dass γ1-COP die Neuritenverlängerung spezifisch erleichtert, eine paralogspezifische Funktion des COPI-Signalwegs unterstreicht und Hinweise auf die Rolle von COPI-beschichteten Vesikeln bei der neuronalen Polarisation liefert. Um den Mechanismus der γ1-COP-spezifischen Funktionen während der Differenzierung pluripotenter Zellen in Neuronen zu untersuchen, wurde die kombinationsnäherungsabhängige Biotinylierung mit Affinitätsreinigung und Massenspektrometrie (AP-MS) angewendet, um zu analysieren, ob das Interaktom von γ-COPs Paralog zeigt. spezifische Ladungen oder Regulierungsbehörden. Im Lichte der Analyse der markierungsfreien Quantifizierung (LFQ) wurden verschiedene Neurogenese-verwandte Proteine im γ1-COP-Interaktom signifikant angereichert, was darauf hinweist, dass γ1-COP solche Proteine während des Prozesses der neuronalen Differenzierung pluripotenter Zellen bevorzugt transportieren kann.

Table of Contents

1. Introduction 13
1.1 Secretory pathway 13
1.2 Maintenance of Early Secretory Pathway homeostasis 14
1.3 Transport vesicles within secretory pathway 15
1.3.1 COPII coated vesicles 15
1.3.2 COPI coated vesicles 15
1.3.2.1 Coat protein subunits in COPI coated vesicles 15
1.3.2.2 COPI biogenesis 16
1.3.2.3 Cargo sorting 17
1.3.2.4 Scission of COPI coated vesicles from Golgi membrane 18
1.3.2.5 COPI coated vesicles disassemble 18
1.3.2.6 COPI coated vesicles tethering and fusion 19
1.3.3 Clathrin coated vesicles 19
1.4 Specific role of COPI vesicles in the neuronal differentiation of mouse pluripotent cells 20
1.5 Proteomics to study transport vesicle 21
1.5.1 ultraID 21
1.5.2 ultraID as a tool to study transient associated interactom 22
1.5.3 ultraID coupled to mass spectrometry (ultraID-MS) as a tool to probe the composition of protein complexes 23
1.6 Objectives 24
2. Results 24
2.1 Depletion of γ1-COP or γ2-COP does not induce apoptosis 25
2.2 Depletion of γ1-COP or γ2-COP does not induce ER stress 26
2.3 Generation of P19 cells expressing γ1-COP-GFP KI, γ2-COP-GFP KI and GFP KI from Copg1 locus 28
2.4 Characterization of the knock-in insertions 29
2.5 Bi-allelic insertion of the transgenes 31
2.6 Expression of either γ1-COP or γ2-COP from the Copg1 locus supports the formation of a tight embryonic body 34
2.7 γ1-COP promotes the neurite extension 35
2.8 Generation of P19 cells expressing γ Chimera-COP-GFP from Copg1 locus 37
2.9 Chimera constructs knock-in characterization 39

2.10 Bi-allelic insertion of the exogenous coding gene in γ Chimera-COP-GFP KI cells 40
2.11 The formation of tight EBs is not due to an absent specific function mediated by γ1-COP 42
2.12 Expression of γ-COP chimeras from the Copg1 locus does not fully compensate for the absence of γ1-COP during neurit outgrowth 43
2.13 γ-COP paralogs tag ultraID cells construction 45
2.14 The workflow of the ultraID-based efficient proximity labelling approach to identify proximal proteins to γ-COPs 46
2.15 Characterisation of ultraID in γ-COP paralogs tag ultraID undifferentiated cell lines 47
2.16 Testing the pulldowns of the ultraID-based approach to confirm the successful labelling of interactome in γ-COP paralogs tag ultraID undifferentiated cell lines 49
2.17 The co-localization of γ-COPs with biotinylated proteins in undifferentiated cells 51
2.18 Identifying the interactome of either γ1-COP or γ2-COP in P19 undifferentiated cells 54
2.19 Different membrane-associated interactome between γ1-COP and γ2-COP in undifferentiated P19 cells 57
2.20 Identification of the different interactome between γ1-COP and γ2-COP in P19 undifferentiated cells 61
2.21 Characterization of ultraID-based labeling in P19 differentiated neurons 64
2.22 Localization of tagged γ-COPs and biotinylated proteins in differentiated cell lines 66
2.23 Identification of the interactome of either γ1-COP or γ2-COP in P19 differentiated neurons 69
2.24 Different membrane-associated interactome of γ1-COP and γ2-COP in P19 differentiated neurons 72
2.25 Identification of the different interactome between γ1-COP and γ2-COP in P19 differentiated neurons 76
3. Discussion 81
4. Materials and methods 87
4.1 Materials 87
4.1.1 Primers and oligos 87
4.1.2 Plasmids and cassette 88

4.1.3 Chemicals, kits and enzymes 92
4.1.4 Medium, buffer and supplements for Prokaryotic strains culture 94
4.1.5 Cell lines 95
4.1.6 Medium, buffer and supplements for cell culture 96
4.1.7 Buffer and chemical stuff 97
4.1.8 Antibodies 99
4.1.9 Equipment 100
4.2 Molecular Biological Methods 101
4.2.1 Plasmids and PCR cassette constructs 101
4.2.2 Restriction digestion 103
4.2.3 Oligo annealing 104
4.2.4 Polymerase chain reaction (PCR) 104
4.2.5 Agarose Gel Electrophoresis 104
4.2.6 Gel Extraction and PCR product Purification 105
4.2.7 Ligation 105
4.2.8 Gibson assembly 105
4.2.9 Transformation of E. coli 105
4.2.10 Plasmids purification and Determination of DNA concentration 106
4.2.11 Plasmids Precipitation 106
4.3 Cell biology methods 106
4.3.1 Cell culture 106
4.3.2 Heat inactivation of serum 106
4.3.3 Generation of stable cell lines 107
4.3.3.1 Construction of CRISPR knock-in cell lines 107
4.3.3.2 Construction of a doxycycline inducible ultraID tag gene expression cell lines 107
4.3.4 Plasmids transfection 108
4.3.5 Fluorescence-Activated Cell Sorting (FACS) 109
4.3.6 Cell Colony picking 109
4.3.7 Poly-D-Lysine coating 109
4.3.8 Hanging drop assay 109
4.3.9 P19 cells differentiation 110
4.3.10 COPI formation inhibition and biotinylation induction 110
4.3.11 Immunostaining 110
4.3.12 Cellular apoptosis detection 111

4.3.13 Fluorescence Microscopy Techniques 111
4.4 Biochemical Methods 112
4.4.1 Cell lysis for western blot 112
4.4.2 Sodium-dodecyl sulfate polyacrylamide gel electrophoresis (SDS-PAGE) ...112
4.4.3 Protein Concentration Determination (Bradford Assay) 112
4.4.4 Western Blot Analysis 113
4.4.5 Chemical modification of streptavidin-sepharose beads for trypsin resistance 113
4.4.6 Preparation of protein lysates for MS 113
4.4.7 Streptavidin affinity pulldowns 114
4.4.8 Mass spectrometry data acquisition and analysis 114
Reference 118
Abbreviations 132

List of Figures

Figure 1: Transport vesicle mediated trafficking 20
Figure 2: The structure of ultraID 22
Figure 3: Schematic indication of the two-stage P19 neuronal differentiation protocol 25
Figure 4: The absence of γ1-COP or γ2-COP neither elevates cellular apoptosis nor ER stress 27
Figure 5: CRISPR strategy to acquire KI cell lines 29
Figure 6: Identification of knock-in insertions in CRISPR knock-in cells 30
Figure 7: Bi-allelic insertion identification by PCR mapping 33
Figure 8: γ1-COP -GFP KI and γ2-COP-GFP KI rescue the formation of tight Embryoid bodies (EB) in vitro 35
Figure 9: Expression of γ1-COP promotes neurite outgrowth. 37
Figure 10: The structure of γ-COP (Annotations of 5NZT_G) 38
Figure 11: CRISPR strategy to acquire KI cell lines 38
Figure 12: Identification of knock-in insertion proteins in CRISPR knock-in cells 40
Figure 13: Bi-allelic insertion identification by PCR mapping 42
Figure 14: γ-COP chimeras support the formation of tight Embryoid bodies (EB) in vitro 43
Figure 15: Partial compensation of the deletion of γ1-COP during neurite outgrowth in Chimera-COP KI cells 45
Figure 16: Workflow for the identification of transient-interacting or proximal proteins by following an ultraID-based approach 47
Figure 17: The ultraID-based approach to identify membrane-associated proximal proteins to coatomer 48
Figure 18: Characterization of clonal cell lines expressing ultraID fusion proteins 49
Figure 19: Characterization of ultraID base-labelling in P19 undifferentiated cell lines 50
Figure 20: Co-localization of γ-COPs with biotinylated proteins in p19 undifferentiated cells 53
Figure 21: Volcano plots showing the differential abundance of isolated biotinylated proteins in P19 undifferentiated cells 55
Figure 22: Volcano plots and venn diagram depicting Golgi membrane-associated γ-COP interactome in P19 undifferentiated cells 60
Figure 23: Volcano plots and venn diagram depicting differential interactomes between γ1-COP and γ2-COP in P19 undifferentiated cells 63
Figure 24: Characterization of ultraID-based labeling in P19 differentiated neurons 66

Figure 25: Colocalization of γ-COPs with biotinylated proteins in differentiated neurons 68
Figure 26: Volcano plots showing the differential abundance of isolated biotinylated proteins in P19 differentiated neurons 70
Figure 27: Volcano plots and venn diagram depicting Golgi membrane-associated γ-COP interactome in P19 differentiated neurons 74
Figure 28: Volcano plots and venn diagram depicting differential interactomes between γ1-COP and γ2-COP in P19 differentiated neurons 78

List of Tables

Table 1: Significantly enriched genes in γ1-COP-ultraID over ultraID-Ago2 in P19 undifferentiated cells with P-value<0.01 56
Table 2: Significantly enriched genes in γ2-COP-ultraID over ultraID-Ago2 in P19 undifferentiated cells with P-value<0.01 57
Table 3: Venn figure indicating γ1-COP membrane-associated interactome in P19 undifferentiated cells with P-value<0.01 60
Table 4: Venn figure indicating γ2-COP membrane-associated interactome in P19 undifferentiated cells with P-value<0.01 61
Table 5: Venn figure indicating overlapped membrane-associated interactome between γ1-COP and γ2-COP pool in P19 undifferentiated cells with P-value<0.01 61
Table 6: The significantly enriched proteins in γ1-COP-ultraID samples in P19 undifferentiated cells with P-value < 0.01 64
Table 7: The significantly enriched proteins in γ2-COP-ultraID samples in P19 undifferentiated cells with P-value < 0.01 64
Table 8: Significantly enriched genes in γ1-COP-ultraID over ultraID-Ago2 in P19 differentiated neurons with P-value<0.01 71
Table 9: Significantly enriched genes in γ2-COP-ultraID over ultraID-Ago2 in P19 differentiated neurons with P-value<0.01 71
Table 10: Significantly enriched genes in γ1-COP-ultraID over ultraID-Ago2 in P19 differentiated neurons with P-value<0.05 71
Table 11: Significantly enriched genes in γ2-COP-ultraID over ultraID-Ago2 in P19 differentiated neurons with P-value<0.05 72
Table 12: Venn figure indicating γ1-COP membrane-associated interactome in P19 differentiated neurons with P-value<0.01 74
Table 13: Venn figure indicating γ2-COP membrane-associated interactome in P19 differentiated neurons with P-value<0.01 75
Table 14: Venn figure indicating overlapped membrane-associated interactome between γ1-COP-ultraID and γ2-COP-ultraID in P19 differentiated neurons with P-value<0.01 75
Table 15: Venn figure indicating γ1-COP membrane-associated interactome in P19 differentiated neurons with P-value<0.05 75
Table 16: Venn figure indicating γ2-COP membrane-associated interactome in P19 differentiated neurons with P-value<0.05 76
Table 17: Venn figure indicating overlapped membrane-associated interactome between γ1-

COP-ultraID and γ2-COP-ultraID in P19 differentiated neurons with P-value<0.05 76
Table 18: The significantly enriched proteins in γ1-COP-ultraID samples in P19 differentiated neurons with P-value < 0.01 79
Table 19: The significantly enriched proteins in γ2-COP-ultraID samples in P19 differentiated neurons with P-value < 0.01 79
Table 20: The significantly enriched proteins in γ1-COP-ultraID samples in P19 differentiated neurons with P-value < 0.05 79
Table 21: The significantly enriched proteins in γ2-COP-ultraID samples in P19 differentiated neurons with P-value < 0.05 81
Table 22: Donor PCR cassettes for generating CRISPR knock-in cell lines 102
Table 23: Py109-crRNAs assay plasmid containing a Cas12a/Cpf1 gene and crRNA arrays for the generation of CRISPR knock-in cell lines 103
Table 24: Py109_2-crRNAs array plasmid, originating from Py109-crRNAs assay plasmid formed by the puromycin selection gene deletion for the generation of CRISPR knock-in cell lines 103
Table 25: Recombination reporter plasmid (pMB1610-crRNA2 targets) to assist with CRISPR cell line selection via puromycin treatment 103
Table 26: Doxycycline induction gene expression within a PiggyBac (PB) transposon plasmid for the generation of protein coding gene tag ultraID cell lines 103
Table-M1: Oligo 87
Table-M2: Primer 88
Table-M3: Plasmids 88
Table-M4: Chemicals used in this study with their respective product number and manufacturer 92
Table-M5: Kits used in this study with their respective product number and manufacturer 94
Table-M6: Enzymes used in this study with their respective product number and manufacturer 94
Table-M7: Prokaryotic strains 94
Table-M8: Prokaryotes culture medium 95
Table-M9: Other chemical stuff for prokaryotes culture 95
Table-M10: Eukaryotic strains 95
Table-M11: Chemicals for cell culture 96
Table-M12: Buffers 97
Table-M13: Primary antibodies 99
Table-M14: Secondary antibodies 100

Table-M15: Equipment 100
Supplementary Table1: Restriction digest protocols 114
Supplementary Table2: Oligo annealing protocols 115
Supplementary Table3: PCR protocols 115

1. Introduction

1.1 Secretory pathway

The secretory pathway is accountable for the synthesis, post-translational modification, and traffic of lipids and proteins to their final destination and consists of compartments from rough endoplasmic reticulum (rough ER), ER exit sites (ERESs) and the ER-to-Golgi intermediate compartment (ERGIC) via the Golgi complex and trans-Golgi network (TGN) to the lysosome, plasma membrane, or the exterior of the cell.[1-4] Protein translation begins at the ribosome attached on the Endoplasmic Reticulum (ER) membrane. About 30% of proteins[5] in the eukaryotic cells are targeted and translocated to ER. Many ER-resident proteins play a significant part on protein quality control maintaining for further synthesis such as folding, disulfide bound formation[6] or glycosylation[5,7]. The ER is also the entry site of most newly synthesized proteins to the secretory system.

In mammals, after fundamental modifications for maturation in ER, proteins leave through ER exit sites (ERES) to the ER-to-Golgi intermediate compartment (ERGIC) mainly transported via COPII vesicles according to two distinct models directed transport and bulk flow[8]. The directed transport model proposes that cargos are encapsulated into COPII vesicles through transmembrane capture receptors[9]. In the bulk flow model, cargo proteins without receptor selection through passive are integrated to membrane and fluid.[8,10] According to the recent evidence, both mechanisms probably co-exist in the traffic pathway from ER to Golgi.[11]

The Golgi plays a central role in the secretory pathway to fulfill two major functions which are in charge of exporting secreted proteins to the endolysosomal system or the cell surface via a cis-Golgi to trans-Golgi direction, and protein glycosylation.[12] Glycosylation is a complicated multi-step process that requires a series of enzymes with a diverse gradient concentration within the Golgi stacks to ensure correct glycan chains are attached to secretory proteins[13,14]. The mechanism of cargo delivery within the Golgi apparatus from the cis- to trans-cisterna remains controversial. The vesicular transport theory and dynamic cisternal maturation theory are proposed. In the vesicular transport model, anterograde coated vesicles are responsible for transferring secreted cargos and distribution of resident proteins across the stable Golgi stacks[14-16]. In the cisternal maturation theory, the Golgi cisterna matures gradually as the carrier to traffic cargos via sorting driving force from stack movement

(retrograde transport).[14-18] Moreover, retrograde traffic from the Golgi to the ER plays a key role on retrieving the ER resident proteins that escaped from ER to Golgi.[19,20] The anterograde membrane flow from ER to cis-Golgi compartment regulated by COPII vesicles is counter-balanced by a retrograde membrane trafficking pathway[21] that mediates the recycling of inappropriate folded or misassembled proteins back to the ER.[12,21]

In the post Golgi trafficking, Clathrin coated vesicles (CCVs) and other carriers have been reported to play a crucial role in membrane, endocytosis, and exocytosis recycling pathways for homeostasis maintaining within the cell.[22-26]

1.2 Maintenance of Early Secretory Pathway homeostasis

Newly synthesized proteins in the ER acquire proper modifications and conformations to pass through the quality control by folding enzymes and chaperones containing N-glycosylation, proline isomerization or disulfide bond formation.[27] Two major ER chaperones, glucose-regulated protein 78 (GRP78) and GRP94[28] assist to fold the unmodified proteins by binding to their hydrophobic regions with conformational changes[29] as well as ATPase domains regulating ATP hydrolysis.[30] The ER transmembrane receptors PERK comprises a luminal stress sensing domain to sense accumulation of unfolded proteins.[31,32] Under non-stress conditions, PERK bind to GRP78 and thus limits its activity, while under ER stress condition, GRP78 is released from PERK luminal domain due to competitive interactions with misfolded proteins[33]. Additionally, another type of chaperones and co-chaperones are responsible for keeping the function of ATPase-domain from GRP78 to assist recruitment of its substrates.[34] GRP78 also controls the activity of targeting post-translational modifications. Likewise, the inhibition of the combination between GRP78 and PERK results in the activation of the unfolded protein response (UPR).[35,36] If ER stress perdures for a long time, the UPR activates the pro-apoptotic pathway. The main pro-apoptotic pathway is regulated by the transcription factor CHOP.[37] CHOP targets a series of genes including apoptosis relative genes and death receptor in cell surface such as GADD34[38] and DR5[39] that causes caspase activation cascades, as well as the involvement of ER-stress induced apoptosis in cancer cell lines.[10,40]

1.3 Transport vesicles within secretory pathway

Secreted and transmembrane proteins are mainly transported by protein-coated vesicles with a lipid membrane-structure (**Figure1**).[41] The coated proteins are distinct among the various vesicles and thereby distinguish different vesicle type.[42] In eukaryotes, three main types of coated vesicles are characterized by COPII vesicles, COPI vesicles and Clathrin-coated vesicles that mediate membrane trafficking in the different part of the secretory pathway.[43,44] COPII vesicles dominate cargo transport within anterograde pathway from ER to the Golgi apparatus.[44] COPI vesicles regulate retrograde pathway from the Golgi apparatus back to ER as well as within different Golgi stacks.[45] Clathrin coated vesicles convey secretory proteins in many post-Golgi transport routes.[26,43]

1.3.1 COPII coated vesicle

COPII vesicle formation is mainly activated at ERES, after proteins are translated and folded correctly[46,47], by the exchange on the small GTPase Sar1 of GDP for GTP with the assistance of the membrane-bound guanidine nucleotide exchange factor (GEF) Sec12[48]. Sar1-GTP recruits the inner COPII coat layer composed of the Sec23/24 lattice as a pre-budding complex[49] and further combines with the other large heterodimeric complexes Sec13/31 to deform the ER membrane and buds into a vesicle.[49-51] The uncoating of COPII vesicles is dependent on the hydrolysis of GTP[52-54] whereas the scission process is mediated by sar1-GTP independent of GTP hydrolysis.[53,55,56] Varying cargo-binding sites have been elucidated on the surface of Sec24 a major delivery binding module of the COPII vesicle[4,57,58] that recognize diverse cargo with specific motives found on e.g. SNARE complexes[58] or various cargo proteins. Moreover, Cargo selection by COPII vesicles can also be identified by transmembrane domains of delivery protein[59], oligomerization[60] multimeric sorting signals[61] or other quality control procedure.[49,62]

1.3.2 COPI coated vesicle

1.3.2.1 Coat protein subunits in COPI coated vesicles

COPI coatomer is composed of intertwingled caged subcomponent that contains α-COP (140 KD), β'-COP (107 KD) and ε-COP (34 KD) and adaptor subcomplex that is made up of β-COP (107 KD), δ-COP (61 KD) γ-COP (98KD) and ζ-COP (20KD).[63,64] The caged

subcomplex-binding KKXX sorting sequence can directly interact with α and/or β'-COP.[65] Two WD40 β-propeller domains with α-solenoid were reported in both α- and β'-COP.[66,67] In the large adaptor subunits, both β- and γ-COP include a N-terminus α-solenoid trunk domain that interacts with Arf1-GTP to recruit the coat to the membrane, combined by short unstructured linker with a β sandwich appendage domain.[68,69] In the cytoplasm, the recruitment of the heptameric coatomer complex to the membrane is *en bloc*.[68] Coatomer in the cytosol and bound to the Golgi membrane is present as one complex with the cage subcomplex and adaptor subcomplex intertwined among the subunits[70] instead of two dividing layers like in the COPII or Clathrin coats.[71] Moreover, a three-fold triad structure is comprised with three molecules of coatomer and six molecules of Arf1 within the assembled coat[71], which link together on the membrane surface to generate vesicles of variable shape and size.[71,72] γ-COP and ζ-COP in higher eukaryotes have emerged for the presence of paralogues (γ1-COP, γ2-COP, ζ1-COP and ζ2-COP).[73,74] At the protein level, the paralogues of γ-COP share about 80% identity while ζ-COP share 75% identity.[26,74] Three populations of COPI vesicles are defined by different isotypes of coatomer containing different combinations of a γ/ζ subcomplex designated by γ1/ζ1-, γ1/ζ2-, or γ2/ζ1-COP with a ratio of about 2:1:2 respectively in mammals.[75] The p24 proteins (type I transmembrane proteins) is a main component of COPI-coated vesicles with FFXXBB(X)n sorting signals (B: basic amino acid)[45,76-78], which interact with γ-COP at two individual sites, one in trunk domain and the other one in appendage domain at its cytoplasmic domains.[79] In cryo-electron microscopy derived structures of coatomer, no electron density for residues from 555 to 603 was detected, indicating that there is a flexible linker between two subdomains of γ1-COP.[80] For residues 604-874, the structure of the appendage domain was reported, similar to previous X-ray structures of the isolated domain.[80]

1.3.2.2 COPI biogenesis

The biogenesis of COPI coated vesicle initiates from the recruitment of cytoplasmic coatomer to the Golgi membrane.[81] With the assistance of a guanine exchange factor (GEF), after Arf1-GDP change into Arf1-GTP, the N-terminal myristoylated amphipathic helix of Arf1 is exposed to insert into the Golgi membrane.[82-89] Three different guanine exchange factors[90] were observed in the Golgi and endosomal systems with different functions and localizations including GBF1 (Arf1 GEFs—Golgi-associated brefeldin A (BFA)-resistant GEF 1) , BIG1 and BIG2 (BFA-resistant guanine nucleotide exchange protein 1 and 2).[88-93] ArfGEF GBF1 binds directly to the γ-COP appendage on the Golgi membrane to anchor the coatomer

spatially surrounding the activated Arf1.[90] GTP-hydrolysis plays a critical role in regulating the dissociation between Arf1 and membranes. Thus, GAPs (GTPase-activating proteins) act as a kind of GTPase timer to release Arf1 to cytoplasm. ArfGAP1, ArfGAP2 and ArfGAP3 have been found to be associated to the COPI function.[94] In vitro reconstitutions, ArfGAP2 was found to be in the vicinity of γ-Arf (arf1 directly interacts with γ-COP)[68,81] rather than to β-Arf (arf1 directly interacts with β-COP)[68]. ArfGAP1 contains an ALPS motif (ArfGAP1 lipid-packing sensor motif) that initiates an amphipathic helix on membrane by recognizing lipid packing and the activity of ArfGAP1 is higher when bound to membranes with increase curvature.[95-97] By contrast, the activity of ArfGAP2 and 3 is not influenced by membrane curvature like ArfGAP1[98], since no ALPS motif is found in these regulators.[99,100] In summary, the fundamental elements for the formation of COPI vesicles consist of coatomer, Arf1 and its regulators the ArfGEFs and ArfGAPs.[81,101-103]

1.3.2.3 Cargo sorting

Cargo sorting by COPI is mainly regulated by recognition signals on cytosolic domains of retrieved proteins such as di-lysine motifs (KKxx and KxKxx) that interact with propeller domain of β' or α-COP in the vicinity of the membrane surface for recycling to the ER.[65,104-106] Another type of retrieval recognition signal is the Arginine (R)-based sequence ϕRxR (ϕ: hydrophobic amino acid)[81] on cytosolic domains[107,108] to assist a quality control mediated by COPI vesicles, so as to prevent the transport of dysfunctional complexes to cell membrane[81]. Indeed, Arg-based signals are covered in the correct folded cargos but exposed in the improperly assembled proteins.[109-112] In addition to retrieval proteins sorting, another site is found in the propeller domain of β'-COP to regulate the exocytic SNARE Snc1 by the recognition of polyubiquitylated Snc1.[81,113] Various studies indicate that p24 family play a key role in recruitment of coatomers and classification of cargoes which leads to mouse embryonically lethal after the deletion of one member of p24 family.[77,101,114-120] p24 proteins with short cytoplasmic domains FFxxBB(x)n sequence (B: basic amino acid) interacts with two distinct sites in γ-COP.[45,81] A few protein adaptors interact with COPI regulating cargo sorting such as KDEL receptors, Rer1 and Vps74.[121] KDEL adaptors specifically recognize ER luminal resident chaperones with C-terminal KDEL sequence to retrieve them from the Golgi to the ER in a PH- and Zinc-dependent way.[122-127] Vps74 (a member of the GOLPH3 family) mediates glycosyltransferases traffic within Golgi by the recognition of sorting signals with cytosolic domain.[128] Likewise, Rer1 regulates retrieval signals attached with the transmembrane domain of many proteins.[129-132] In early stage, GTP-hydrolysis by Arf

proteins emerges as important to ensure correct cargo sorting. If GTP-hydrolysis is blocked, less cargo is capsuled into vesicles. In one model, ArfGAPs binding to the cargos act as cargo recognition adaptors to sort proteins into vesicles.[43,81,115,126,133-136]

1.3.2.4 Scission of COPI coated vesicles from Golgi membrane

The COPI vesicles start fission from the Golgi membrane at the neck of the bud and scission of vesicles from membranes dependent on oligomerization of Arf1.[81,137-139] The accurate mechanism of driving vesicle scission by Arf1 is deficiently clear. Vesicle scission from the donor membrane is independent of GTP hydrolysis.[55] A bud scar observed on cytosolic COPI vesicles by cryo-electron tomography in living cells also indicate that the formation of a completely closed cage is not necessary.[67] Some additional factors have been suggested to participate in the scission step of COPI vesicles such as CtBP/BARS, acyl-COA and PLD2.[81,136,140-142]

1.3.2.5 COPI coated vesicles disassemble

Once the vesicles are released to the cytosol, uncoating is activated. Uncoating of COPI vesicles is blocked by Q71L a mutant form on Arf1 that is unable to hydrolyze GTP.[143] Similar results were obtained from the vitro reconstitution assays with this GTP-locked form of Arf1, highlighting that GTP-hydrolysis by Arf1 is necessary for vesicle uncoating.[144] Although it is established that GTP-hydrolysis performs a critical role in the process of coat disassemble, the precise timing of GTP hydrolysis on Arf1 is not clear. The distinct half-lives between COPI and Arf1 on membranes[143] supports that the polymerized COPI coatomers remains longer on membrane than Arf1, probably owing to binding to cargo and lipids, after GTP-hydrolysis and Arf1 release from membranes.[143,145,146] On the membrane-associated coat, GTP hydrolysis is speculated to be mediated in a curvature-independent manner at the triad central area by ArfGAP2 close to the γ-COP/Arf1 while a curvature-dependent manner at peripheral triad area by ArfGAP1 close to the β-COP/Arf1.[68,81,109] In eukaryotes, inactivation of one specific sub-type of ArfGAPs (ArfGAP1, or ArfGAP2 and -3) is not lethal [99], suggesting a certain degree of overlapping function among them. It is not elucidated how the role of one ArfGAP would be replaced by the other. However, combined depletion of both sub-types of ArfGAPs critically affects cell viability.[81,99,147,148]

1.3.2.6 COPI coated vesicles tethering and fusion

In the ultimate stage of COPI vesicle transport, specific localization is mediated to the target organelles by tethers to identify and bind vesicles either directly or indirectly through some factors, such as Rab GTPases and SNAREs.[149] A variety of tethers were observed within Golgi trafficking pathway such as the trafficking protein particle II (TRAPPII) complex[150], the conserved oligomeric Golgi (COG) complex[151] and p115 (Uso1)[152] . During the intra-Golgi transport, tethers were proposed to catch different types of COPI vesicle for targeting to distinct cisternae.[153] In retrograde trafficking, the COPI vesicles are captured by the ER-linked tethering complex Dsl1[154-157] COPI vesicles contain SNARE proteins. Association of specific SNAREs on opposite membranes leads to the formation of SNARE pins as a prelude for membrane-membrane fusion.[158-163] The SNARE family contains v-SNAREs on vesicles and t-SNAREs on target membranes.[163] The combination of v- and t SNAREs leads to the fusion of two opposing membrane.[164] After fusion, the v- and t-SNAREs will not be separated and localize within the same membrane referred to cis-SNARE which is disassembled in an ATP-dependent manner to facilitate to release of individual SNARE proteins that are recycled back to their original membrane through vesicular transport.[165-170] According to several studies, vesicle uncoating is probably half-complete with remaining residual coat on vesicle surface allowing specific vesicle tethering and fusion.[81,102]

1.3.3 Clathrin coated vesicles

Clathrin coated vesicles regulate many post Golgi traffic route. They have a lattice shaped coat structure that is comprised of three light chains and three heavy chains[171] to form a triskelion. One heavy chain binds with one light chain to form pair of trimers.[171,172] The backbone of the Clathrin lattice is constructed by the heavy chains while the light chains regulate the biogenesis and uncoating of Clathrin. Polymerization of these triskelia result in the formation of flat lattices (6-sided rings structure) and curved lattice (5-sided rings structure) in appropriate conditions.[173] Clathrin is recruited to membrane or indirectly binds to cargo through adaptor proteins (AP). At present, five different AP complexes (AP1-5) are described. Cargo transport between the TGN and endosomes[174,175] is mediated by AP1[176] and AP4[177], while among the early endosomes to late endosomes or lysosomes-like organelles routes, AP-3 dominate the cargos shipping.[174,178] Additionally, AP-2 coated vesicles[179] play an important role in endocytosis. AP-5 adaptor protein complex is presumed to be structurally similar to APs 1–4 and localizes to a late endosomal/lysosomal compartment for membrane

traffic.[180] Moreover, it is observed that AP-5 functions as a backup pathway for retrieval in late endosomes to Golgi.[180] With the assistance of Arf1, the adapter protein complexes, with the exception of AP-2, are recruited to membranes.[174,181] Some other Adaptor molecules such as AP180 and epsin can also recruit Clathrin to membranes and contribute to polymerization.[182,183]

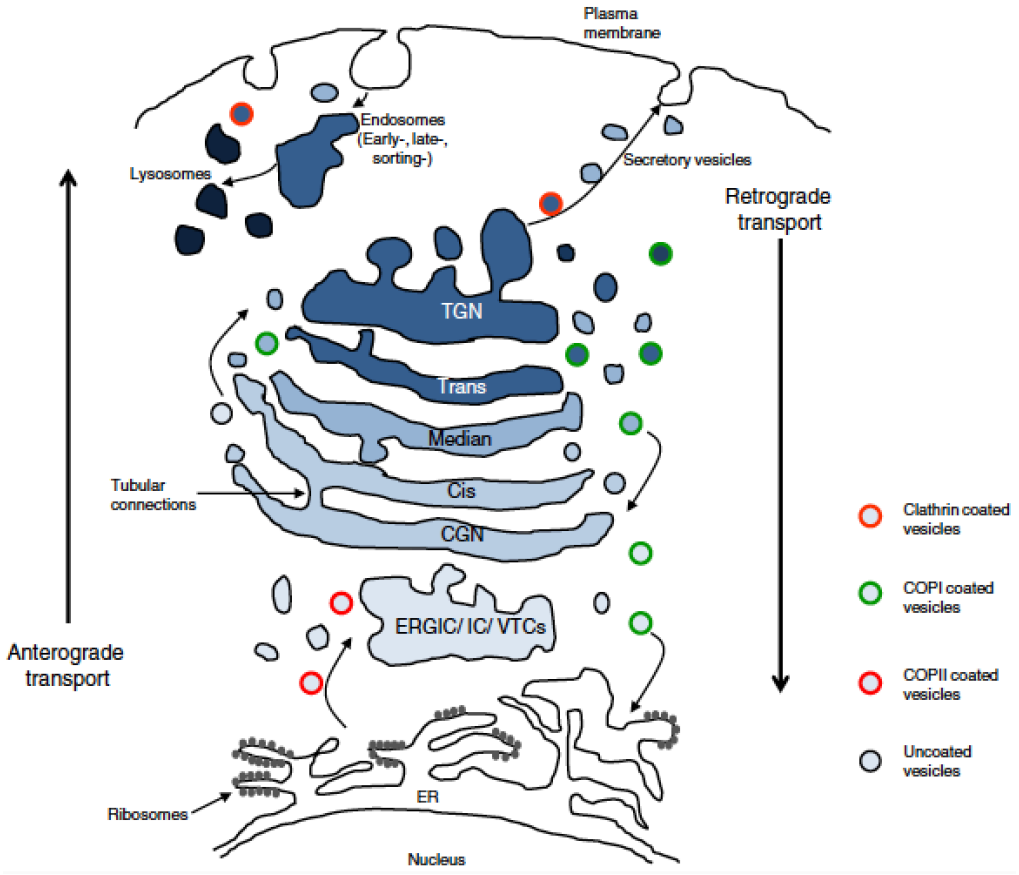

Figure 1. Transport vesicle mediated trafficking. Figure reused from Glycoconjugate Journal. Copyright (2013) Rosnoblet et al[184], with permission from Clearance Center's RightsLink® service, License number: 5071451166119

1.4 Specific role of COPI vesicles in the neuronal differentiation of mouse pluripotent cells

It was observed that knock down of α-COP lead to a striking decline of both axonal and dendritic growth in primary cortical neurons.[185-187] Additionally, α-COP was localized along the neurites to the axonal growth cone indicating COPI vesicles regulate long-range transport through the axon besides transport between Golgi and ER in the neuron cell body.[186] In motor neurons, the survival motor neuron protein associates with α-COP to facilitate neurite

extension.[186,187] From a previous study from our lab, mRNA expression of Copg1 (γ1-COP encoded gene) is up regulated whereas Copg2 (γ2-COP encoded gene) is down regulated during murine pluripotent P19 cells neuronal differentiation.[188] In the following of the specific KO of Copg1 or Copg2 P19 cells construction, neither of the two paralogs is necessary for cell survival when the other is present in the cells.[188] Furthermore, the knock-out of Copg1 results in the disruption of embryoid bodies (EBs) formation and reduced neurite outgrowth, during the retinoic acid (RA)-induced neuronal differentiation of P19 cells.[188] By contrast, the disruption of Copg2 does not P19 cell neuronal differentiation.[188] However, how RA-inducted P19 cells differentiation is regulated by COPI transport vesicles is currently unclear. At the beginning of this project, the only hint of a functional difference between γ-COP paralogues was a distinct Golgi localization. It was reported that γ1-COP is preferentially localized at the cis-Golgi while γ2-COP is more present at the trans-Golgi.[188,189]

1.5 Proteomics to study transport vesicle

1.5.1 ultraID

In E. coli, biotin is activated at the expense of ATP to form biotinyl-5'-adenylate (bio-5'-AMP), a reaction catalyzed by BirA, a biotin protein ligase (BPL).[190] The product of this reaction biotinyl-5'-AMP is then attached to an available lysine residue of the biotin carboxyl carrier protein (BCCP) coupled with the release of AMP.[191] It was reported that BirA*, the R118G variant of BirA (also named BioID) is a BPL capable of biotinylation of nearby protein substrates in a proximity dependent manner.[190] With the assistance of BioID, the reactive biotinyl-5'-AMP covalently binds to lysine residues of prey proteins within the distance of 10nm over a period of time in a natural cellular setting.[192] After denaturation and solubilization of proteins, only the biotinylated proteins are selectively isolated on streptavidin conjugated beads to be later identified by mass spectrometry.[190,192,193] Since marked proteins rather than intact complexes are isolated from cell lysates, BioID is particularly suited for the determination of transient or weak proximity contacts.[192] Furthermore, an improved BPL for proximity-dependent biotinylation was developed in our lab and designated microID (μID). It corresponds to a truncated form of BioID2[194], the derived mutant from A. aeolicus' BPL (unpublished data from the Béthune lab). The ligase activity of μID was further improved through a directed evolution approach from the collaboration of the Kolmar group (TU Darmstadt). The resulting variant, ultraID

(**Figure 2**) was characterized as an hyperactive BPL that outperforms all currently available enzymes for proximity-dependent biotinylation.[195] It was therefore used in this thesis.

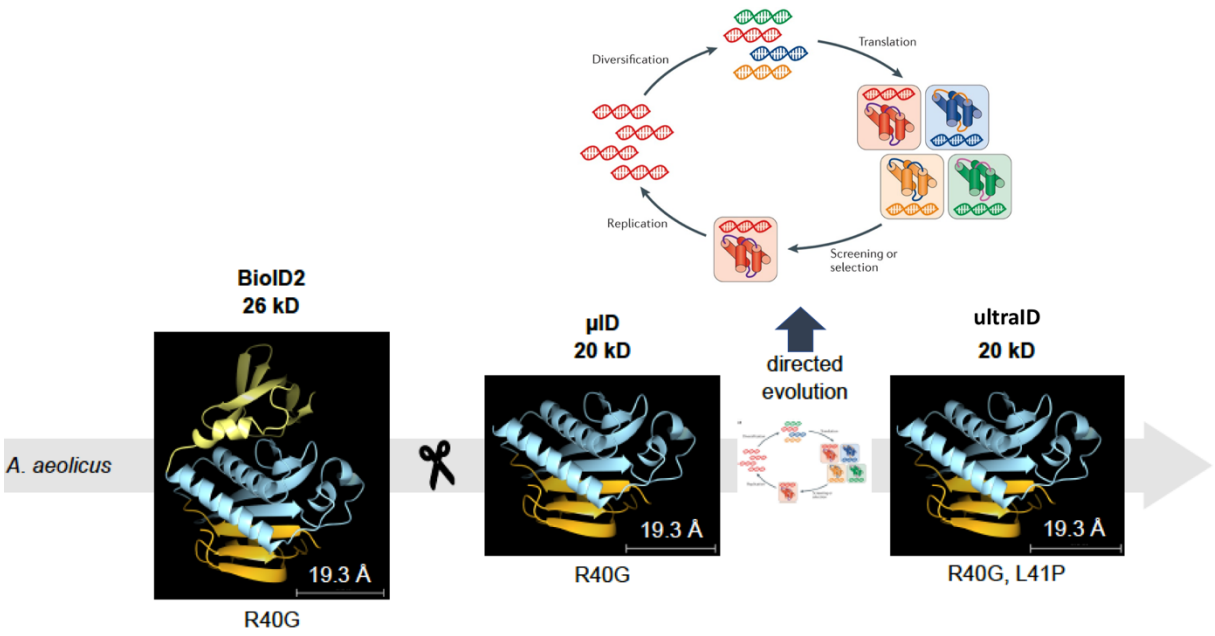

Figure 2. The structure of ultraID.
The figure reused from Bachelor thesis of Lea Kubitz[195] (September, 2020). The BPLs derived from A. aeolicus with specific molar mass and mutated sites gained from the RCSB database (PDB ID: 2EAY MMDB ID: 53025) and illustrated with the software of CCP4mg.[196] The schematic figure of directed evolution reused from nature reviews genetics Journal. Copyright (2015) Packer et al[197], with permission from Clearance Center's RightsLink® service, License number: 5071510253620

1.5.2 ultraID as a tool to study transient associated interactome

In ultraID experiments, a bait protein is tagged with ultraID and expressed in cells. Upon addition of extra biotin in the growth medium, proximity-dependent labeling is induced and results in the biotinylation of proximal proteins to the fusion protein. Typically, stable cell lines are constructed that express the fusion protein at a level close to the endogenous counterpart. In this thesis, the PiggyBac (PB) transposon plasmid containing doxycycline induction gene expression was adopted to generate stable cell lines.

Previous work in the lab showed that in these conditions, efficient proximity dependent biotinylation with ultraID is achieved after a 10 min labeling time in Hela cell lines, induced

by supplementation of biotin in the growth medium.[195] The labeling radius of ultraID is estimated to be about 10 to 15 nm. In the following steps, streptavidin pulldown is applied to purify the biotinylated proteins and process them for identification by LC-MS/MS (Liquid chromatography-mass spectrometry).[195]

1.5.3 ultraID coupled to mass spectrometry (ultraID-MS) as a tool to probe the composition of protein complexes

All cellular pathways are regulated by protein complexes. The determination of the composition of these complexes, assembly regulators and dynamic interactome still remains challenging. One way to analyze protein complexes is to use proximity-dependent biotinylation coupled to LC-MS. To identify specific proximal proteins to a given bait fused to the BPL enzyme, protein enrichment over a negative control experiment have to be performed. To quantify enrichments, label-free quantitative (LFQ) proteomic methods are available.[198-200] The intensities of LFQ precisely indicate the relative abundance of the analysis proteins across samples and is usually performed to compare two conditions, each with at least 3 replicated samples. Two fundamental algorithms to LFQ includes intensity based absolute quantification iBAQ[201-203], and the LFQmax method integrated in the program MaxQuant. iBAQ utilizes the sum of intensity from all replicated samples that is separated by the amount of short tryptic peptides in length of 6-30 amino acids. Additionally, iBAQ data is rational to the molar abundance of analysis proteins.[204] After removing all the contaminated background, the iBAQ algorithm can approximately evaluate the relative amounts of the proteins within each sample.[205] Since the quantified peptides varies in different samples, protein abundance profiles are global assembly using the information from MS signals.[206] LFQmax is a generic label-free quantification approach compatible with any protein or peptide separation before LC-MS analysis and applied to different biological pregress.[206,207]

In this thesis, peptides were identified by the software of MaxQuant[207]. The relative abundance of each protein across samples was calculated by LFQ[206] and relative enrichment were calculated with the R-package proDA[208]. ProDA (for probabilistic drop out analysis) manages the missing LFQ values (either reflecting a real absence of the corresponding proteins, or a lack of detection in the particular sample) by deducing from the missing data the associated variance of the mean LFQ intensity for each quantified protein.[208,209]

1.6 objectives

The two paralogues of γ-COPs share similar structure of a large stacked helical trunk domain at the N-terminus joined by a low complexity linker with little or no secondary structure to an appendage domain at the C-terminus. Potential distinct function between the γ1-COP and γ2-COP in the early secretory pathway during neuronal differentiation were investigated in this study. A recent study by a PhD student of our lab revealed that disrupting the expression of γ1-COP, but not of γ2-COP, results in the failure to generate tight embryoid bodies and neurite extension during P19 cells neuronal differentiation.[188] To validate the specific role of γ1-COP during neuronal differentiation and explore the underlying mechanisms in P19 cells, in the extent of this thesis, the following major questions were addressed:

(1) Does the γ1-COP protein play a role in neuronal differentiation or are other regulatory elements within the Copg1 locus also involved?
(2) Do the phenotypes of γ1-COP KO cells result from the absence of the γ1-COP protein or rather of a reduced combined expression of the γ-COP paralogues?
(3) Can a specific domain be mapped within the γ1-COP protein that explains its activity during P19 cells neuronal differentiation?
(4) Do γ1-COP interactors with a specific set of proteins that may explain its unique function during neuronal differentiation?

2. Results

In the previous study, a Cas9-mediated genome editing method was used with an individual particular single guide RNA (sgRNA) to target Copg1 and Copg2 in P19 pluripotent cells and so result in frame shift insertions and deletions (indels).[188] Following this, the P19 cells were differentiated into neurons to explore a potential specific role for the distinct paralogue of γ-COP. In this study, the same two-stage neuronal differentiation procedure is adopted in P19 cells for a duration of 8 days (**Figure 3**). The cells under non-adherent conditions are first inducted by a retinoic acid (RA)-containing medium for the first 4 days to generate embryoid bodies (EBs). Then, the trypsin-dissociated EBs are seeded in poly-L-lysin-coated plates to form post-mitotic neurons (day 4-8). At day 6, an anti-mitotic agent known as the arabinosylcytosine C (Ara-C) is used to reduce the population of the non-neuronal cells (the detailed differentiation protocol is described in the method and material session).[26,188]

During the first stage of the differentiation process monitored on days 2 and 4, it was observed through microscopy with 10X magnification that the EBs had dark boundaries and the cells were tightly connected with each other in the P19 WT and Copg2 KO cells, while they were lacking sharp boundaries and had loose connections in the Copg1 KO cells. In the second stage, analysed on day 8, the cells were stained with an antibody against the neuron marker Tuj1. Images from the immunofluorescence microscopy showed neurite extensions in the Copg2 KO cells of similar averaged length to those observed in the P19 WT cells. By contrast, none or only extremely short neurites were detected in the Copg1 KO cells.[26,188] According to the above study, deletions of the γ1-COP leads to the failure of neurite growth during P19 cells differentiation.

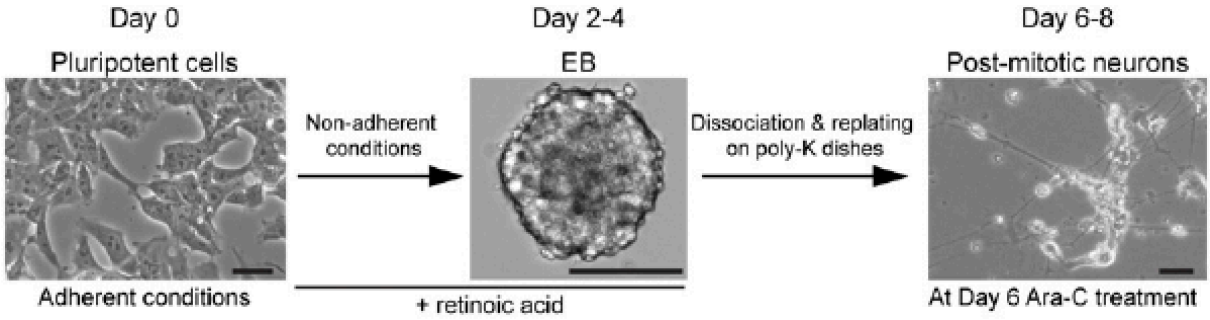

Figure 3. Schematic indication of the two-stage P19 neuronal differentiation protocol. Scale bar 50 μm.

2.1 Depletion of γ1-COP or γ2-COP does not induce apoptosis

It has been reported that disruption of the COPI pathway can lead to apoptosis.[210,211] In addition, increased apoptosis can affect neuronal differentiation.[212-214] Hence it is important to check if deletion of γ1-COP or γ2-COP leads to increased apoptosis because this could be the reason why we observed a defect in neurite extension in γ1-COP KO cells. The caspases are central components of the apoptotic process and so, to analyse whether the γ1-COP or γ2-COP KO cells are prone to apoptosis, they were stained with Fluorescent Labelled Inhibitors of Caspases probes (FLICA) to track the activity of caspase-3/-7.[215] The membrane

impermeant DNA stain Propidium iodide (PI) was adopted to distinguish early apoptotic (positive for caspase activity but intact membrane), late apoptotic (positive for caspase activity and disrupted membrane) and necrotic cells (negative for caspase activity and disrupted membrane). In addition, an apoptosis positive sample was prepared by treating P19 WT cells with staurosporine to induce cell apoptosis through the activation of caspase-3.[216] The dot plots in **Figure 4A** depict 4 quadrants in which living (PI and FLICA negative), necrotic (PI positive and FLICA negative), early apoptosis (PI negative and FLICA positive) and late apoptosis (PI and FLICA positive) cells can all be found. When compared to P19 WT, **Figure 4A** shows that the apoptotic activity did not increase in either the Copg1$^{-/-}$ or Copg2$^{-/-}$ cells, meaning therefore, that the absence of γ1-COP or γ2-COP does not result in elevating apoptosis.[188]

2.2 Depletion of γ1-COP or γ2-COP does not induce ER stress

The absence of COP subunits may result in ER stress.[217,218] It was reported that ER stress could have an effect on neuronal differentiation in P19 cells[219], and so, whether an absence of γ1-COP or γ2-COP could induce ER stress was investigating by analysing the expression levels of two ER stress markers – GRP-78 (also known as Bip) and CHOP. It was observed that the low expression of GRP-78 and CHOP in WT, was comparable to γ1-COP KO and γ2-COP KO cells (**Figure 4 B and C**). By contrast, much higher expression levels were visible in the cells following treatment with tunicamycin, which is a glycosylation inhibitor that induces the unfolded protein response[220] (**Figure 4B**). Interestingly, when compared with WT and Copg2$^{-/-}$ cells, a lower GRP-78 and a higher CHOP expression was observed in Copg1$^{-/-}$ cells following the tunicamycin treatment. GRP-78 is an ER luminal protein with a KDEL (Lys-Asp-Glu-Leu) retention signal at its C terminus.[122] The KDEL signal is recognised at the Golgi by its receptor, and is then be regulated and trafficked back to ER by the COPI vesicles.[221] CHOP activates the apoptotic pathway and is up-regulated dependent on the chronic ER stress which results from the elevated misfolded protein in the ER.[37] One prospect that could explain the different responses to the tunicamycin treatment in Copg1$^{-/-}$ cells is that the retrograde traffic back to ER might be affected in Copg1$^{-/-}$ cells to a higher extent than in Copg2$^{-/-}$ cells. This would lead to a less efficient retention of GRP-78 in the ER, which would subsequently result in cells that cannot cope as efficiently with ER stress, which in turn might explain the higher activation of apoptosis through the CHOP pathway after induced ER stress.

Anyhow, our data indicate that the absence of γ1-COP or γ2-COP does not lead to increased ER stress.[188]

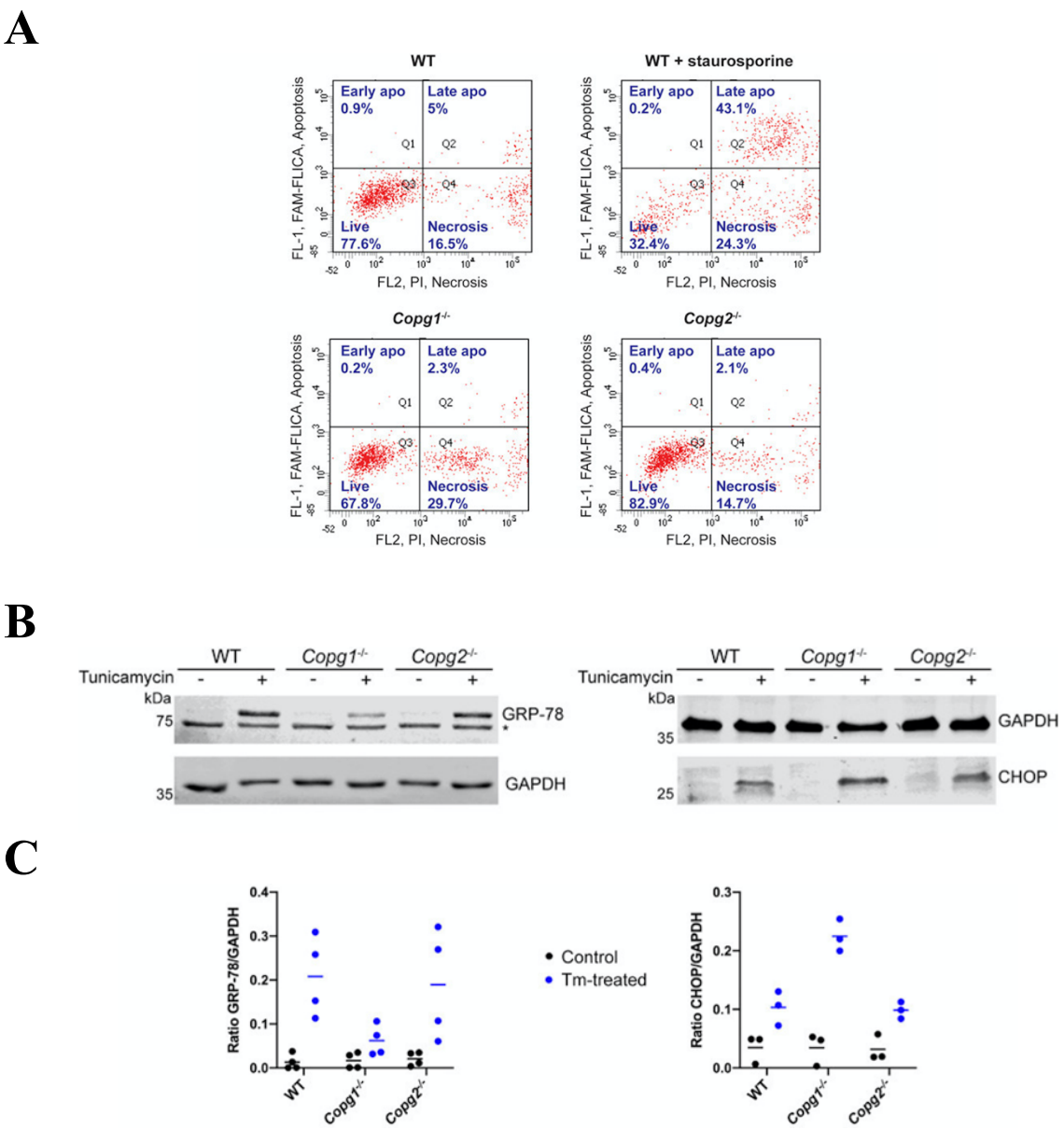

Figure 4. The absence of γ1-COP or γ2-COP neither elevates cellular apoptosis nor ER stress. Figure published in Life Sci Alliance Journal. Copyright © 2020 Goyal, Zhao et al[188]. This figure is licensed under the Creative Commons Attribution 4.0 International License. To view a copy of this license, visit http://creativecommons.org/licenses/by/4.0/ or send a letter to Creative Commons, PO Box 1866, Mountain View, CA 94042, USA.

(A) Dual fluorescence flow cytometry assay was used to detect activated caspase-3/7 (FL1, FAM FLICA) and membrane damage (FL2, propidium iodide) in P19 WT, Copg1−/− and Copg2−/− cells. Apoptosis (apo) was induced in WT cells with staurosporine, as previously indicated. The percentage of cells detected in each quadrant is indicated (n = 4,686–7,145

cells). (B) Western blot analysis was carried out on the expression of the ER stress markers GRP-78 and CHOP, as well as of GAPDH in P19 WT, Copg1−/− and Copg2−/− cells. When indicated, ER stress was induced with tunicamycin. * nonspecific signal. (B, C) Quantification of (B). Tm, tunicamycin.

2.3 Generation of P19 cells expressing γ1-COP-GFP KI, γ2-COP-GFP KI and GFP KI from Copg1 locus

As described above, Copg1$^{-/-}$ and Copg2$^{-/-}$ cells were constructed following a Cas9-mediated genome editing approach by inducing the formation of insertion-deletion (Indel) within the corresponding encoded gene Copg1 or Copg2 to knock out γ1-COP or γ2-COP. Following a neuronal differentiation induction, the Copg1$^{-/-}$ cells were unable to form the long neurite length as P19 WT cells and Copg2$^{-/-}$ cells. In addition, after making these observations, a previous study used bacterial artificial chromosome (BACs) plasmids to generate the P19 Copg1$^{-/-}$-Copg1-GFP cells harbouring the murine Copg1 locus in Copg1$^{-/-}$. Impressively, the P19 Copg1$^{-/-}$-Copg1-GFP cells showed a similar neurite outgrowth to the WT and Copg2$^{-/-}$ cells.[188]

In order to validate if the contribution and significance of COPI in neuronal differentiation is specified in the expression of γ1-COP, but not in the regulatory elements from the Copg1 locus, we constructed the γ1-COP-GFP knock-in (KI) cells and GFP KI as a negative control cell line. Instead of introducing frame-shift mutations by Cas9 nuclease, the whole Copg1 locus was eliminated using Cas12a enzyme guided by two CRISPR RNAs (crRNAs). This was done to induce two single cuts prior to knocking in the coding sequence of either γ1-COP-GFP (γ1-COP-GFP KI cell line) or GFP (GFP KI cell line) as a control. Furthermore, in the missing γ1-COP cells, it remained unclear whether the amount of γ2-COP could play a significant role in the process of neurites outgrowth. To avoid the fluctuation of the amount of coatomer between two distinct γ-COPs, γ2-COP-GFP KI cell line (the coding sequence of γ2-COP-GFP knock-in Copg1 locus) was generated following the same Cas12a-mediated genome editing method as the P19 GFP KI and P19 γ1-COP-GFP KI cell lines. The schematic of knock-in cell lines generation is shown in **Figure 5**.

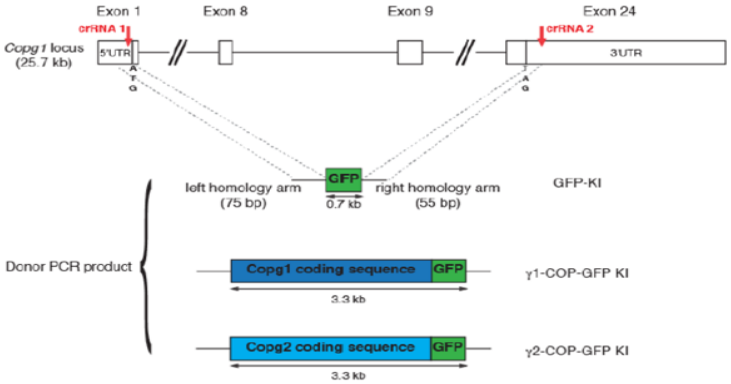

Figure 5. CRISPR strategy to acquire KI cell lines. Figure reproduced from Life Sci Alliance Journal. Copyright © 2020 Goyal, Zhao et al[188]. The reproduced figure is licensed under the Creative Commons Attribution 4.0 International License. To view a copy of this license, visit http://creativecommons.org/licenses/by/4.0/ or send a letter to Creative Commons, PO Box 1866, Mountain View, CA 94042, USA.

The schematic shows the sites targeted by the crRNAs in the Copg1 genomic locus in order to induce two cleavages by Cas12a. The knock-in PCR cassettes with short homology arms that direct homology-directed repair is also demonstrated.

2.4 Characterisation of the knock-in insertions

Confocal microscopy and western blot were used to identify the stable cell lines expressing the proteins of knock-in insertions. Confocal microscopy with 100 magnification demonstrates that the cell lines show a Golgi-scattered or whole cell-scattered GFP signal. **Figure 6A** shows that the GFP KI cell lines displayed the whole cell-scattered GFP protein expression, whereas all the other cell lines expressing the γ-COP fused to GFP proteins were localised at the Golgi. As is shown in **Figure 6B**, the proteins of the knock-in insertions were detected at the correct size by western blot.

A

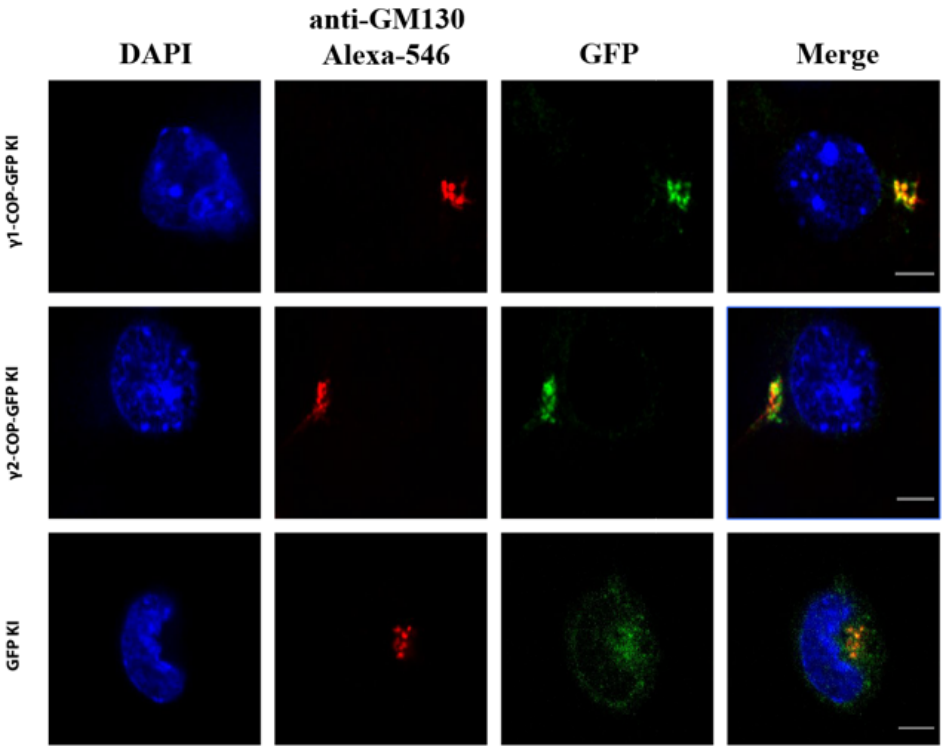

B

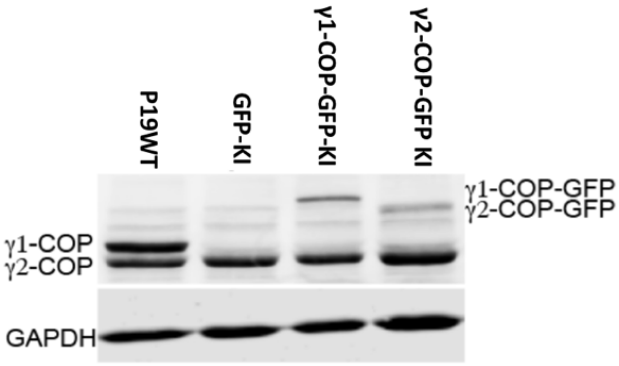

Figure 6. Identification of knock-in insertions in CRISPR knock-in cells.

(A) the localisation of the knock-in insertions in P19 cells, and in the γ1-COP-GFP and γ2-COP-GFP, were aggregated around the Golgi (co-localisation with the GM130 marker) whereas the GFP knocked-in protein was scattered in the cell. (B) Figure published in Life Sci Alliance Journal. Copyright © 2020 Goyal, Zhao et al[188]. This figure is licensed under the Creative Commons Attribution 4.0 International License. To view a copy of this license, visit http://creativecommons.org/licenses/by/4.0/ or send a letter to Creative Commons, PO Box 1866, Mountain View, CA 94042, USA. Western blot analysis of the γ1-COP and γ2-COP

expression level from P19 WT and GFP-KI, as well as of the expression levels of γ1-COP-GFP and γ2-COP-GFP from P19 γ1-COP-GFP KI and γ2-COP-GFP KI cell lysates, respectively.

2.5 Bi-allelic insertion of the transgenes

PCR mapping was performed to detect the bi-allelic insertion in the Copg1 locus. To verify the knock-in insertions in the Copg1 locus, the primers around the cutting sites were designed for a PCR test. For GFP KI cells, the expected PCR product should be 595bp for the amplified fragment that spans the cutting site in 5'UTR of the Copg1 locus. For γ1-COP-GFP KI cells, it should be 1241bp and for γ2-COP-GFP KI cells, 1234bp. For all three KI cells, the expected PCR product should be 699bp for the amplified fragment spanning the cutting site in the 3'UTR. As shown in **Figure 7A**, the product of all the PCR products are consistent with expectations.

In order to determine the bi-allelic insertion of the fragments in the Copg1 locus, two other pairs of primers were designed in the exons (exon8 and exon9) and UTR (5'UTR and 3'UTR) of the WT locus. Primer locations and two heterozygous situations are shown in the following schematics (**Figures 7B and C**). If the cells are monoallelic, as in heterozygous situation 1, the expected PCR product should be 1079bp, whereas, in bi-allelic samples, it should be about 5000bp for γ-COP knock-in cells, and 1923bp for GFP knock-in cells (**Figure7B**). In addition, if the cells are monoallelic, as heterozygous situation 2, the expected PCR product should be 1221bp (**Figure7C**). According to **Figures 7B and C**, neither 1079bp nor 1221bp was found in the PCR mapping. Thus, in summary, all the cell lines are the product of a bi-allelic insertion.

A

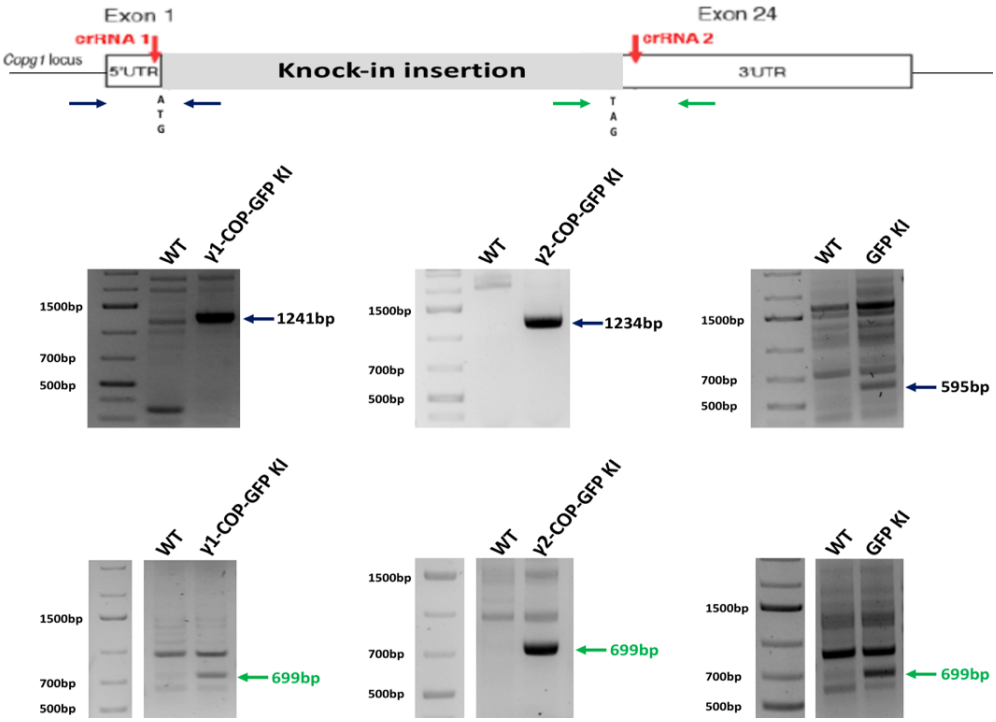

B

Heterozygous Situation1

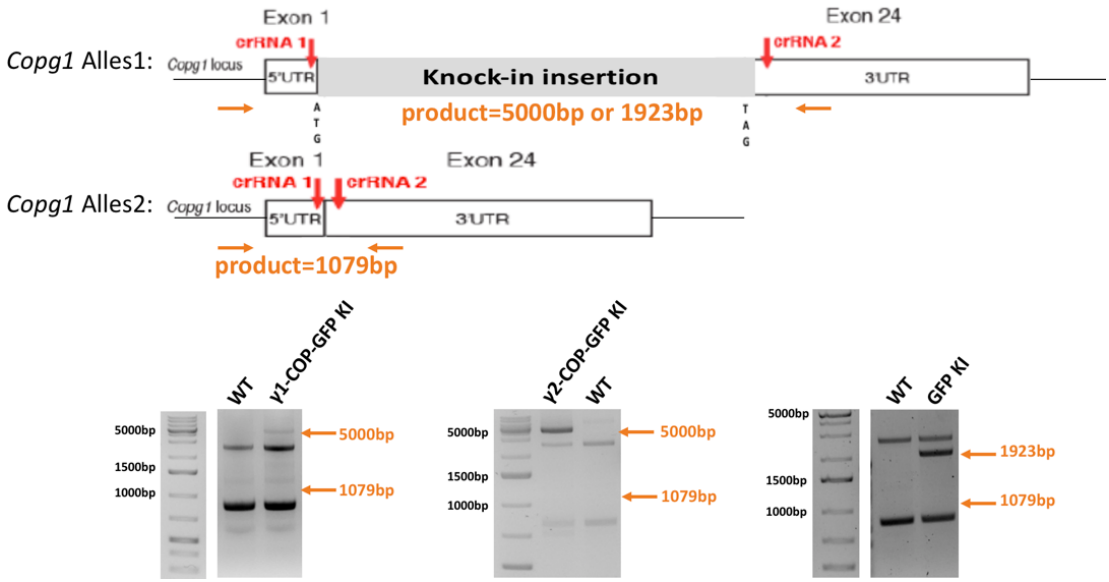

C

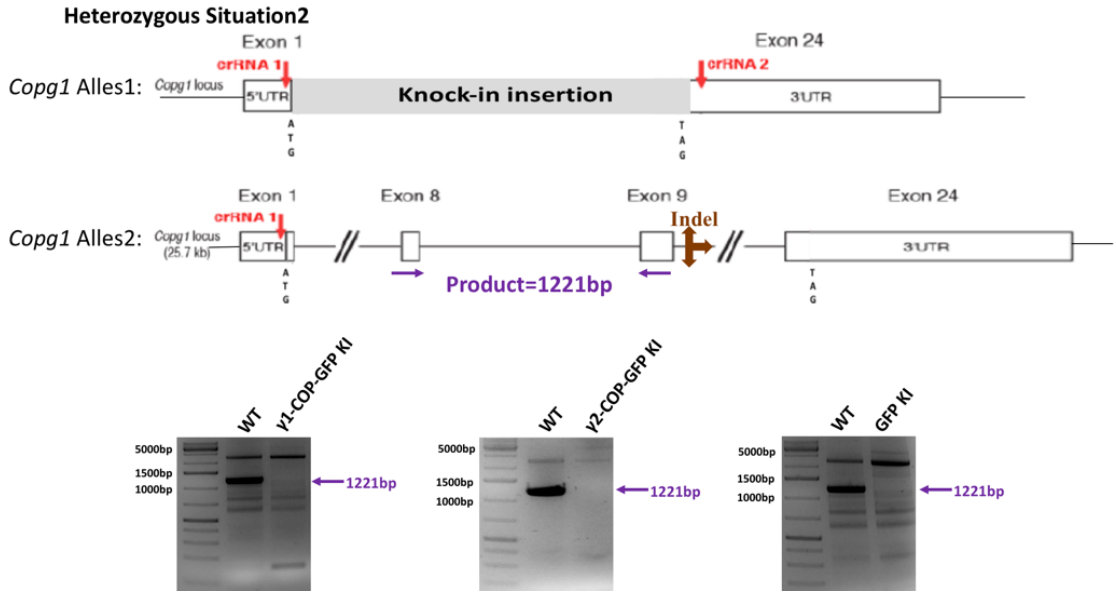

Figure 7. Bi-allelic insertion identification by PCR mapping.

Schematic overview of the positions of the crRNA cutting sites in the Copg1 locus to assist knock-in insertions by Cas12a. PCR analysis of the amplification of genomic DNA with the respective primers to detect the wild-type alleles and knock-in samples. (A) Coloured arrows represent the location of genotyping primers spanning the flanked positions of the inserts. The expected PCR product size around crRNA1 between the black arrows is 1241bp for γ1-COP-GFP KI, 1234bp for γ2-COP-GFP KI, and 595bp for GFP KI. The expected PCR product size around crRNA2 between the green arrows is 699bp for all samples of γ1-COP-GFP KI, γ2-COP-GFP KI, and GFP KI. (B) Coloured arrows represent the location of the genotyping primers spanning from the 5'UTR to 3'UTR of the Copg1 locus to check the bi-allelic samples. In accordance to the schematic figure, no PCR product size of 1079bp was detected when using the primers depicted by the orange arrows in any of the γ1-COP-GFP KI, γ2-COP-GFP KI, or GFP KI samples, but only PCR products of about 5000bp for γ-COP knock-in cells and 1923bp for GFP knock-in cells, which means that all samples are bi-allelic. (C) Coloured arrows represent the location of the genotyping primers spanning from the Exon8 to Exon9 of the Copg1 locus to check the bi-allelic samples. According to the schematic figure, no PCR product size of 1221bp is detected between the purple arrows in any of the γ1-COP-GFP KI, γ2-COP-GFP KI, or GFP KI samples, which means that all samples are bi-allelic.

2.6 Expression of either γ1-COP or γ2-COP from the Copg1 locus supports the formation of a tight embryonic body

In order to verify if γ1-COP carries out specific functions during pluripotent cells differentiation, all the KI cells were submitted to the classical two-step differentiation protocol. In the first step, a spherical embryoid body (EB) with dark boundaries was formed by a retinoic acid (RA) induction in P19 WT cells for subsequent neurites outgrowth.[222,223] For the investigation of EB morphology, the hanging drop method was adopted and 20 μL of volume containing 200 cells was used in each drop (the detailed method is shown in the method session). Then, on days 2 and 4 the pictures were obtained using light microscopy with 10X magnification. According to **Figure 8**, the γ1-COP-GFP KI cells can form tight EBs, which are similar to the WT cells on day 2 and day 4, whereas the GFP KI cell failed to form the ball-shaped EBs, which thus suggests that γ1-COP expression is essential for tight EB formation. Strikingly, as shown in **Figure 8**, γ2-COP-GFP KI cells were able to form tight EBs, just like WT cells. This demonstrated that the failure to generate EB by GFP KI cells is in fact not due to the absence of γ1-COP but rather to having a too low expression level of γ-COP, regardless of the paralog identity. In brief, expressions of either γ1-COP or γ2-COP paralogs from the Copg1 locus can support the formation of EBs.

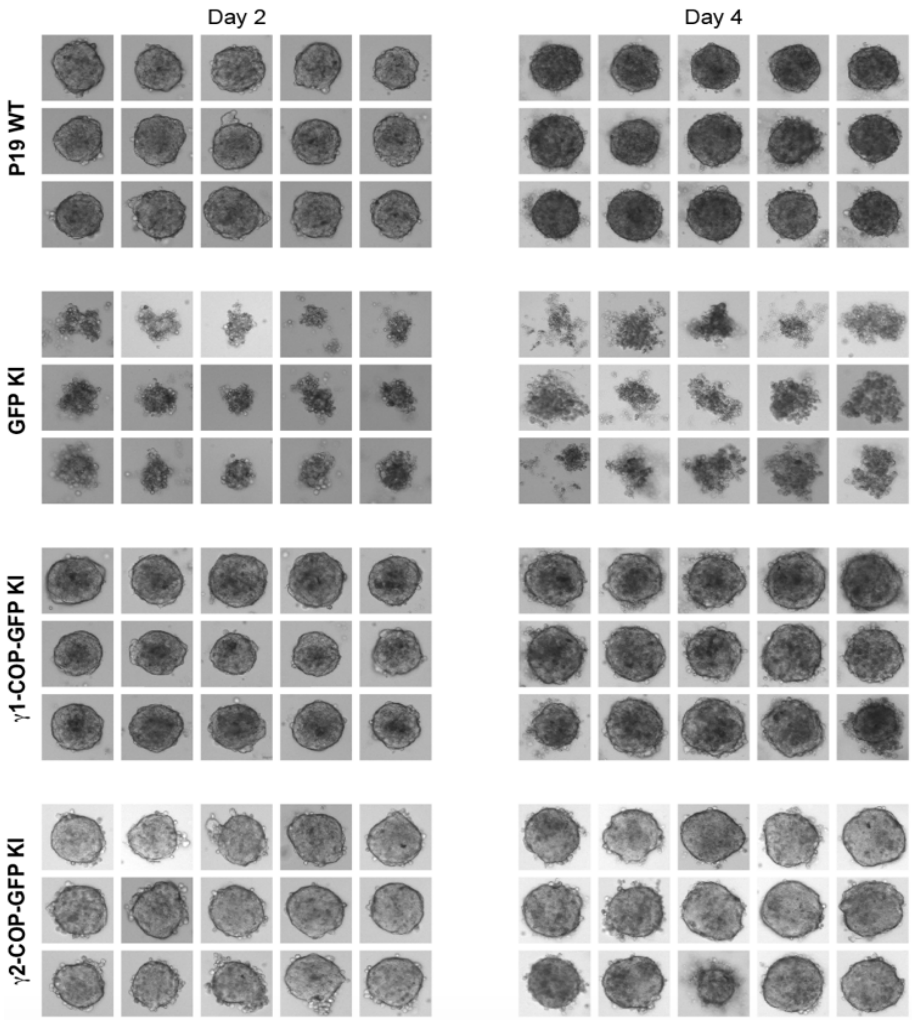

Figure 8. γ1-COP -GFP KI and γ2-COP-GFP KI rescue the formation of tight Embryoid bodies (EB) in vitro.

Compared to P19 WT cells, the formation of EB in GFP KI cells is disrupted by the knock-out of the Copg1 locus. In γ1-COP-GFP KI or γ2-COP-GFP KI cells, the formation of EB is similar to P19 WT cells and is achieved through the expression of either γ1-COP or γ2-COP from their coding sequences in the Copg1 locus.

2.7 γ1-COP promotes the neurite extension

Following the above, I analysed if the γ1-COP paralog has a specific function in promoting neurite outgrowth during the second step of in vitro P19 cells differentiation. 10^6 cells per dish were cultured with an RA-containing medium for four days in non-adherent bacterial dishes. Then, aggregated EBs were trypsinised and 80,000 cells per well were seeded on the poly-L-lysine-coated 8-well ibidi slide. Following 8 days of differentiation, cells were stained with the antibody Tuj1 to detect the neuron specific marker Tubulin β III through detection by

immunofluorescence microscopy (the detailed differentiation protocol is shown in the method session). According to the microscopic analysis depicted in **Figure 9A**, it appears that γ1-COP-GFP KI cells showed a network of long neurites similar to WT cells. In contrast, as shown in **Figure 9A**, P19 GFP KI cells failed to extend long neurites. Additionally, in the light of **Figure 9A**, the neurites of the γ2-COP-GFP KI cells could stretch out longer than GFP KI, but were not comparable in length to those of WT and γ1-COP KI cells. These findings were supported by the software quantification of the averaged neurite length per cell in **Figure 9B**. In consequence, this revealed that γ1-COP plays a specific role, that can only be partially taken over by γ2-COP, in neurogenesis during the late differentiation stage of the P19 cells.

A

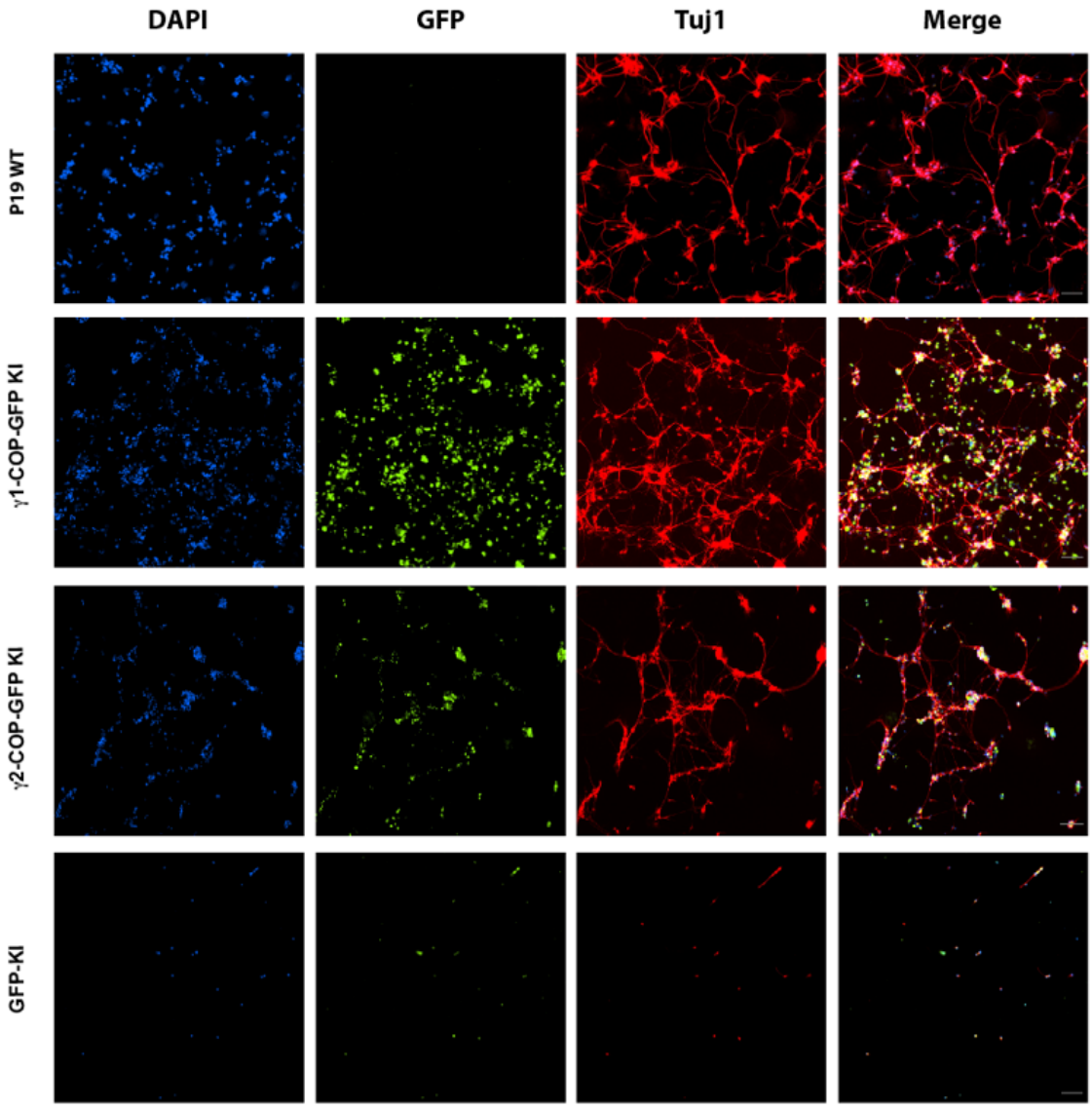

B

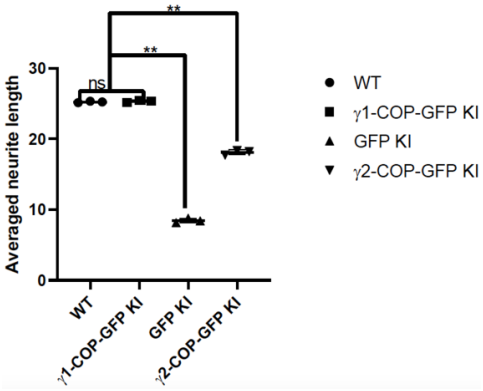

Figure 9. Expression of γ1-COP promotes neurite outgrowth.

(A) Fluorescent microscopy images for the analysis of the expression of the neuronal marker Tuj1 and GFP channel of knock-in insertions in γ1-COP-GFP, γ2-COP-GFP and GFP KI cells at day 8 of neuronal differentiation. The blue channel represents the nucleus stained by DAPI. The green channel represents the expression of knock-in insertions by GFP tag. The red channel represents the Golgi marked by GM130. Scale bar is 100μm. (B) Quantification of the averaged neurite length (neurite length/cell number). Each dot indicates the quantity gained from 5 random images (corresponding to about 1000 cells), as in (A). ** represents P-value < 0.005, ns, nonsignificant.

2.8 Generation of P19 cells expressing γ Chimera-COP-GFP from Copg1 locus

The γ-COP protein is made up of two subdomains, the designated amino-terminal trunk domain and carboxyl-terminal appendage domain, combined with a flexible linker (**Figure 10**).[80] Based on the available structures, in γ1-COP, the amino-terminal region of COP (residues 1–554) joins a carboxyl-terminal appendage (residues 604–874) through a linker (residues 555–603).[68,80] Though the structure of γ2-COP has not been reported in detail, its carboxyl-terminal appendage can be predicted from residue 602 to 871, which, according to the 80% amino acid sequence identity between the two proteins in mammals, corresponds to the appendage domain of γ1-COP.[73] To investigate if there is a specific domain of γ1-COP that is responsible for its activity in promoting neurite extension, two chimeric constructs were generated containing the region of the γ1-COP trunk plus the linker combined with the γ2-COP appendage (comprised of residues 1–603 from γ1-COP fused to residues 602–871 from γ2-COP and designated γ1-2-COP), and the region of the γ2-COP trunk plus the linker combined with the γ1-COP appendage (comprised of residues 1–601 from γ2-COP fused to

residues 604–874 from γ1-COP and designated γ2-1-COP). This led us to knock-in the chimera constructs in the Copg1 locus to generate P19 γ1-2-COP-GFP KI and γ2-1-COP-GFP KI cell lines according to the same Cas12a-mediated genome editing strategy that was used to in the P19 GFP KI and P19 γ1-COP-GFP KI cell lines.[188] The schematic of knock-in cell lines generation is shown in **Figure 11**.

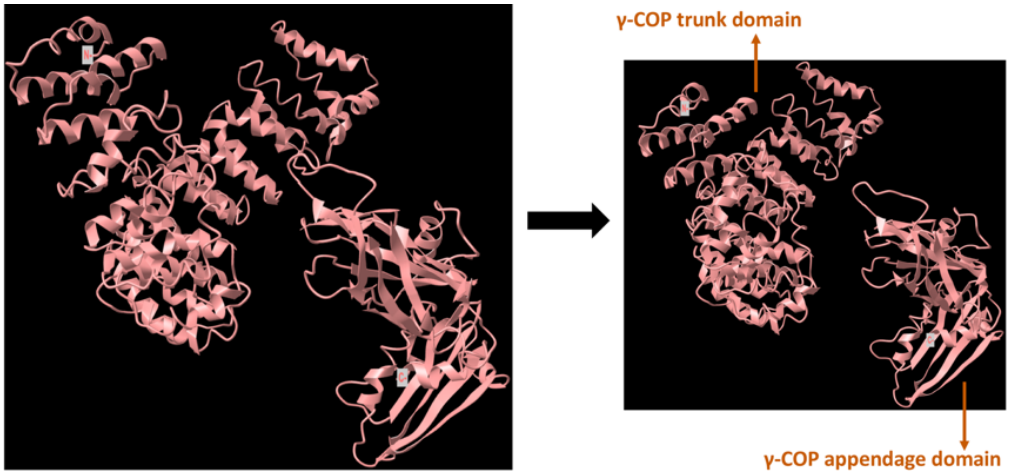

Figure 10. The structure of γ-COP (Annotations of 5NZT_G) cited from[68,80]. The protein structures were obtained from the RCSB protein data bank. PDB ID: 5NZT MMDB ID: 152192

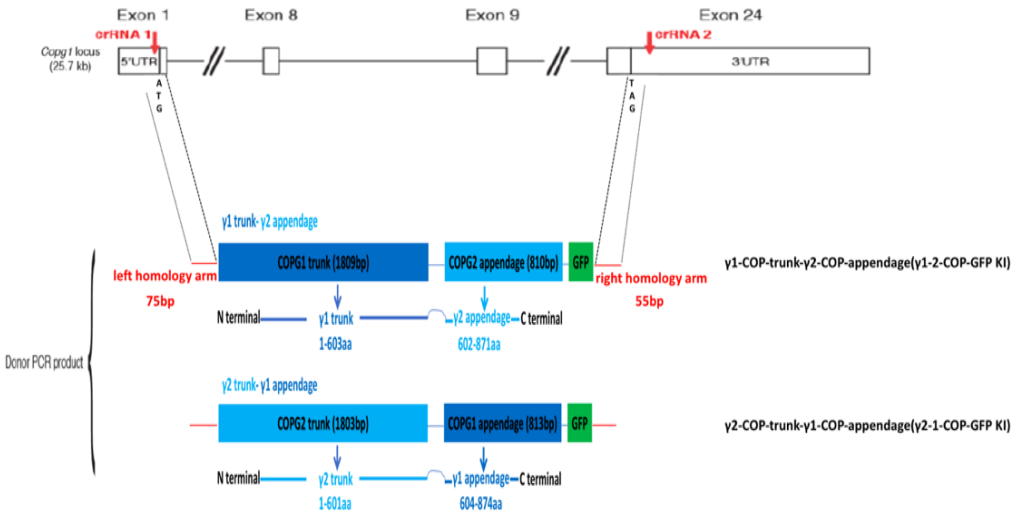

Figure 11. CRISPR strategy to acquire KI cell lines.

Figure reproduced from Life Sci Alliance Journal. Copyright © 2020 Goyal, Zhao et al[188]. The reproduced figure is licensed under the Creative Commons Attribution 4.0 International

Schematic shows the sites targeted by the crRNAs in the Copg1 genomic locus to induce two cleavages by Cas12a. The chimera PCR cassettes with short homology arms are directed to knock-in the Copg1 locus. Figure reproduced from[188].

2.9 Chimera constructs knock-in characterisation

Chimera knock-in insertions were characterised by confocal microscopy and western blot. The specific protein expression of either γ1-2-COP or γ2-1-COP was demonstrated by confocal microscopy with a GFP signal (green channel) co-localised with the signal for the Golgi marker GM130 (red channel) in the cell lines (**Figure 12A**). Additionally, as shown in **Figure 12B**, the chimera fusions' proteins were detected at their expected size by western blot.

A

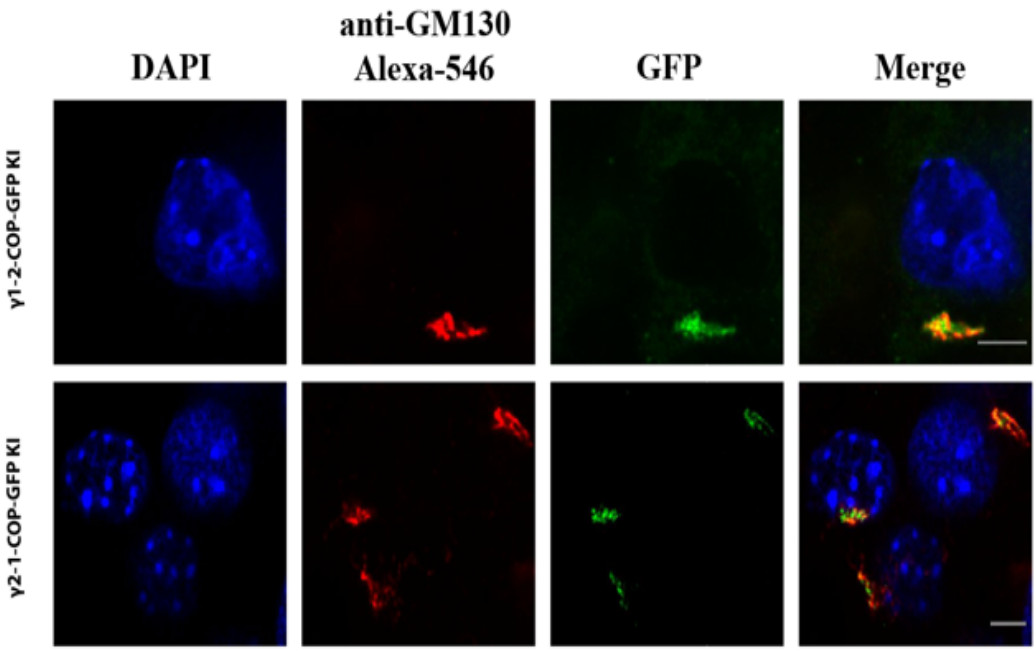

B

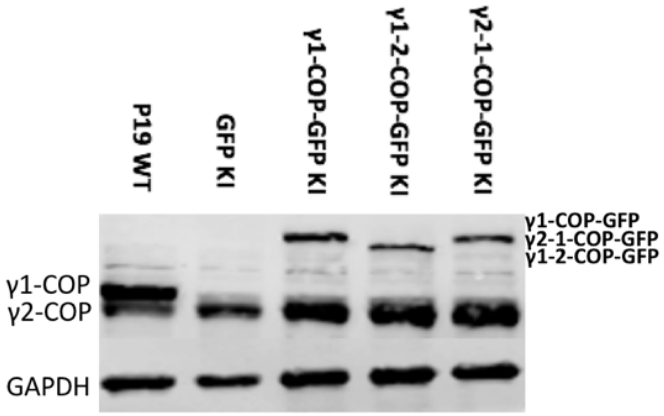

Figure 12. Identification of knock-in insertion proteins in CRISPR knock-in cells.
(A) The GFP tag γ1-2-COP and γ2-1-COP localise in the Golgi marked by GM130. The scale bar is 5μm. (B) Western blot analysis of the γ1-2-COP and γ2-1-COP expression level compared with P19 WT, GFP KI as well as with the migrated expression levels in γ1-COP-GFP KI.

2.10 Bi-allelic insertion of the exogenous coding gene in γ Chimera-COP-GFP KI cells

PCR mapping was carried out to identify the bi-allelic insertion in the Copg1 locus by following the same strategy and using the same mapping primers that were used to identify the insertions in P19 GFP KI, γ1-COP-GFP KI and γ2-COP-GFP KI cell lines. For the γ1-2-COP-GFP KI cells, the expected PCR product should be 1241bp, with the primers flanking the cutting site in 5'UTR of the Copg1 locus, and 1234bp in the γ2-1-COP-GFP KI cells. For both of the chimera KI cells, the expected PCR product should be 699bp, with the primers flanking the cutting site in 3'UTR. According to **Figure 13 A**, all the PCR products correspond to expectations. Furthermore, to determine whether the insertion was bi-allelic and in order to exclude the two heterozygous situations shown in **Figures 13 B and C,** the same primers used in **Result 2.5** were used once more. In heterozygous situation 1, an amplified product of 1079bp was expected, but instead only the PCR product of about 5000bp, that corresponds to the inserted coding sequence of the chimeras, was detected in the KI cell lines (**Figure 13B**). In heterozygous situation 2, a PCR product of 1221bp, spanning intron 8 was expected, but it was absent from the KI cell lines (**Figure 13C**). In the light of **Figures 13 B and C**, no monoallelic-specific band was found in the PCR mapping. Therefore, all the cell lines were bi-allelic insertion samples.

A

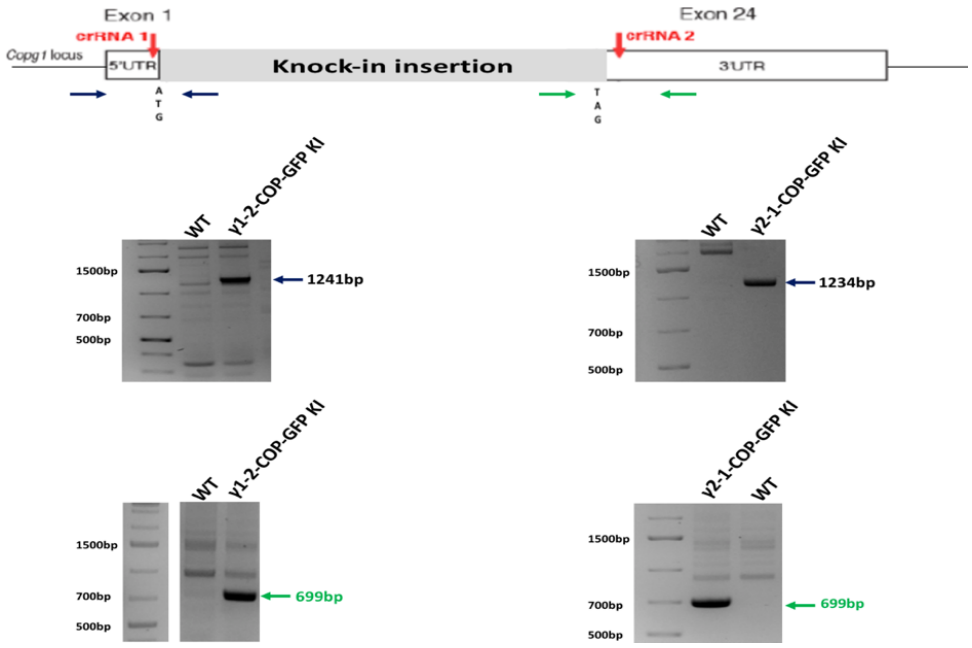
Exon 1
crRNA 1
Copg1 locus
5'UTR
Knock-in insertion
Exon 24
crRNA 2
3'UTR
A T G
T A G
WT
Y1-2-COP-GFP KI
1500bp
700bp
500bp
1241bp
WT
Y2-1-COP-GFP KI
1500bp
700bp
500bp
1234bp
WT
Y1-2-COP-GFP KI
1500bp
700bp
500bp
699bp
Y2-1-COP-GFP KI
WT
1500bp
700bp
500bp
699bp

B

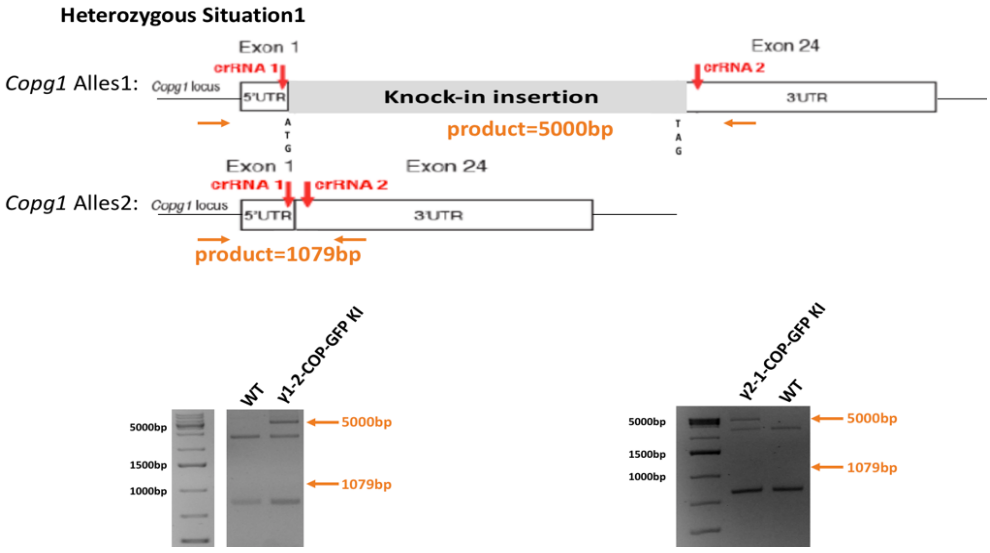
Heterozygous Situation1
Copg1 Alles1:
Exon 1
crRNA 1
Copg1 locus
5'UTR
Knock-in insertion
Exon 24
crRNA 2
3'UTR
A T G
product=5000bp
T A G
Copg1 Alles2:
Exon 1
crRNA 1
crRNA 2
Exon 24
Copg1 locus
5'UTR
3'UTR
product=1079bp
WT
Y1-2-COP-GFP KI
5000bp
1500bp
1000bp
5000bp
1079bp
Y2-1-COP-GFP KI
WT
5000bp
1500bp
1000bp
5000bp
1079bp

C

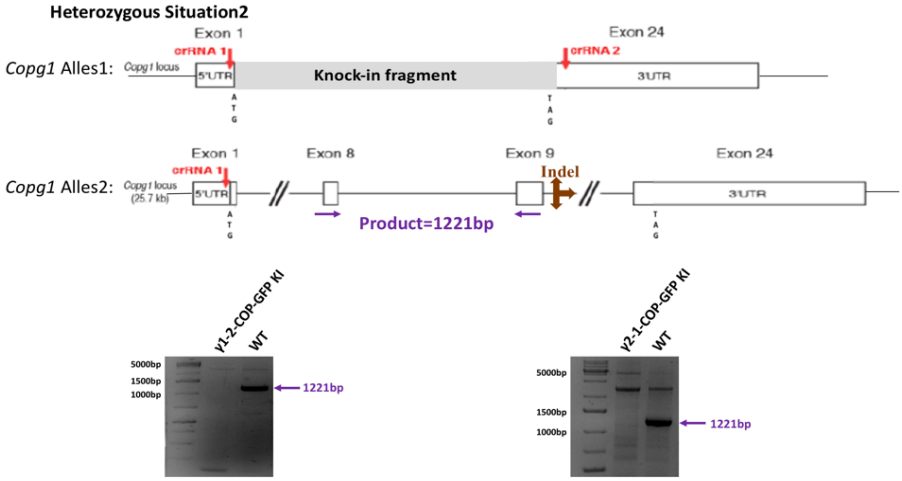

Figure 13. Bi-allelic insertion identification by PCR mapping.
Schematic overview of the crRNA cutting site positions in the Copg1 locus to assist knock-in insertions by Cas12a. PCR analysis of the insertion of the indicated cassettes in the genomic DNA with the respective primers detecting the wild-type alleles and knock-in samples. (A) Coloured arrows represent the location of the genotyping primers spanning the flanked positions of the inserts. The expected PCR product size around crRNA1 and found between the black arrows in the schematic figure are 1241bp for γ1-2-COP-GFP KI, and 1234bp for γ2-1-COP-GFP KI. The expected PCR product size around crRNA2 and found between the green arrows in the schematic figure is 699bp among all the samples of γ1-2-COP-GFP KI and γ2-1-COP-GFP KI. (B) Coloured arrows represent the location of the genotyping primers spanning from the 5'UTR to 3'UTR of Copg1 locus to verify the bi-allelic insertion of the cassettes. No PCR product of a size of 1079bp but instead a product of about 5000bp is detected, when using the primers depicted by the orange arrows, in any of the samples of γ1-2-COP-GFP KI and γ2-1-COP-GFP KI, which means that all samples are bi-allelic. (C) Coloured arrows represent the location of the genotyping primers spanning from Exon8 to Exon9 of Copg1 locus to check the bi-allelic insertion of the cassettes. No PCR product size of 1221bp is detected between the purple arrows among any of the samples of γ1-2-COP-GFP KI and γ2-1-COP-GFP KI, which means all samples are bi-allelic.

2.11 The formation of tight EBs is not due to an absent specific function mediated by γ1-COP

From previous data shown in **Figure 8**, I found that a sufficient amount of the γ-COP, rather than a specific paralogous sub-unit, is the key factor in regulating the early stage of P19 cells

differentiation. I thus expected both chimeras to support the correct EB formation. To challenge this prediction therefore, I used the γ1-2-COP-GFP KI and γ2-1-COP-GFP KI cell lines for an EB morphology investigation. As is shown in **Figure 14**, the expression of both γ-COP chimeras from the Copg1 locus supports the formation of tight EBs, which is in contrast to the GFP KI cells. Again, these data validate the idea that the formation of tight EBs is not specifically mediated by γ1-COP.

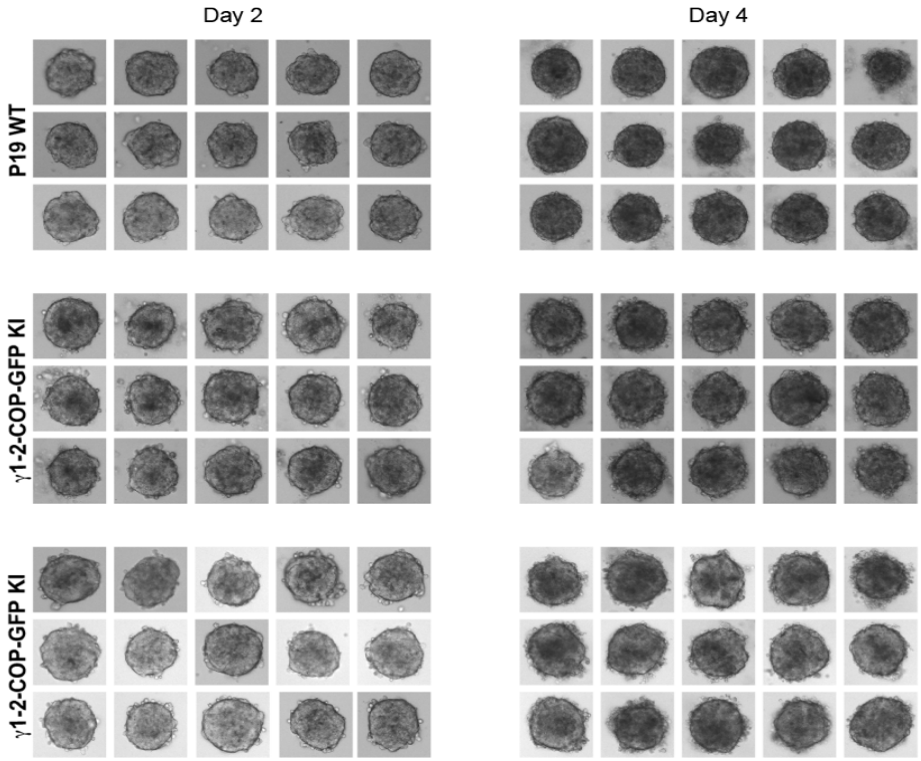

Figure 14. γ-COP chimeras support the formation of tight Embryoid bodies (EB) in vitro.

In chimera KI cells, the formation of EB was similar to P19 WT cells through either the expression of the γ1-2-COP or γ2-1-COP coding sequence in the Copg1 locus.

2.12 Expression of γ-COP chimeras from the Copg1 locus does not fully compensate for the absence of γ1-COP during neurite outgrowth

In contrast to the formation of EB, I found that γ2-COP cannot fully compensate for the absence of γ1-COP during the neurite extension phase of neuronal differentiation (**Figure 9**). Therefore, in order to analyse whether a specific γ1-COP domain mediates neurite outgrowth,

in vitro differentiation of P19 cells was performed with both γ1-2-COP-GFP KI and γ2-1-COP-GFP KI cell lines.

In the light of the microscopic analysis shown in **Figure 15 A**, in which P19-derived neurons from WT and KI cells were compared, it appears that both γ1-2-COP-GFP KI and γ2-1-COP-GFP have the ability of neurite outgrowth but that the resulting neurites are shorter than in WT cells. To strengthen this observation, the software-mediated quantification of neurite length was performed. As shown in **Figure 15 B**, the quantification of the averaged neurite length in the γ1-2-COP-GFP KI and γ2-1-COP-GFP KI results in no significant difference between the two KI cell lines. However, the quantified averaged neurite length in the chimeric KI cell lines is significantly shorter than that in P19 WT and is thus comparable to what I previously observed for γ2-COP-GFP KI cells. In consequence, these findings reveal that the potential molecular determinant(s) on γ1-COP, which are responsible for its specific activity during neurite extension, are not located in a discrete domain but are rather distributed in both trunk and appendage domains.

A

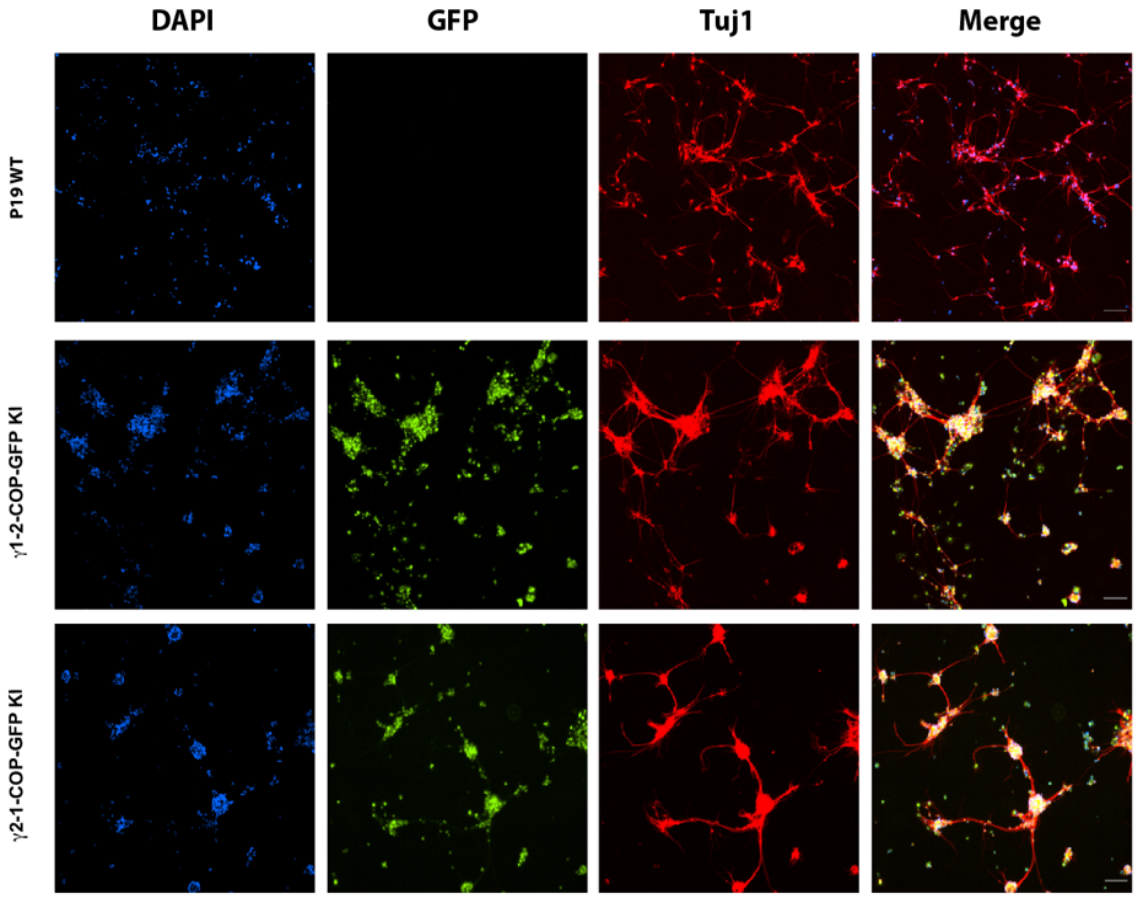

B

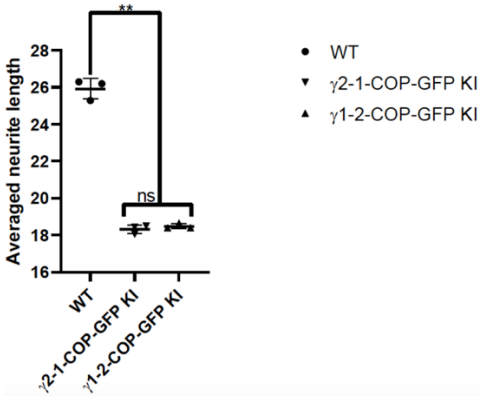

Figure 15. Partial compensation of the deletion of γ1-COP during neurite outgrowth in Chimera-COP KI cells.

(A) Fluorescent microscopy images to analyse the expression of the neuronal marker Tuj1 (red channel) and GFP (green channel) in knock-in insertions in γ1-2-COP-GFP KI and γ2-1-COP-GFP KI cells at day 8 of neuronal differentiation. The blue channel represents the nucleus stained by DAPI. Scale bar is 100 μm. (B) Quantification of the averaged neurite length (neurite length/cell number). Each dot indicates the quantity gained from 5 random images (corresponding to about 1000 cells), as in (A). ** represents P-value < 0.005, ns, nonsignificant.

2.13 γ-COP paralogs tag ultraID cells construction

To identify proximal proteins to γ-COPs during the COPI-mediated transport pathway[71,224], a novel engineered protein biotin ligase was adopted, known as ultraID. It is derived from a truncation of BioID2 and several rounds of directed evolution optimisation (unpublished manuscript in preparation), and we combined it with an optimised affinity purification process on chemically modified streptavidin beads[225] followed by mass spectrometry (MS). The workflow of the integration of ultraID with MS to identify the proximome of γ-COPs in ultraID-tag P19 cells is shown in **Figure 16**.

The stable cell lines expressing ligase (ultraID) tagged proteins under the control of a doxycycline-inducible promoter were generated using the PiggyBac transposition system and clone selection (**Figure 16**). Copg1 or Copg2 KO cells expressing respectively exogenous γ1-COP (T-Copg1-ultraID cell lines) or γ2-COP (T-Copg2-ultraID cell lines), both fused to ultraID at the C-terminal, were constructed. In addition, a control cell line was prepared by

transfecting a PiggyBac construct for the expression of Ago2 fused to ultraID at its N-terminal (T-ultraID-Ago2) (for detailed methods see the Materials and Methods section).

2.14 The workflow of the ultraID-based efficient proximity labelling approach to identify proximal proteins to γ-COPs

We next assessed the interactomes of the different γ-COPs using ultraID-tag cells lines. The workflow of the ultraID-based efficient proximity labelling approach to characterize the interactome of γ-COPs is demonstrated in **Figure 16**. Notably, the identified proteins by the ultraID-based approach should fall into three categories: direct interactions, indirect interactions and proximal proteins within approx. 10 nm[193,226]. Although proximity-dependent biotinylation allows for the identification of transient or weak contacts, it must be carefully controlled in order to filter out any random background biotinylation. Here, the protein Ago2[227] was used as a negative control to remove the background proteins identified by the ultraID approach, since it is functionally unrelated to the COPI pathway but shows at a partial localisation the ER and Golgi[228,229] (**Figure 17**).

Furthermore, it is known that on the basis of its core component coatomer, COPI vesicles contribute in initiating the intracellular transport and allow for both the sorting of cargo and deformation of the donor membrane to bud a vesicle carrier at the Golgi membrane. Once the COPI vesicles are released to the cytoplasm from the Golgi membrane, the coatomer complexes will then soon be disassembled in the cytoplasm. As ultraID is fused to γ-COPs, the labelling of proximal proteins will occur both with membrane-attached and cytosolic coatomer. To identify the γ-COPs interactome on the Golgi membrane, cells were treated with Brefeldin A (BFA) as it is a known reversible inhibitor of the guanine exchange factor GBF1, and it can thus prevent the recruitment of coatomer to the Golgi membrane. The schematic figure (**Figure 17**) presents the application of an ultraID-based approach to identify proteins specially associated with membrane-bound coatomer. As is shown in **Figure 17**, following BFA treatment, coatomer is released from the Golgi membrane to the cytoplasm. In the following experiment cells were treated with BFA (5μg/mL) for 1h prior to addition of biotin with the goal of releasing coatomer from membranes before starting labelling proximal proteins. These samples were then compared to mock-treated cells in which labelling occurs both at the membrane and in the cytosol. The biotinylation activity was found to be similar in BFA-treated and mock-treated samples (**Figure 19A**).

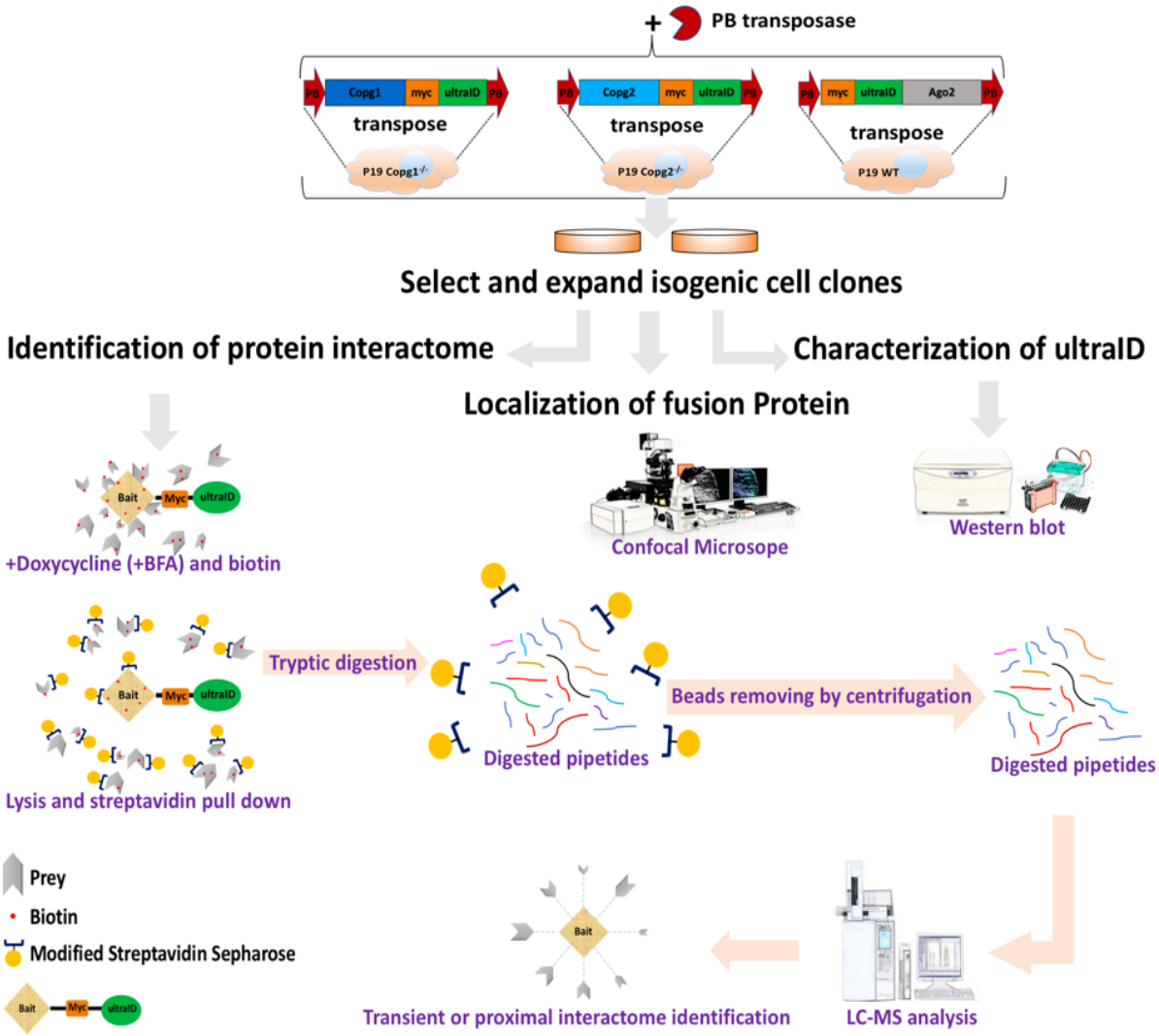

Figure 16. Workflow for the identification of transient-interacting or proximal proteins by following an ultraID-based approach.

2.15 Characterisation of ultraID in γ-COP paralogs tag ultraID undifferentiated cell lines

As described above, we generated doxycycline inducible clonal cell lines that express exogenous γ-COPs fused ultraID at C-terminal in P19 γ-COP KO (T-Copg1-ultraID#1&2 and T-Copg2-ultraID#1&2) and Ago2 tagged ultraID at N-terminal as control cell line (T-ultraID-Ago2). (see the Materials and Methods section)

The expression of specific γ-COP paralogue was detected in a doxycycline (5ng/ml) induction dependent manner by western blot analysis as showed with antibodies against γ1-COP and γ2-

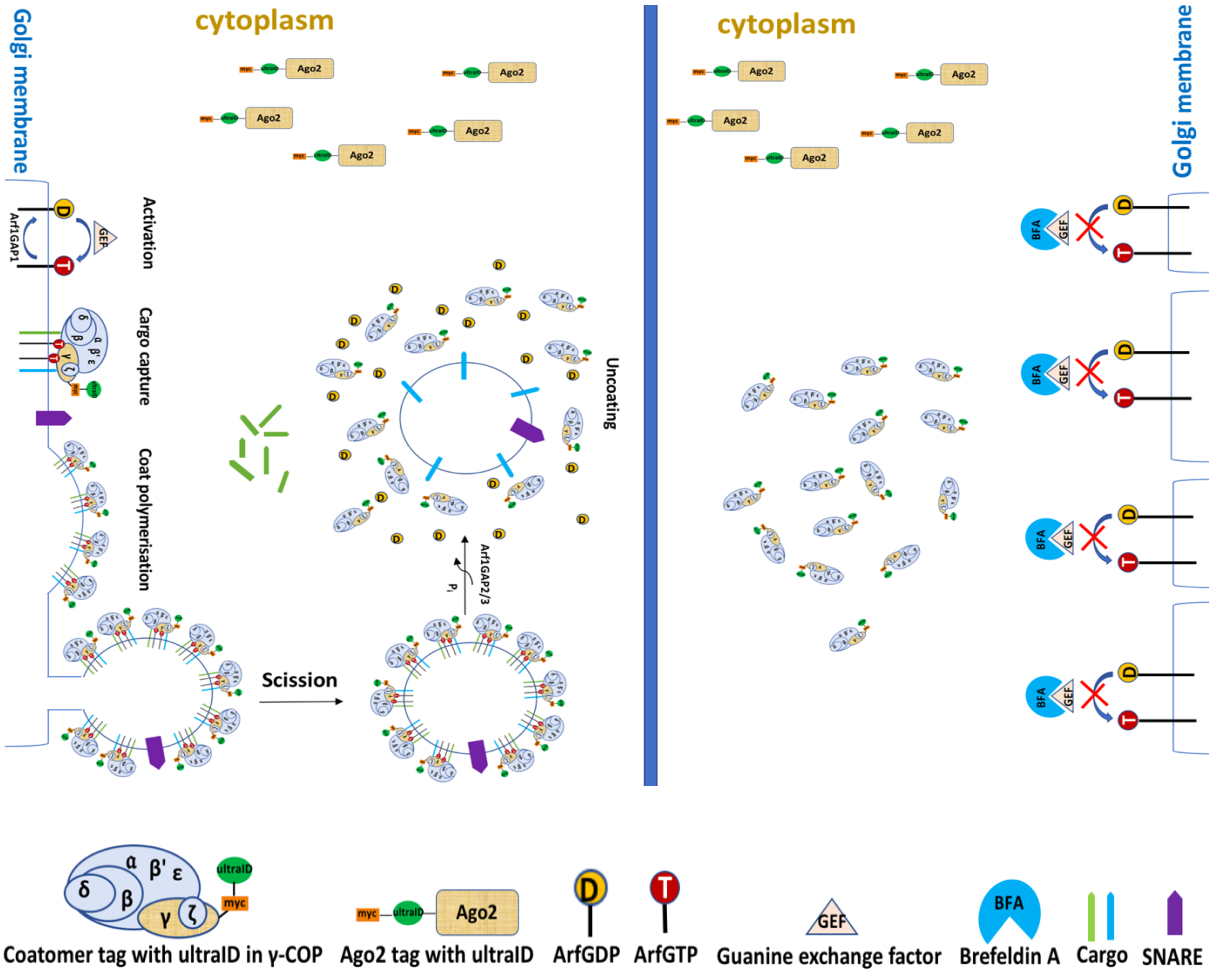

Figure 17. The ultraID-based approach to identify membrane-associated proximal proteins to coatomer.

With the help of Arf1GEF and the recruitment of Arf-GTP to the membrane for coatomer binding, the formation of COPI transport vesicles begins to become activated. Following membrane deformation with cargo and coat polymerisation, the vesicles are released to the cytoplasm. Once the Arf-GTP is hydrolysed by the ArfGTPase, coatomer is rapidly released upon Arf1-mediated GTP hydrolysis. Brefeldin A can bind with the Guanine exchange factor (GBF1) to block the exchange of ArfGDP to ArfGTP, and then, the coatomers will be released from the Golgi membrane to the cytoplasm. Ago2 is a cytoplasm residence protein.

COP as indicated in **Figure 18 A**. Moreover, the expression of γ-COP paralogues in T-Copg1-ultraID#2 and T-Copg2-ultraID#2 cell samples appeared similar to that of P19 WT cells (**Figure 18 A**). Hence, in the following experiment, T-Copg1-ultraID#2 and T-Copg2-ultraID#2 were adopted. To verify the ultraID-based efficient labelling proximity proteins, biotinylation activity was detected after a period of 4h biotin (50μM) incubation using

streptavidin conjugate 680 (**Figure 18 B**), and all the clones yielded abundant biotinylated proteins.

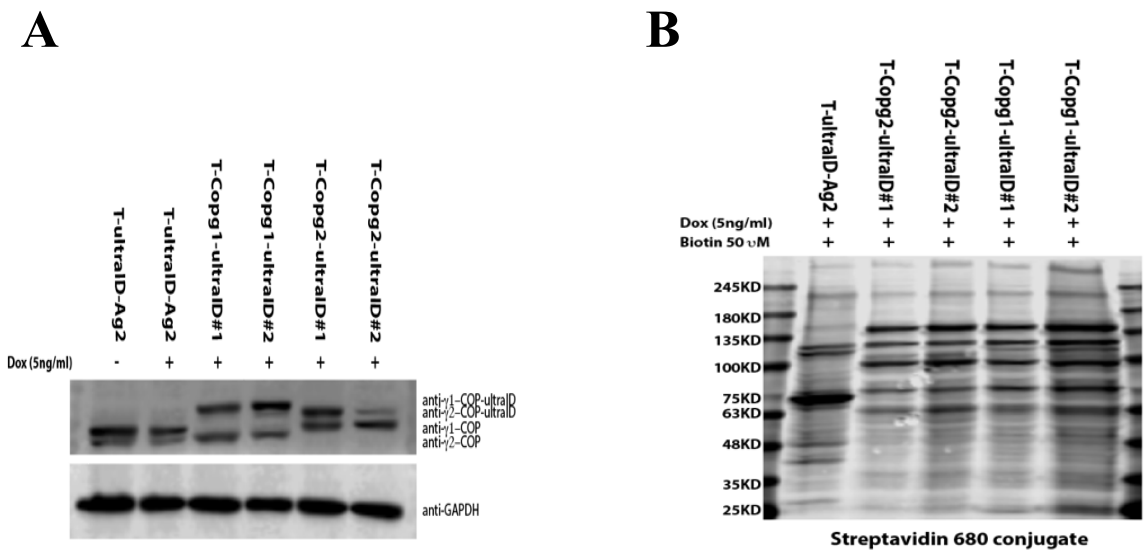

Figure 18. Characterization of clonal cell lines expressing ultraID fusion proteins. (A) The biotinylated proteins were labelled by streptavidin 680 conjugate. (B) The expression of different paralogues of COPI transport vesicle in different doxycycline induction cell clones.

2.16 Testing the pulldowns of the ultraID-based approach to confirm the successful labelling of interactome in γ-COP paralogs tag ultraID undifferentiated cell lines

The ultraID-based efficient proximity labelling procedure for affinity purification of proximal protein was adapted to isolate biotinylated proteins from cell lysates that specifically associate with the γ1-COP and γ2-COP ultraID fusion protein. As shown in **Figure 19 A and B**, the expression of fusion proteins (γ1-COP and γ2-COP) was detected by western blot, with the mix antibody of γ1-COP and γ2-COP and efficient biotinylation being detected with the streptavidin conjugate 680. As a positive control for labelling specificity, we analysed the coatomer sub-unit α-COP, which is always stably associated with the γ-COPs within the coatomer complex. As shown in **Figure 19 C**, the α-COP protein could be detected by both the anti-α-COP antibody and the labelled streptavidin in T-Copg1-ultraID#2 and T-Copg2-ultraID#2 cells, whereas labelled streptavidin did not decorate that band in the T-ultraID-Ago2 control cell line. As a negative control for labelling specificity, we analysed the GAPDH which was never described as being associated with coatomer or Ago2. As shown in

Figure 19 D, GAPDH was detected with anti-GAPDH antibodies but not labelled by streptavidin in all the cell lines. The results support the theory that the ultraID-based proximity labelling system could be a reasonable method for the exploration of the interactome in the different paralogues of γ-COP.

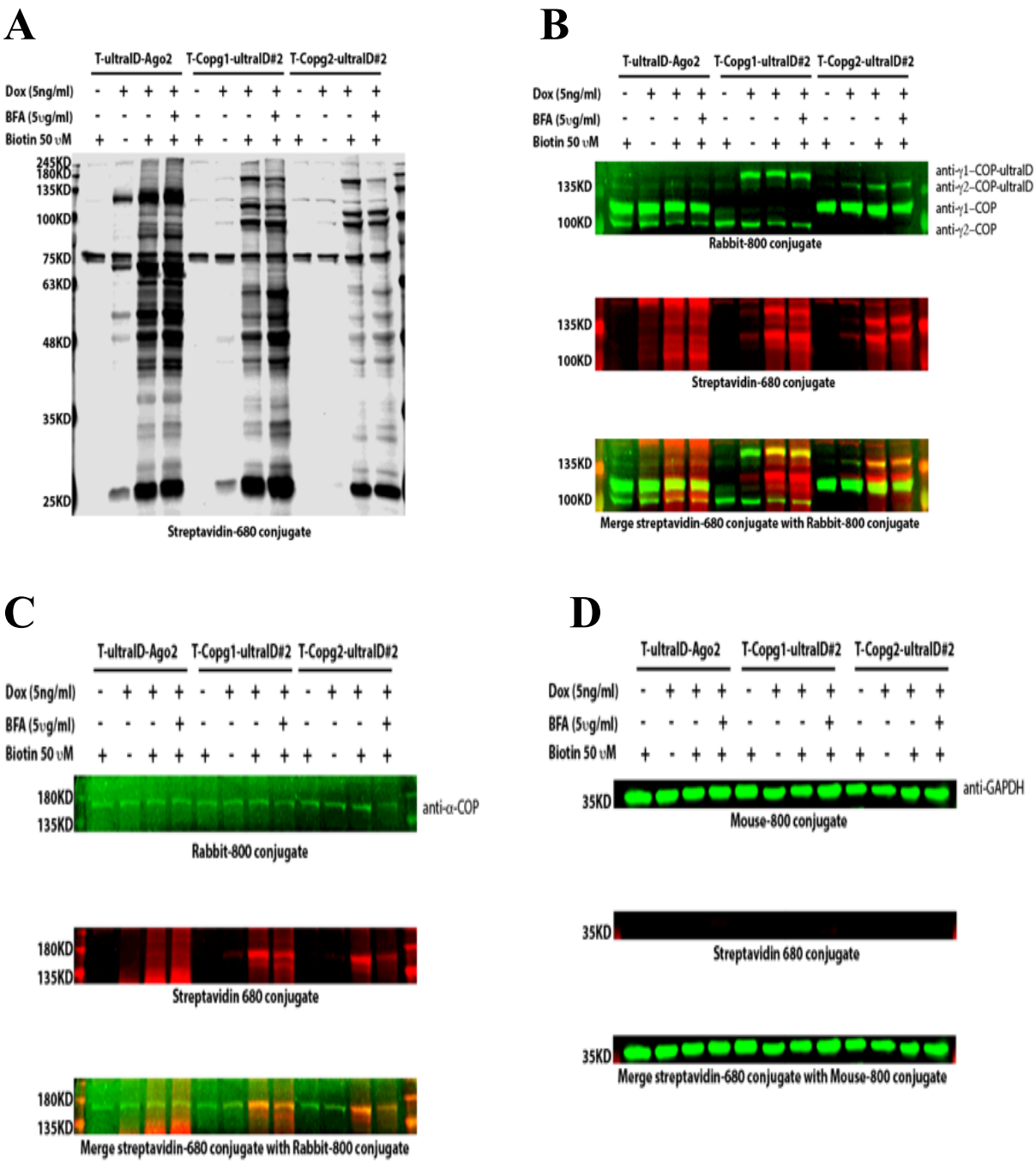

Figure 19. Characterization of ultraID base-labelling in P19 undifferentiated cell lines. (A) The biotinylation activity in all cell samples treated with Brefedin A (BFA) or without BFA. (B) In the top blot, the expression of the fusion protein was detected with an anti-γ1-COP and γ2-COP antibody (green channel). In the middle blot, the endogenous biotinylated

proteins were detected using streptavidin 680 conjugate (red channel). In the bottom blot, the signal of the bait protein merged with that of the biotinylated proteins. (C) In the top blot, the coatomer sub-unit α-COP was detected using an anti-α-COP antibody (green channel). In the middle blot, the biotinylated proteins were labelled by streptavidin 680 conjugate (red channel). In the bottom blot, the signal of α-COP merged with that of biotinylated proteins (D). In the top blot, the negative control protein GAPDH was detected with an anti-GAPDH antibody (green channel). In the middle blot, the biotinylated proteins were detected by streptavidin 680 conjugate (red channel). In the bottom blot, the signal for biotinylated proteins merged with the GAPDH detection.

2.17 The co-localization of γ-COPs with biotinylated proteins in undifferentiated cells

In order to further characterise the ultraID-fusion proteins, their localisations and that of the biotinylated proteins were analysed using confocal fluorescence imaging in a biotin or a doxycycline induction dependent manner in P19 undifferentiated cells. The fusion proteins were detected by an anti-myc antibody and an Alexa Fluor 488-conjugated goat anti-rabbit antibody, as well as by biotinylated proteins with streptavidin Alexa 647 conjugate. Nucleus DNA was stained by DAPI, and Golgi was stained with an antibody against the Golgi marker protein GM130. In T-Copg1-ultraID#2 or T-Copg2-ultraID#2 cells, γ1-COP or γ2-COP (**Figures 20 A and B**) co-localised with their labelled proteins at the Golgi membrane while the biotinylated proteins in the T-ultraID-Ago2 cell line appeared to be restricted with Ago2 to the cytosol (**Figure 20 C**).

As describe above, for the identification of the Golgi membrane-associated interactome, the cytosolic interactome of γ-COP can be determined through the assistance of the BFA-treated control samples. To validate our approach in comparing BFA-treatment to mock conditions, we next sought to analyse the localisation of the biotinylated proteins after a 1h pre-treatment with BFA and subsequent 4h incubation with biotin (still in the presence of BFA). As indicated in **Figure 20 A-C**, the Golgi apparatus was disrupted by BFA into a fragmented perinuclear structure. Additionally, it is shown in **Figures 20 A and B** that the γ-COPs and the biotinylated proteins were released to the cytoplasm following BFA treatment. By contrast, as shown in **Figure 20 C**, Ago2 and its biotinylated proteins did not seem to be affected by the BFA treatment.

A

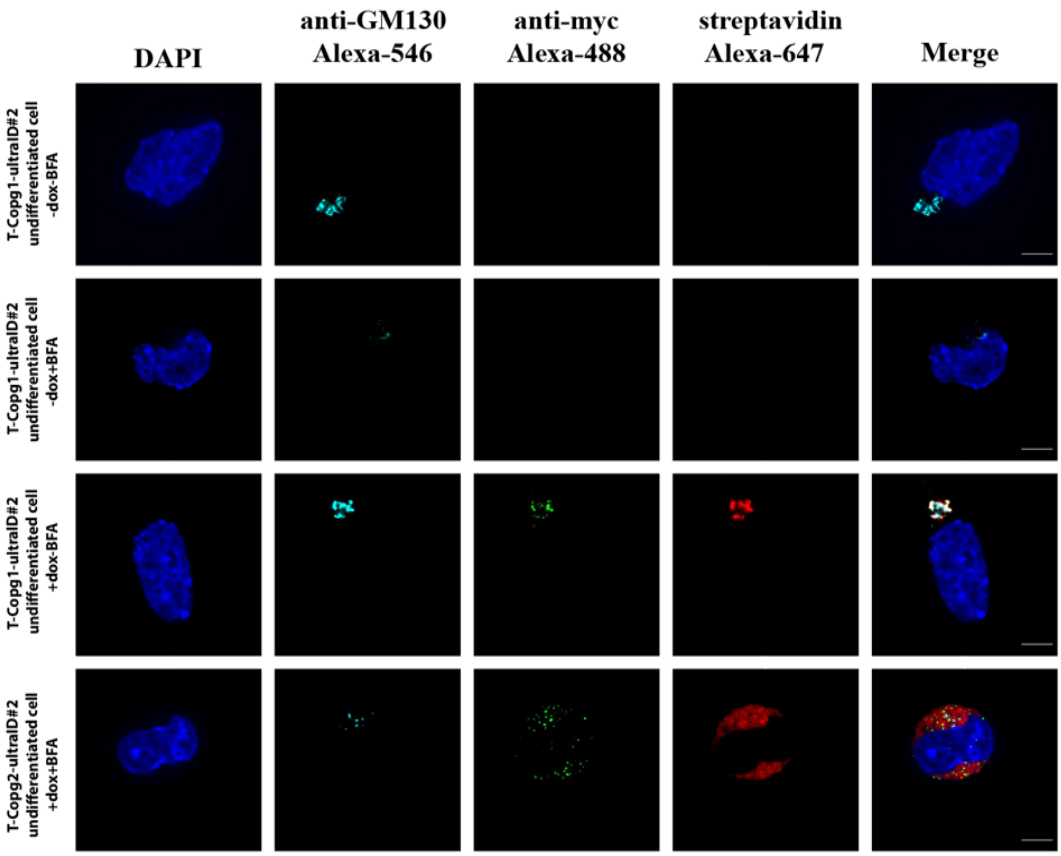
DAPI
anti-GM130 Alexa-546
anti-myc Alexa-488
streptavidin Alexa-647
Merge
T-Copg1-ultraID#2 undifferentiated cell -dox-BFA
T-Copg1-ultraID#2 undifferentiated cell -dox+BFA
T-Copg1-ultraID#2 undifferentiated cell +dox-BFA
T-Copg2-ultraID#2 undifferentiated cell +dox+BFA

B

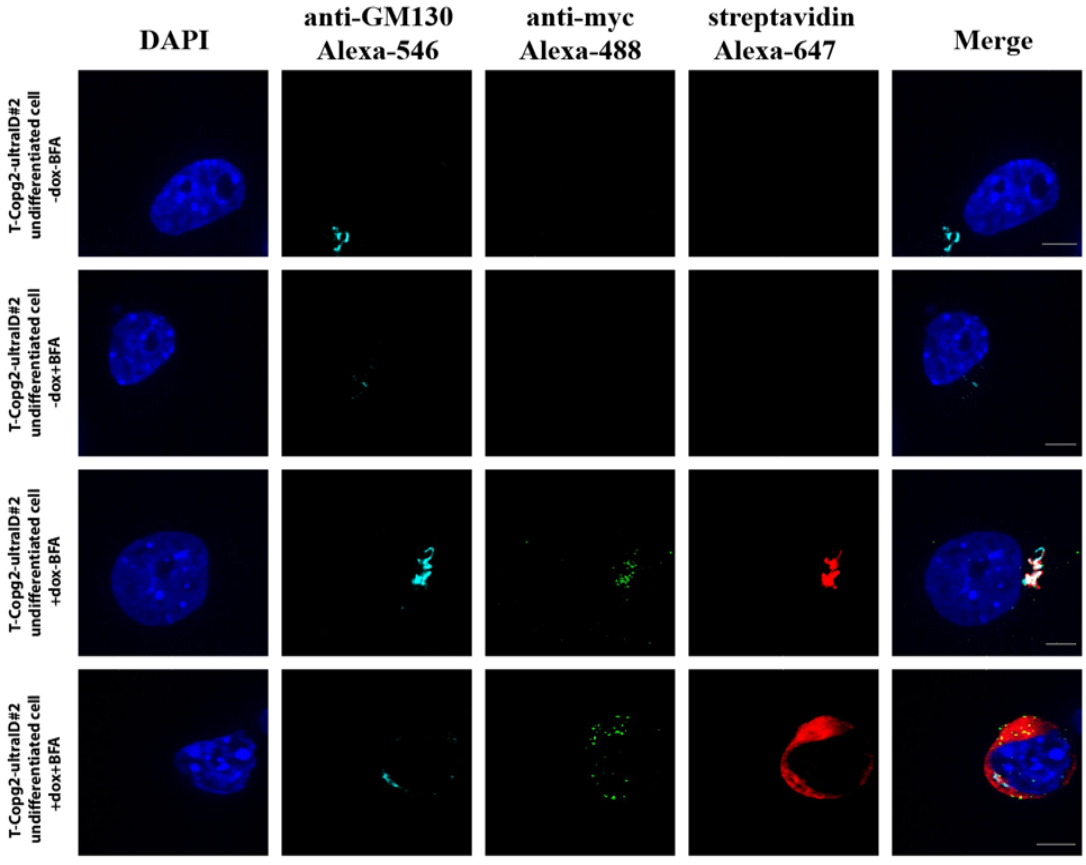
DAPI
anti-GM130 Alexa-546
anti-myc Alexa-488
streptavidin Alexa-647
Merge
T-Copg2-ultraID#2 undifferentiated cell -dox-BFA
T-Copg2-ultraID#2 undifferentiated cell -dox+BFA
T-Copg2-ultraID#2 undifferentiated cell +dox-BFA
T-Copg2-ultraID#2 undifferentiated cell +dox+BFA

C

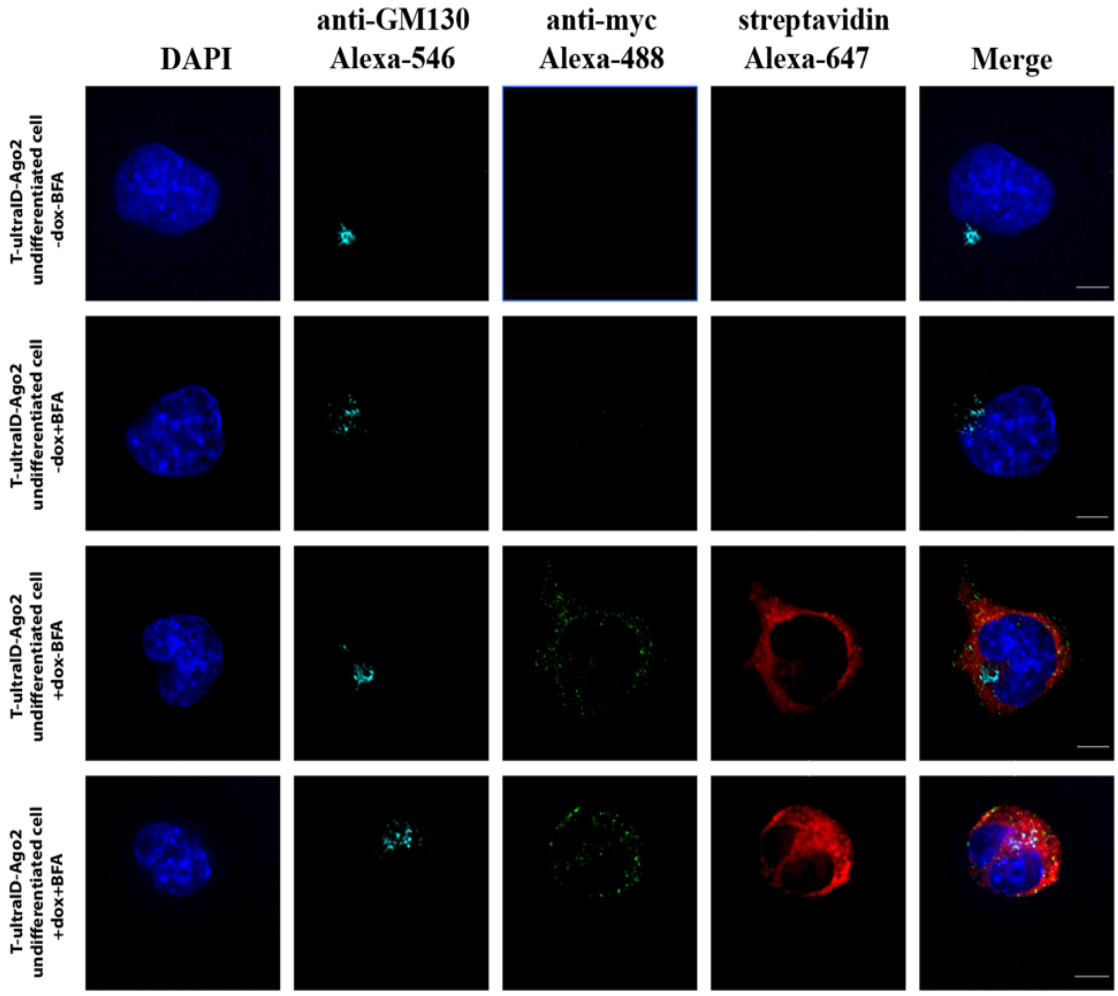

Figure 20. Co-localization of γ-COPs with biotinylated proteins in P19 undifferentiated cells.

Immunostaining with streptavidin (647nm, red channel) to detect biotinylated protein. DAPI (405nm, blue channel) is used to stain DNA. GM130 (546nm, cyan channel) is visualised to mark Golgi. Brightness intensity is in the same range for the images' cyan channel (2000-12000), green channel (1000-1600) and red channel (2000-6000). The scale bar is 5 μm. (A) Confocal visualisation of the colocalisation of the γ1-COP with an ultraID-based approach for labelling proteins plus or minus BFA. γ1-COP is observed in the anti-myc channel (488nm, green channel). (B) Confocal visualisation of the colocalisation of the γ2-COP with an ultraID-based approach for labelling proteins plus or minus BFA. γ2-COP is observed in the anti-myc channel (488nm, green channel). (C) Confocal visualisation of the colocalisation of the Ago2 with an ultraID-based approach for labelling proteins plus or minus BFA. Ago2 is observed in the anti-myc channel (488nm, green channel).

2.18 Identifying the interactome of either γ1-COP or γ2-COP in P19 undifferentiated cells

In order to further uncover the role that γ1-COP plays in neurites outgrowth, a classic neuronal differentiation was performed on the T-Copg1-ultraID#2, T-Copg2-ultraID#2 and T-ultraID-Ago2 P19 cell lines according to the protocol outlined in the method. From the workflow shown in **Figure 16**, the ultraID-based approach enables proteomic mapping. This involves streptavidin affinity pull-downs followed by tryptic digestion of the biotinylated proteins and later identification of the digested peptides by liquid chromatography-mass spectrometry (LC-MS/MS), as described in material and in the method. The raw data of the ultraID experiment was processed in Maxquant for protein identification and assignment of an LFQ value for label-free quantification. For the determination of enriched proteins in one sample compared to another, the data was first processed with the proDA[208] package using a Probabilistic Dropout Analysis. This assigns a mean LFQ value for each identified protein and a calculated variance taking into account the missing values and relative intensities in each replicate. This approach is much more powerful than imputing random values in place of missing values in the datasets. As described in the results, a pCutoff for p value was set to 0.01 and an FCcutoff for fold change to ±2 as presented in the figures and tables below. As previously stated, ultraID-Ago2 was used as a control bait protein in order to acquire proximity proteins of γ1-COP or γ2-COP. The volcano plots revealed the statistically significant enrichment of affinity proteins by either γ1-COP-ultraID or γ2-COP-ultraID over ultraID-Ago2 respectively (**Figure 21 A and B**) in P19 undifferentiated cells. The data is listed in **Table 1 and Table 2**.

As previously described, the intensities of iBAQ data and the determination of specific peptides are used to approximately evaluate the expression of the proteins within each sample. When considering the iBaq values, we observed that some proteins were missed by the LFQ analysis but were detected in all three replicates of either γ1-COP or γ2-COP while not at all in any replicate of the other sample. Hence, we added those "iBaq hits" to the datasets that fulfilled the following criteria: detection in all three replicates of one condition with at least two peptides in each replicate, and no peptide detected in any replicate of the other condition. The protein-coding genes of all the iBaq hits are highlighted in red in **Table 1 and Table 2**.

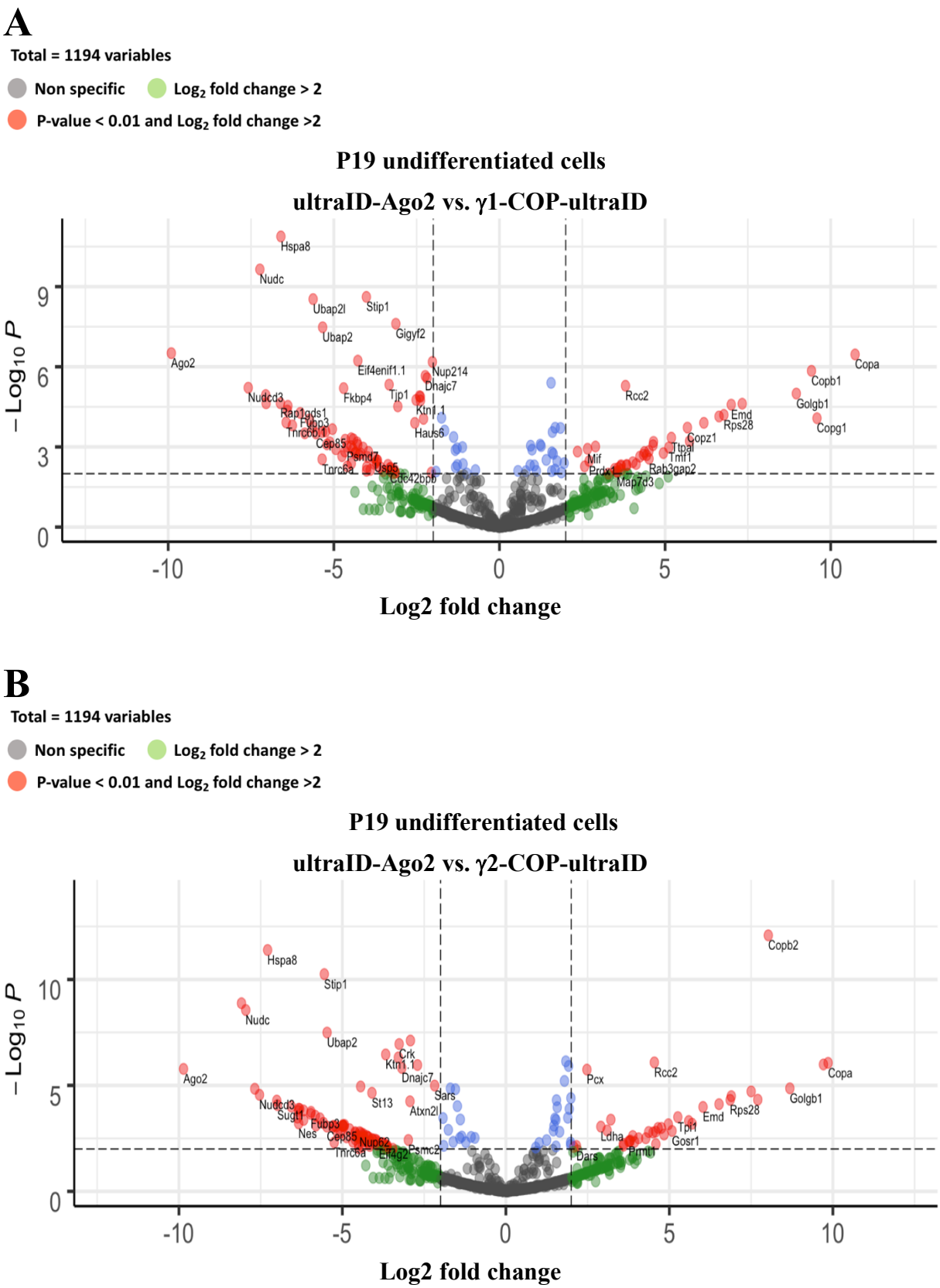

Figure 21. Volcano plots showing the differential abundance of isolated biotinylated proteins in P19 undifferentiated cells.

The differential protein abundance was calculated after LC-MS/MS analysis of ultraID samples in three biological replicates for each cell line. The thresholds for significance (P-value < 0.01 and |log2 fold change|>2) are indicated by the dashed lines. Graph (A) shows a statistically significant enrichment of biotinylated proteins by γ1-COP-ultraID over biotinylated proteins by ultraID-Ago2 in P19 undifferentiated cells. Spots on the top-right quadrant illustrate significantly enriched proteins of the γ1-COP samples, whilst significantly enriched proteins of Ago2 samples in P19 undifferentiated cells is shown on the top-left. Detailed information is listed in **Table 1**. Graph (B) shows statistically significant enrichment of biotinylated proteins by γ2-COP-ultraID over biotinylated proteins by ultraID-Ago2 in P19 undifferentiated cells. Spots on the top-right quadrant illustrate proximal proteins to γ2-COP, while proximal proteins to Ago2 are on the top-left. Detailed information is listed in **Table 2**.

Table 1. Significantly enriched genes in γ1-COP-ultraID over ultraID-Ago2 in P19 undifferentiated cells with P-value<0.01. iBaq hits were indicated with red colour.

Copb2	Ubap2l	Copa	Dnajc7	Rcc2	Gigyf1	Fxr2	Emd
Hspa8	Gigyf2	Eif4enif1.1	Crk	Nudcd3	Ankrd17	Rap1gds1	Fam21
Nudc	Ubap2	Nup214	Pcca	Fkbp4	Hsph1	Sugt1	St13
Stip1	Ago2	Copb1	Tjp1	Golgb1	Ktn1.1	Arcn1	Prrc2a
Fubp3	Copg1	Arfgap2	Copz1	Aars	Fkbp5	Ankrd49	Arf3
Rps28	Atxn2l	Haus6	Pgk1	Nufip2	Cep85	Samd4b	Cdc37
Gcc1	Cops5	Cacybp	Vdac3	Vdac2	Pcbp2	Eftud2	Hdlbp
Ppid	Tnrc6b.1	Nudcd2	Ppp6r3	Tnrc6c.1	Ttpal	Scyl1	Pcm1
Mccc1	Pcx	Eif3f	Mif	Strap	Ppp5c	Fmr1	Scyl3
Ttc1	Smyd5	Tmf1	Rpap3	Txn	Arfgap1	Gosr1	Nes
Tpi1	Psmd7	Psme3	Sec16a	Vcpip1	Dcun1d4	Fam193a	Stx5a
EG433182	Dars	Sars	Eef1a1	Tmem263	Ttc4	Arfip1	Pum1
Vps51	Tnrc6a	Prdx1	mCG_6739	Nasp	Paics	Glod4	Ddb1
Pgls	Atp5a1	Vdac1	Prrc2b.1	Ophn1	Prmt1	Txnl1	Hook1
Usp5	Fubp1	Rpl12	Bicd2	Uba1	Eef2	Ubap2l.1	Pex5
Rab3gap2	Uri1.1	Ankhd1	Ppp2r2a	G3bp1	Rpl10	Pgam1	Cct3
Cdc42bpb	Gbf1	Flna	Srp54	Trim71	Tgs1	Trip11	Scfd1
Wnk1	Eif5a	Pkm	Rbbp4	Gnb2l1	Nap1l1	Golga4	Impa1
Atp6v1f	Tuba1a	Fus	Fxr1	Prrc2c	Eif2s3x	Golga5	Copz2
Upf1	Eef1d	N4bp2	Map7d3	Usp47	Gcc2	Atp7a	Peg10
Wwox	Gorab	Tmem165	Tomm40	Lman1	Ebag9	Ruvbl1	

Table 2. Significantly enriched genes in γ2-COP-ultraID over ultraID-Ago2 in P19 undifferentiated cells with P-value<0.01. iBaq hits were indicated with red colour.

Copb2	Ktn1.1	Dnajc7	Gigyf2	Rps28	Emd	Fubp3	Pcbp2
Hspa8	Hsph1	Ago2	Cttn	Tubb5	Mccc1	Tjp1	Mif
Stip1	Pcca	Pcx	Arcn1	Gigyf1	Fam21	Tpi1	Pgk1
Ubap2l	Rcc2	Eef1a1	St13	Atxn2l	Pkm	Tnrc6b.1	Cacybp
Nudc	Copa	Sars	Nudcd3	Arfgap2	Eif4enif1.1	Atp5a1	Ppp2r2a
Ubap2	Copb1	Fkbp4	Copz1	Sugt1	Map1b	Yap1	Nudcd2
Rtn4	Ppid	Golgb1	Vdac2	Eif3f	Prrc2a	Cops5	Nes
Crk	EG433182	Strn4	Copg2	Rap1gds1	Fxr2	Eef2	Scyl1
Txn	Slk	Ddx3x	Nup62	Pebp1	G3bp1	Scyl3	Igbp1
Nup214	Tnrc6c.1	Acaca	Tomm40	Cfdp1	Smyd5	Rpap3	Cct3
Nap1l1	Nufip2	Ahnak	Cdc37	Hdlbp	Sec16a	Eps15l1	Ttc4
Ankrd17	Cep85	Gosr1	Ankrd49	Arf3	Ttc1	Psme3	Fmr1
Fkbp5	Ldha	Gcc1	Eftud2	Aars	Prrc2c	Vcpip1	Prmt1
Ppa1	Rpl12	Ran	Pcm1	Crkl	Rbbp7	Nasp	Eif2s3x
Fxr1	Dstn	Arfgap1	Samd4b	Psmd7	Cstf2t	Psmc2	Pum1
Ppp6r3	Larp1	Nap1l4	Sdhb	Nmt2	Rpl10	Vdac3	Haus6
Stx5a	Psmc5	Glod4	Hn1l	Tnrc6a	Zwint	Hpcal1	Fubp1
Fam193a	Plin3	Mllt4.1	mCG_6739	Tmem263	Eif4g2	Usp5	Aspscr1
Strap	Dst	Dnaja1	Hnrnpf	Paics	Pgls	Rpl4	Ubap2l.1
Ppp5c	Csrp1	Dars	Uri1.1	Pdlim1	Gnb2l1	Prrc2b.1	Ankhd1
Scyl2	Golga4	Gcc2	Hspb1	Emg1	Dpysl2	Cul2	Rab3gap2
Tmf1	Scfd1	Wwox	Nudcd1	Rpn1			

2.19 Different membrane-associated interactome between γ1-COP and γ2-COP in undifferentiated P19 cells

COPI transport vesicles are formed on the Golgi membrane by the recruitment of a coatomer complex containing γ-COP. As described above, BFA inhibits the activation of Arf1 on the Golgi membrane, thus preventing the recruitment of a coatomer[230,231](**Figure 17**). Thus, to specifically analyse the transient interactome of γ-COPs on the Golgi membrane, the differential abundance of proteins isolated from γ-COPs-ultraID compared to their BFA-treated samples was analysed and depicted on volcano plots. The pCutoff for p value was set to 0.01 and FCcutoff for fold change set to ±2 (**Figure 22 A and B**).

To further enhance the information of regulators or cargos of different COPI paralogous proteins on the Golgi membrane, the Venn diagram in **Figure 22 C** (**Tables 3-5**) overlapped the associating proteomic data of γ1-COP (**Table 3 and Table 5**) and of γ2-COP on Golgi membrane (**Table 4 and Table 5**). Unsurprisingly, as it is known that Arfs and their ArfGAPs are respectively accountable for coatomer recruitment to, and release from membranes[11],

these proteins were identified as membrane-associated contacts of γ1- and γ2-COP. Similarly, Golgins[232] a family of predominantly coiled-coil proteins distributed over the Golgi apparatus and that act as tethers for transport vesicles were identified as membrane interactors of γ1- and/or γ2-COP. Golgins known to interact with COPI vesicles such as Giantin (Golgb1)[233] , TMF (Tmf1)[151] were found in both datasets, as expected in reference to studies[234], while golgin-84 (Golga5)[235] was observed more enriched in the γ1-COP datasets. In the light of the role of COPI vesicles in retrograde intra-Golgi trafficking, these golgins are located at the Golgi rims[236]. Strikingly, some trans-Golgi network (TGN) localized golgins were identified in both datasets as membrane-associated interactors of coatomer including GRIP and coiled-coil domain-containing protein 1/2 (Gcc1/2) and Golgin subfamily A member 4 (Golga4)[235]. Moreover, the SNAREs known to regulate COPI transport were observed in the data including Golgi SNAP receptor complex member 1 (Gosr1) and Syntaxin-5 (stx5)[237,238]. All but one protein from the MS dataset of membrane-associated proteins are Golgi resident proteins. This protein is Emerin (Emd) and is normally considered as a membrane-anchored protein of the inner nuclear membrane (INM). However, a partial Golgi localisation was also described[239]. We also identified Scyl1, Scyl3 and GORAB in the membrane-associated interactome of coatomer. GORAB in association with Scyl1 form stable domains at the Golgi membrane to recruit coatomers[240], and Scyl3 was observed to interact with coatomer[241]. It is noteworthy that Scyl1 was detected in both γ1-COP and γ2-COP datasets at the membrane. This is in contradiction with previous observation that Scyl1 specifically interacts with γ2-COP[242] while interaction of Scyl3 is with both paralogues[241]. The possibility that might explain the discrepancy is the different cell lines used in the different studies. Additional proteins specifically proximal to membrane-associated γ1-COP were WWOX a protein that localizes to the Golgi with currently unknown function[243-246], TMEM165, a Golgi-localized transporter for Manganese ions, which are an important co-factor of glycosylation enzymes, ATP7A, a copper transporter that resides at the TGN[247], and ERGIC-53 (Lman1). Strikingly, the Protein ERGIC-53 and golgin-84 were exclusively found in the membrane-bound interactome of γ1-COP. This indicates that the γ1-COP rather than γ2-COP is involved in the early secretory pathway at the cis-Golgi, since the ERGIC53 and golgin-84 are thought to be a localized at ERGIC/cis-Golgi interface[248-250]. Altogether, the ultraID approach allowed us to determine a membrane-associated interactome of coatomer that reflects its expected proximal landscape.

A

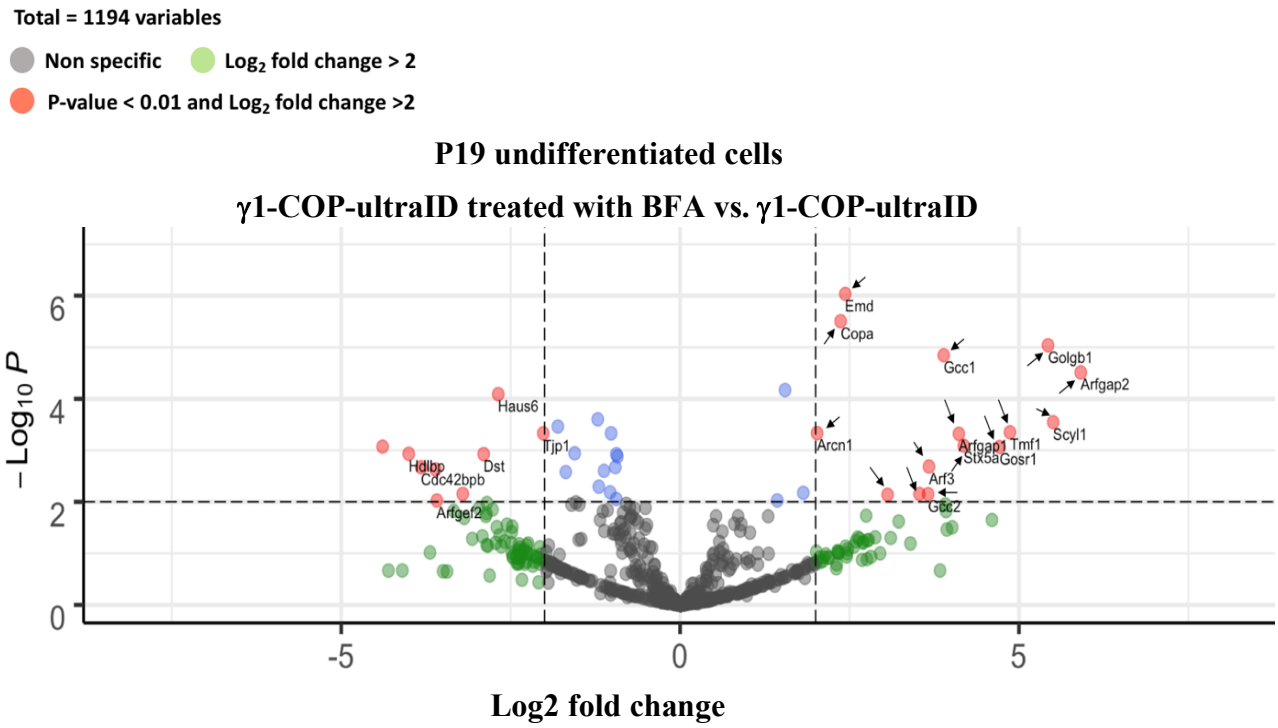
Total = 1194 variables
Non specific
Log2 fold change > 2
P-value < 0.01 and Log2 fold change >2
P19 undifferentiated cells
γ1-COP-ultraID treated with BFA vs. γ1-COP-ultraID
– Log10 P
Log2 fold change
Emd
Copa
Gcc1
Golgb1
Arfgap2
Haus6
Tjp1
Arcn1
Scyl1
Arfgap1
Tmf1
Stx5a
Gosr1
Arf3
Gcc2
Hdlbp
Dst
Cdc42bpb
Arfgef2

B

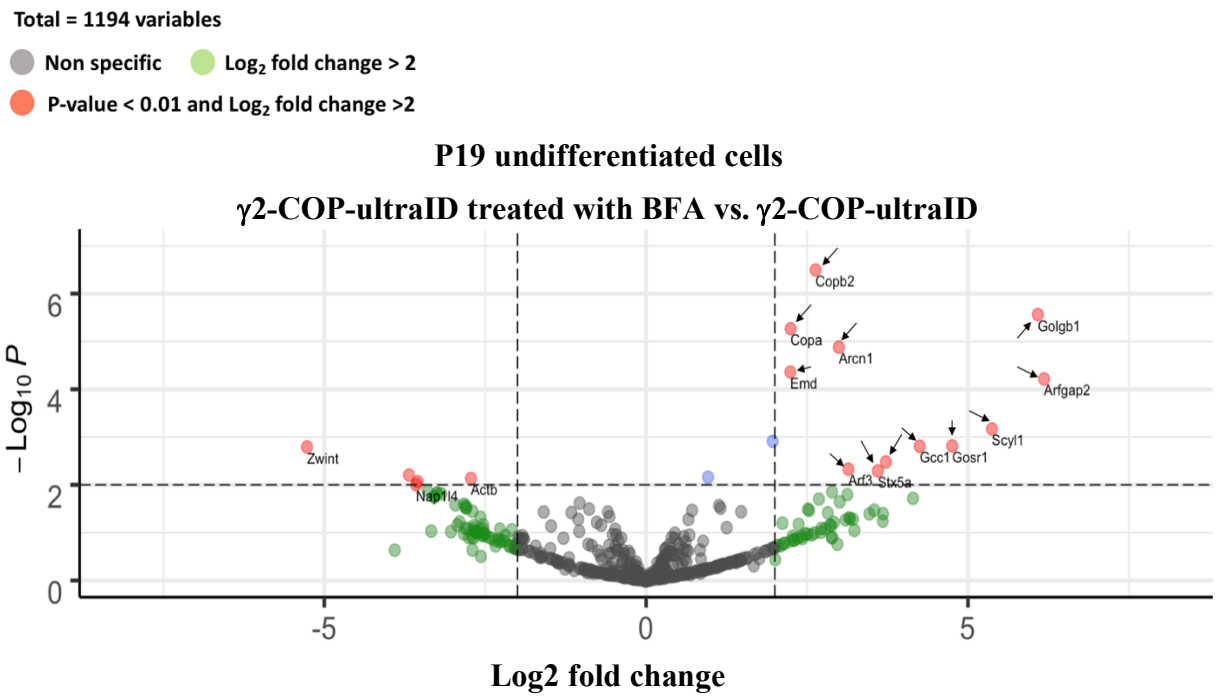
Total = 1194 variables
Non specific
Log2 fold change > 2
P-value < 0.01 and Log2 fold change >2
P19 undifferentiated cells
γ2-COP-ultraID treated with BFA vs. γ2-COP-ultraID
– Log10 P
Log2 fold change
Copb2
Copa
Arcn1
Emd
Golgb1
Arfgap2
Scyl1
Gcc1
Gosr1
Arf3
Stx5a
Zwint
Nap1l4
Actb

C

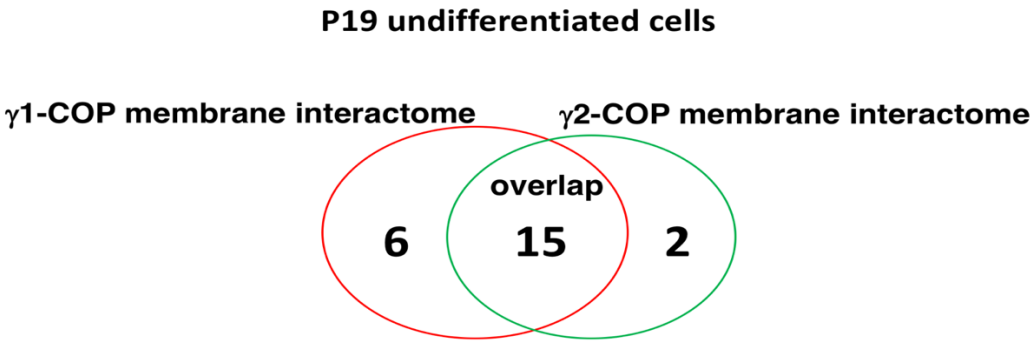

Figure 22. Volcano plots and venn diagram depicting Golgi membrane-associated γ-COP interactome in P19 undifferentiated cells.

The differential protein abundance was calculated after LC-MS/MS analysis of ultraID samples in three biological replicates for each cell line. Significance thresholds (dashed lines) were set to P-value < 0.01 and |log2 fold change|>2. Graph (A) shows enrichment of biotinylated proteins in the γ1-COP-ultraID sample over the BFA-treated γ1-COP-ultraID sample. Proteins that had been analyzed as significant over the Ago2 negative control datasets are indicated in arrows. Graph (B) Same as Graph (A) for the γ2-COP-ultraID samples. Graph (C) is a Venn diagram of the identified membrane-associated proximal proteins to γ1-COP and/or γ2-COP. Only those proteins that had been analyzed as significant over the Ago2 negative control datasets, as well as the iBaq hits were considered. Six membrane-associated proteins of γ1-COP, two membrane-associated protein of γ2-COP and fifteen membrane-associated proteins of both γ-COPs were detected in P19 undifferentiated cells dataset. Detailed information is listed in **Tables 3-5.**

Table 3. Venn figure indicating γ1-COP membrane-associated interactome in P19 undifferentiated cells with P-value<0.01. iBaq hits are indicated with red colour.

Gene name	Protein name	GO molecular Function	localization
Golga5	Golgin subfamily A member 5	Golgi vesicle transport	Golgi apparatus
		Golgi organization	
Atp7a	Golgi apparatus	copper ion transport	Golgi apparatus
		central nervous system neuron development	
		chaperone binding	
		dendrite morphogenesis	
Gorab	RAB6-interacting golgin	positive regulation of smoothened signaling pathway involved in dorsal/ventral neural tube patterning	Golgi apparatus
Tmem165	Transmembrane protein 165	Golgi calcium ion transport	Golgi apparatus
		protein N-linked glycosylation	
		cellular calcium ion homeostasis	
Wwox	WW domain-containing oxidoreductase	skeletal system morphogenesis	Golgi apparatus
		oxidoreductase activity	
Lman1	Protein ERGIC-53	endoplasmic reticulum to Golgi vesicle-mediated transport	cis-Golgi network

Table 4. Venn figure indicating γ2-COP membrane-associated interactome in P19 undifferentiated cells with P-value<0.01.

Gene name	Protein name	GO molecular Function	localization
Scyl3	Protein-associating with the carboxyl-terminal domain of ezrin	cellular protein localization	Golgi apparatus
Copb2	Coatomer subunit beta'	vesicle-mediated transport	Golgi apparatus

Table 5. Venn figure indicating overlapped membrane-associated interactome between γ1-COP and γ2-COP pool in P19 undifferentiated cells with P-value<0.01.

Gene name	Protein name	GO molecular Function	localization
Golga4	Golgin subfamily A member 4	GTPase binding	Golgi apparatus
		positive regulation of axon extension	
		Golgi to plasma membrane protein transport	
Golgb1	Golgin subfamily B member 1	Golgi organization	Golgi apparatus
		Golgi vesicle transport	
Stx5a	Syntaxin-5	SNAP receptor activity	Golgi apparatus
		SNARE binding	
		vesicle fusion with Golgi apparatus	
Arfs	ADP-ribosylation factor	GTP binding	Golgi apparatus
Arcn1	vesicle-mediated transport	coatomer subuunits	Golgi apparatus
Copa	vesicle-mediated transport	coatomer subuunits	Golgi apparatus
Arfgap1	ADP-ribosylation factor GTPase-activating protein 1	GTPase activator activity	Golgi apparatus
Arfgap2	ADP-ribosylation factor GTPase-activating protein 2	GTPase activator activity	Golgi apparatus
Gosr1	Golgi SNAP receptor complex member 1	SNAP receptor activity	Golgi apparatus
		endoplasmic reticulum to Golgi vesicle-mediated transport	
		regulation of vesicle targeting	
Gcc1	GRIP and coiled-coil domain-containing protein 1	small GTPase binding	Golgi apparatus
Gcc2	GRIP and coiled-coil domain-containing protein 2	retrograde transport	Golgi apparatus
		late endosome to Golgi transport	
Scyl1	N-terminal kinase-like protein	retrograde vesicle-mediated transport	Golgi apparatus
		neuron development	
Scfd1	Sec1 family domain-containing protein 1	vesicle-mediated transport	Golgi apparatus
Emd	Emerin	actin binding	Membrane
Tmf1	TATA element modulatory factor	androgen receptor binding	Golgi apparatus
		DNA binding	
		nuclear receptor transcription coactivator activity	

2.20 Identification of the different interactome between γ1-COP and γ2-COP in P19 undifferentiated cells

Next, we directly looked at proteomic differences between the two γ-COP paralogues in P19 undifferentiated cells. The following volcano plots compare protein abundances in the γ1-COP-ultraID vs. the γ2-COP-ultraID samples. As significance threshold pCutoff for the p value was set to 0.01 and FCcutoff for fold change to ±2 in undifferentiated cells (**Figure 23**

A). In addition, to remove biotinylation background, only those proteins that were both enriched over the Ago2 control dataset and the other γ-COP paralogue were considered. After removing the biotinylation background from the Ago2 dataset, the statistically significant enrichment of biotinylated proteins from γ1-COP-ultraID was indicated in Area I in **Figure 23 B and Table 6.** Additionally, the statistically significant enrichment of biotinylated proteins from γ2-COP-ultraID is indicated in Area II in **Figure 23 B and Table 7**.

In the light of the proteomics datasets from the undifferentiated cells (**Figure 23 A and B, Tables 6 and 7**), when comparing the interactomes of γ1-COP and γ2-COP, I only observed a few differences. There were ten enriched proteins in the γ1-COP dataset and five enriched proteins in the γ2-COP dataset. Interestingly, several proteins with a known function related to neurogenesis were detected as specific proximal proteins of γ1-COP, which includes vps51[251] (a subunit of Golgi-associated retrograde protein (GARP) complex), ATP7A (Golgi-localized Cu-transporting ATPases) and OPHN1. OPHN1 is a RhoGAP family member colocalized with and capable of inhibiting Rac1 and Cdc42.[252-254] One striking observation is the seemingly exclusive association of ζ2-COP with γ1-COP. This echoes previous quantifications in different cell lines, that either found no, or at most, 5% γ2/ζ2-COP containing coatomer within the whole cellular coatomer population[75,139]. This may imply that ζ2-COP plays a significant role during the neuronal differentiation of P19 cells.

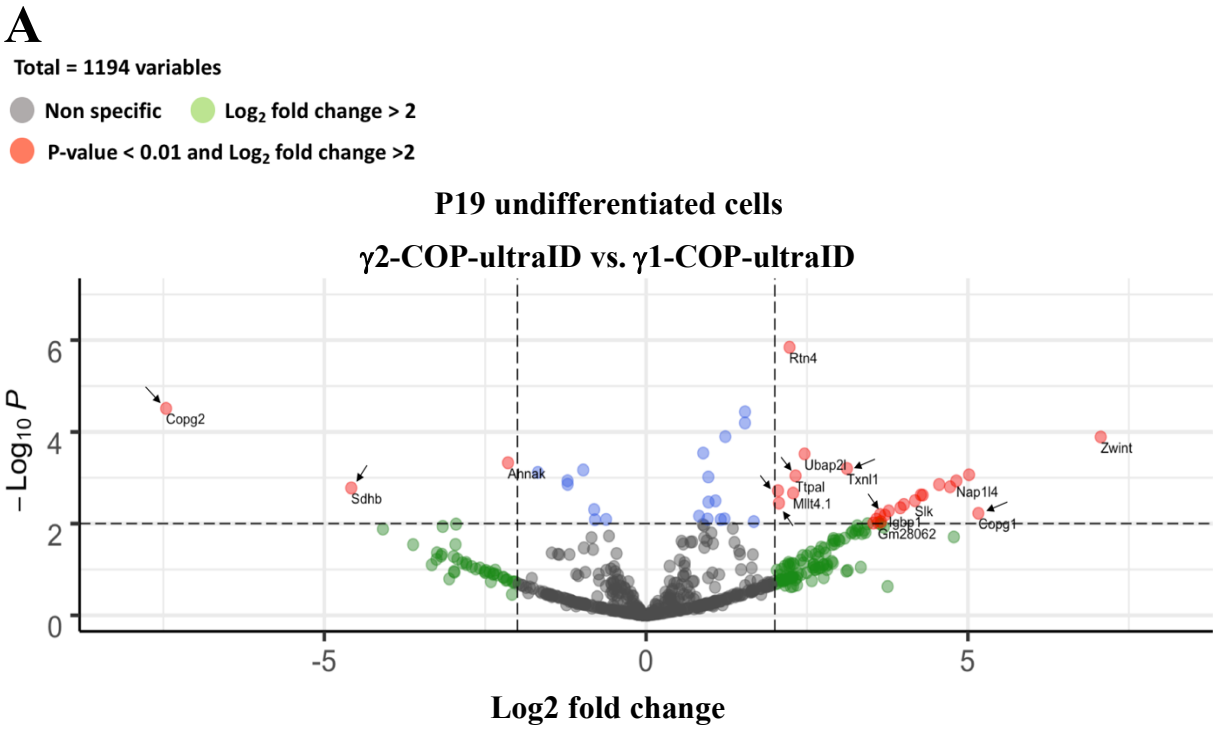

B

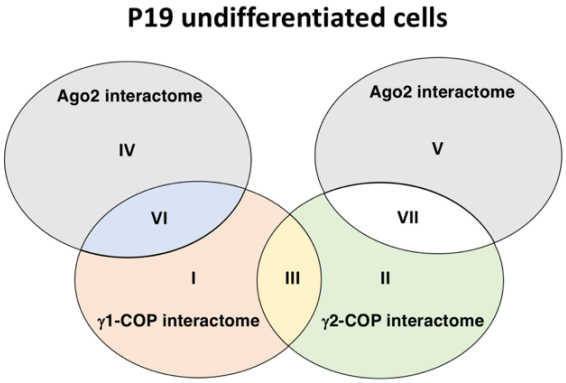

Figure 23. Volcano plots and venn diagram depicting differential interactomes between γ1-COP and γ2-COP in P19 undifferentiated cells.

(A) Volcano plot showing the differential abundance of proteins detected in the γ1-COP-ultraID and γ2-COP-ultraID datasets. Significance thresholds (dashed lines) were set to P-value < 0.01 and |log2 fold change|>2. Dots on the top-right quadrant illustrate significantly enriched hits for γ1-COP while enriched hits for γ2-COP are on the top-left. Proteins that had been analyzed as significant over the Ago2 negative control datasets are indicated in arrows. (B) Venn figure displaying different categories of identified proteins. Only those proteins that had been analyzed as significant over the Ago2 negative control datasets, as well as the iBaq hits were considered. Area I contains the proteins significantly enriched in the γ1-COP samples compared to the γ2-COP and Ago2 samples **(Table 6).** Area II contains the proteins significantly enriched in the γ2-COP compared samples compared to the γ1-COP and Ago2 samples **(Table 7).** Area III contains the overlapped interactome of γ1-COP and γ2-COP. Area IV contains the proteins significantly enriched in the Ago2 samples compared to the γ1-COP samples. Area V contains the proteins significantly enriched in the Ago2 samples compared to the γ2-COP samples. Area VI displaying the overlapped interactome of γ1-COP and Ago2. Area VII displaying the overlapped interactome of γ2-COP and Ago2.

Table 6. The significantly enriched proteins in γ1-COP-ultraID samples in P19 undifferentiated cells (Part I in the Venn figure) with P-value < 0.01. iBaq hits were indicated with red colour.

Gene name	Protein name	GO molecular Function
Copg1	Coatomer subunit gamma-1	vesicle-mediated transport
Txnl1	Thioredoxin-like protein 1	disulfide oxidoreductase activity
Ttpal	Alpha-tocopherol transfer protein-like	phosphatidylinositol bisphosphate binding
Ophn1	Oligophrenin-1	neuron differentiation
		regulation of synaptic transmission
Vps51	Vacuolar protein sorting-associated protein 51 homolog	Golgi vesicle transport
		brain morphogenesis
Gcc1	GRIP and coiled-coil domain-containing protein 1	small GTPase binding
Peg10	Retrotransposon-derived protein PEG10	cell differentiation
Atp7a	Golgi apparatus	copper ion transport
		central nervous system neuron development
		chaperone binding
		dendrite morphogenesis
Gorab	RAB6-interacting golgin	positive regulation of smoothened signaling pathway involved in dorsal/ventral neural tube patterning
Copz2	Coatomer subunit zeta-2	vesicle-mediated transport

Table 7. The significantly enriched proteins in γ2-COP-ultraID samples in P19 undifferentiated cells (Part II in the Venn figure) with P-value < 0.01. iBaq hits were indicated with red colour.

Gene name	Protein name	GO molecular Function
Copg2	Coatomer subunit gamma-2	vesicle-mediated transport
Sdhb	Succinate dehydrogenase [ubiquinone] iron-sulfur subunit	transferring electrons from succinate to ubiquinone
		tricarboxylic acid cycle
Hspb1	Heat shock protein beta-1	chaperone-mediated protein folding
Rpn1	26S proteasome non-ATPase regulatory subunit 2	proteasome-mediated ubiquitin-dependent protein catabolic process
Nudcd1	NudC domain-containing protein 1	proliferation and metastasis

2.21 Characterization of ultraID-based labeling in P19 differentiated neurons

Next, we applied the ultraID-based labeling approach in P19 differentiated neurons. Before a classic in vitro differentiation approach was performed, P19 cells were treated with doxycycline (5ng/ml) for 48 hours. Then, after incubation with retinoic acid for four days and cultivation on the poly-L-lysine coated plates for an additional four days, the differentiated neurons were incubated within a biotin (50μM) supplemented-medium for four hours. In the BFA samples, cells were treated by the BFA (5 μg/ml) for one hour prior to the incubation

with biotin (and BFA). To verify the efficiency of labeling in P19 differentiated neurons, the biotinylation activity was analyzed by western blot with labeled streptavidin. In addition, successful differentiation was monitored by analyzing the expression of the Tuj1 neuronal marker (**Figures 24 A-C**). According to **Figures 24 A-C**, all the P19 differentiated neurons yielded abundant biotinylated proteins as P19 undifferentiated samples. Additionally, it is shown in **Figures 24 A-C** that the expression of Tuj1 in all neuron samples (T-Copg1-ultraID#2, T-Copg2-ultraID#2 and ultraID-Ago2) was higher than in the undifferentiated samples.

A

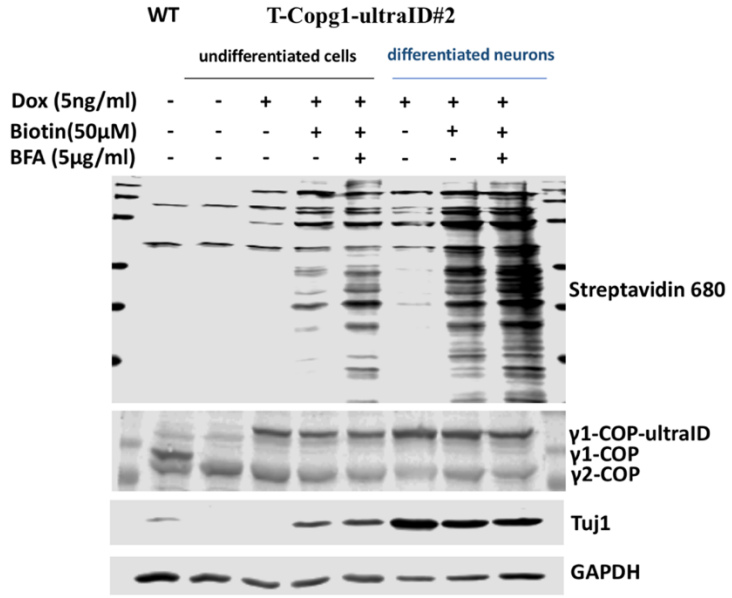

B

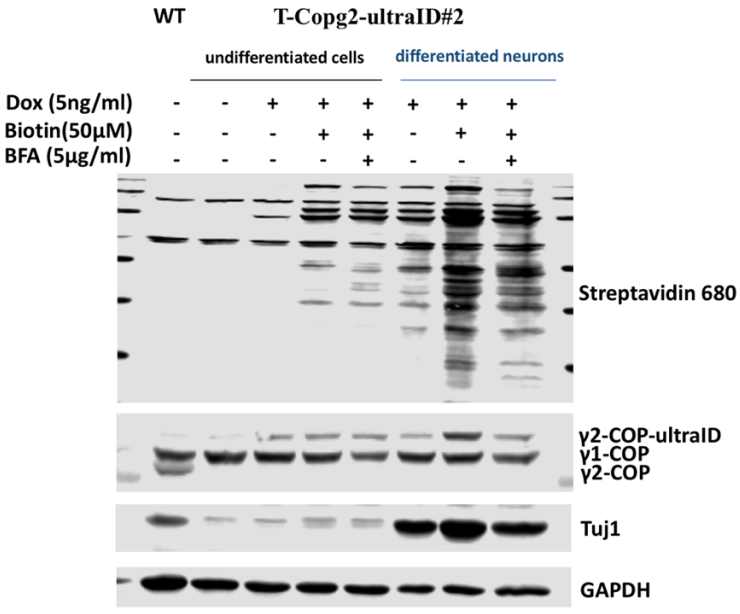

C

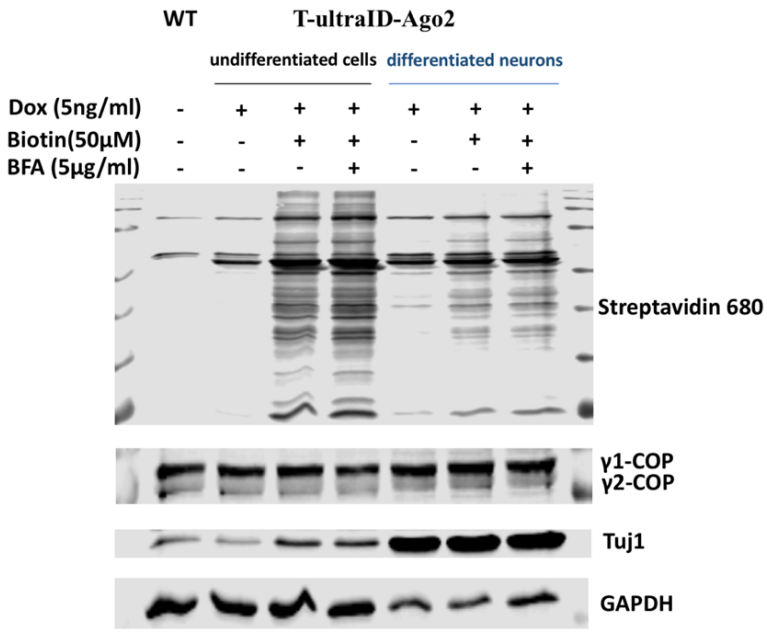

Figure 24. Characterization of ultraID-based labeling in P19 differentiated neurons. (A) Up panels: ultraID-mediated biotinylation in T-Copg1-ultraID cells analyzed by western blot analysis with labeled streptavidin in both non-differentiated cells and differentiated neurons; Lower panels: western analysis of the expression of ultraID tagged γ1-COP and γ2-COP, Tuj1 and GAPDH as indicated. (B) Same as (A) for T-Copg2-ultraID cells. (C) Same as (A) for T- ultraID-Ago2 cells.

2.22 Localization of tagged γ-COPs and biotinylated proteins in the differentiated cell lines

The localization of the fusion proteins and biotinylated proteins was analyzed by confocal fluorescence imaging in biotin and/or doxycycline-treated samples in the P19 cell lines after neuronal differentiation. As indicated above for the non-differentiated cells, the biotinylated proteins were detected with a streptavidin-alexa647 conjugate and the fusion proteins were detected with an anti-myc tag antibody decorated with a goat anti-rabbit alexa488-conjugated antibody. Nuclei were stained with DAPI and Golgi with an antibody against GM130 (alexa546 channel). In differentiated neurons from T-Copg1-ultraID#2 or T-Copg2-ultraID#2, γ1-COP or γ2-COP colocalized with the proximity-dependent biotinylated proteins at the Golgi (**Figures 25 A and B**). The biotinylated proteins in the T-ultraID-Ago2 differentiated neurons by contrast, showed a cytoplasmic staining like Ago2 (**Figure 25 C**). Interestingly, biotinylated proteins colocalized with γ-COP paralogues in Golgi and the axon hillock (the

A

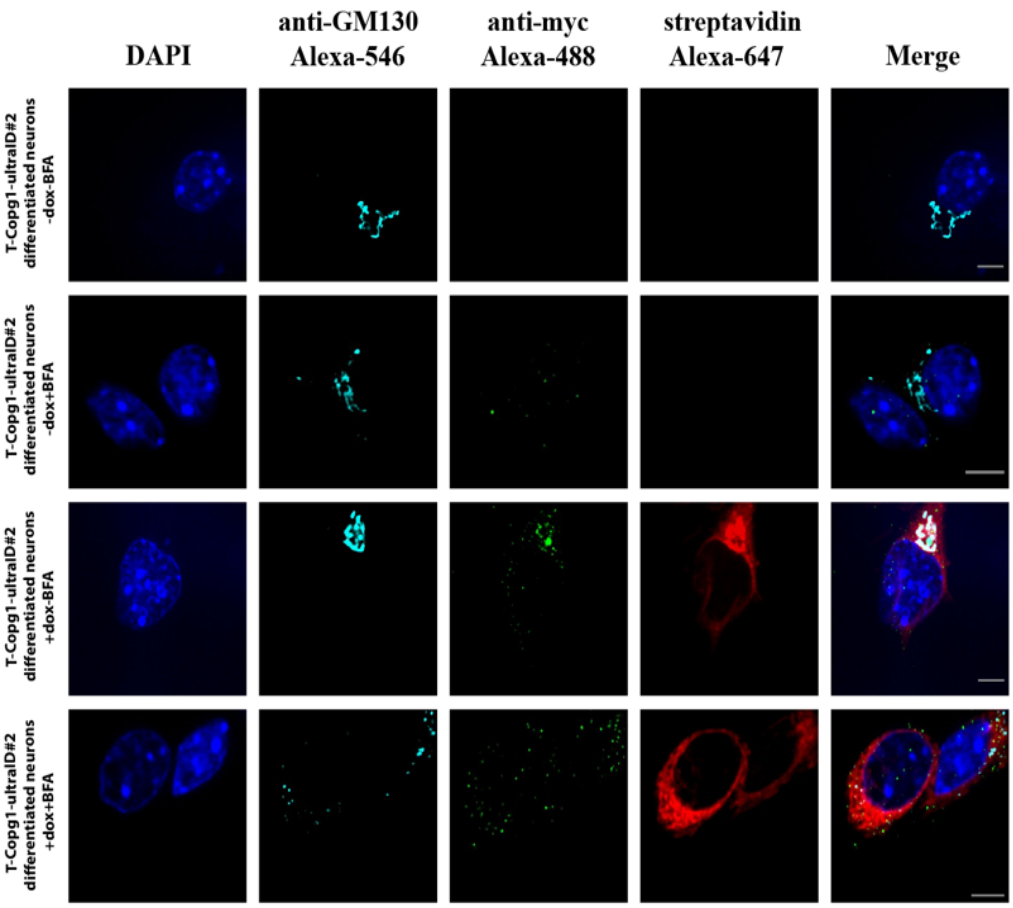
DAPI
anti-GM130 Alexa-546
anti-myc Alexa-488
streptavidin Alexa-647
Merge
T-Copg1-ultraID#2 differentiated neurons -dox-BFA
T-Copg1-ultraID#2 differentiated neurons -dox+BFA
T-Copg1-ultraID#2 differentiated neurons +dox-BFA
T-Copg1-ultraID#2 differentiated neurons +dox+BFA

B

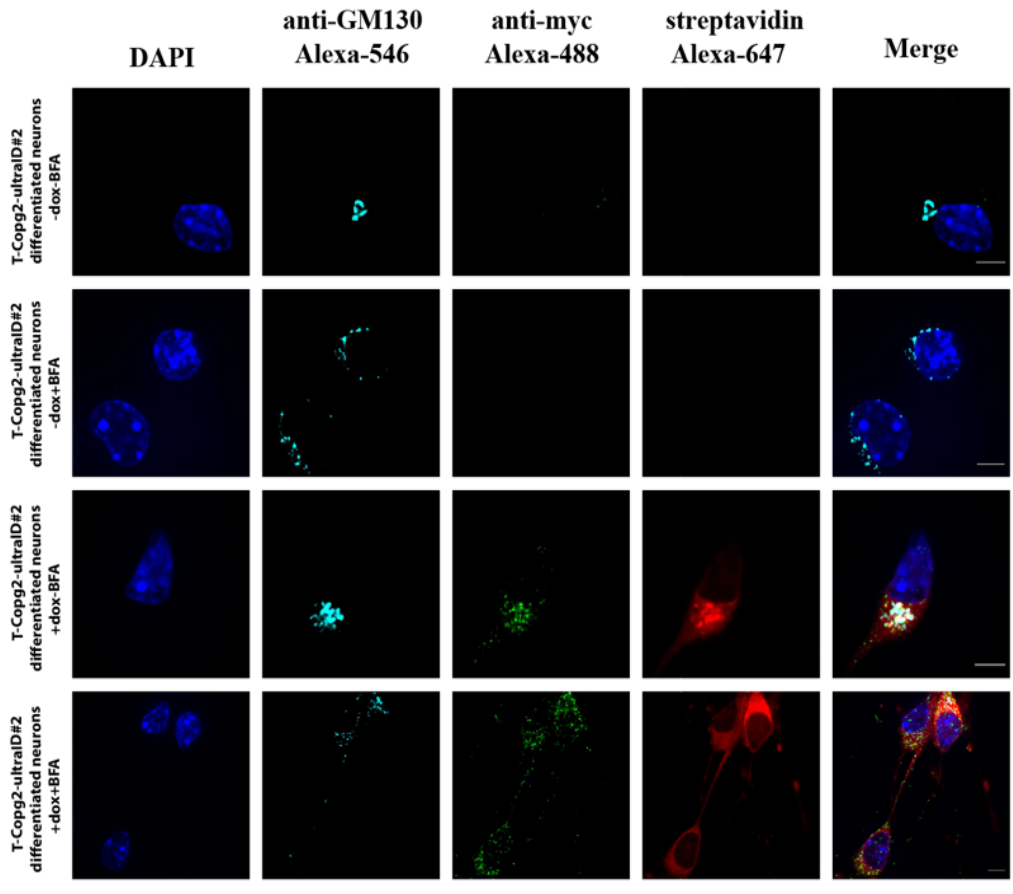
DAPI
anti-GM130 Alexa-546
anti-myc Alexa-488
streptavidin Alexa-647
Merge
T-Copg2-ultraID#2 differentiated neurons -dox-BFA
T-Copg2-ultraID#2 differentiated neurons -dox+BFA
T-Copg2-ultraID#2 differentiated neurons +dox-BFA
T-Copg2-ultraID#2 differentiated neurons +dox+BFA

C

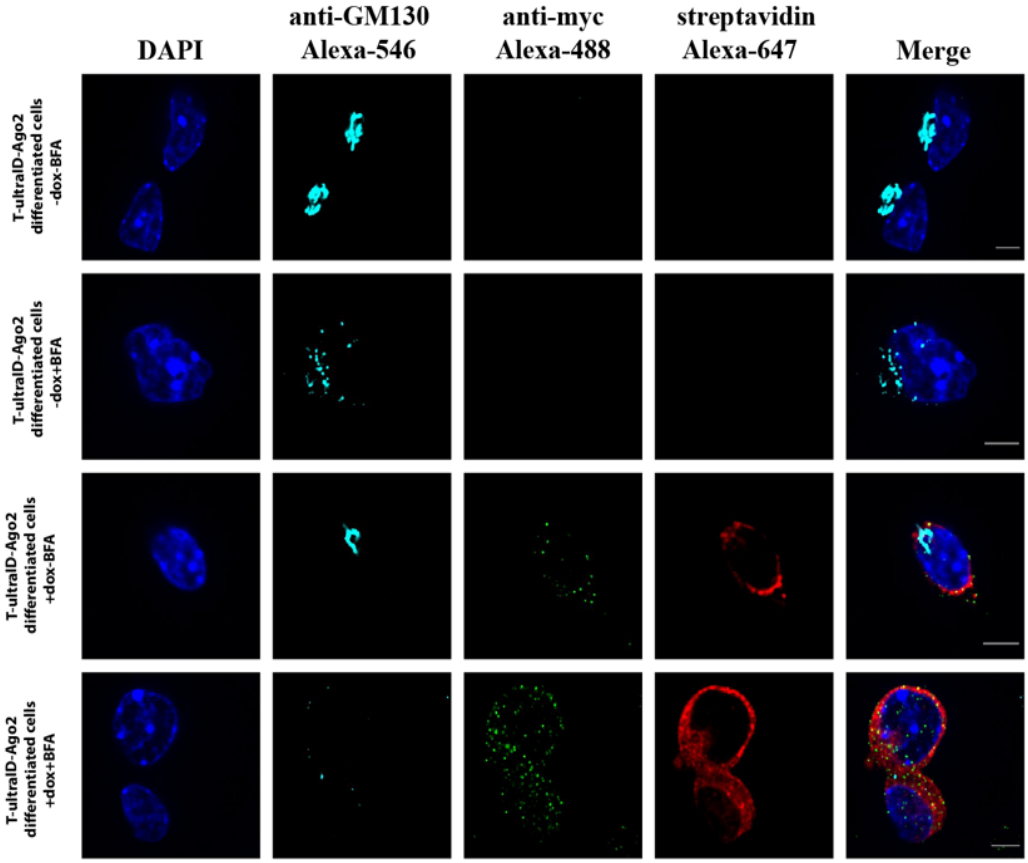

Figure 25. Colocalization of γ-COPs with biotinylated proteins in differentiated neurons. Immunostaining with streptavidin (647nm, red channel) to detect biotinylated protein in P19 differentiated neurons. DAPI (405nm, blue channel) is used to stain DNA. GM130 (546nm, cyan channel) marks the Golgi. The brightness intensity is the same range for all the images: cyan channel (2000-14000), red channel (1000-16000) and green channel (750-1500). The scale bar is 5 μm. The figures are as follows: (A) Confocal visualization of the localization of the γ1-COP and biotinylated proteins plus or minus BFA. γ1-COP is observed in the anti-myc channel (488nm, green channel). (B) Same as (A) for γ2-COP. (C) Same as (A) for Ago2.

swelling part at the start of the axon). In the BFA-treated samples, the Golgi apparatus appeared to collapse (**Figures 25 A-C)** and the γ-COPs as well as the biotinylated proteins were found in the cytoplasm both in the cell bodies and neurites (**Figures 25 A and B)**. By contrast, as demonstrated in **Figure 25 C**, the localization of Ago2 and its biotinylated proteins was not affected by the treatment of BFA.

2.23 Identification of the interactome of either γ1-COP or γ2-COP in P19 differentiated neurons

As described above, the Ago2 served as a control to remove the background proteins. To discover the proteomic difference between the two paralogues in P19 differentiated neurons, the volcano plots were used to analyze the LFQ data. This revealed the statistically significant enrichment of proximal proteins to γ1-COP-ultraID or γ2-COP-ultraID over ultraID-Ago2. For this analysis, the pCutoff for p value was set to 0.01 and the FCcutoff for fold change set to ±2 (**Figure 26 A and B**) (**Tables 8 and 9**). The detailed information with a pCutoff for p value < 0.05 and FCcutoff for fold change to ±2 is listed in **Tables 10 and 11**. The protein-coding genes of all the iBaq hits are highlighted in red in **Table 8 to Table 11**.

A

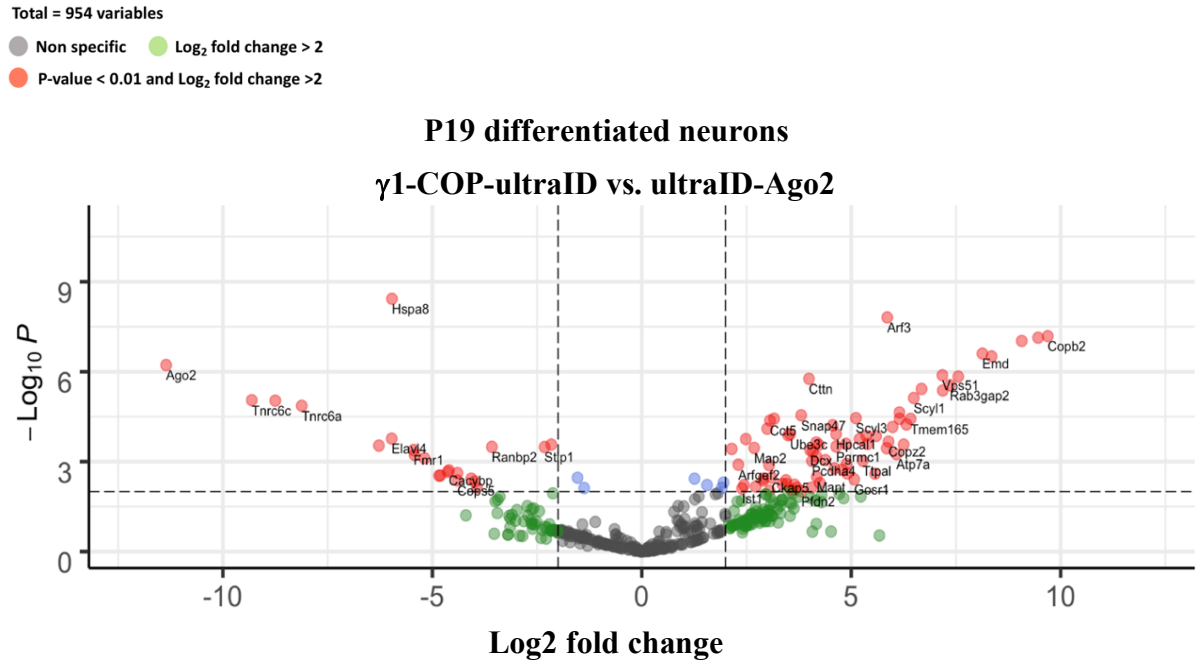

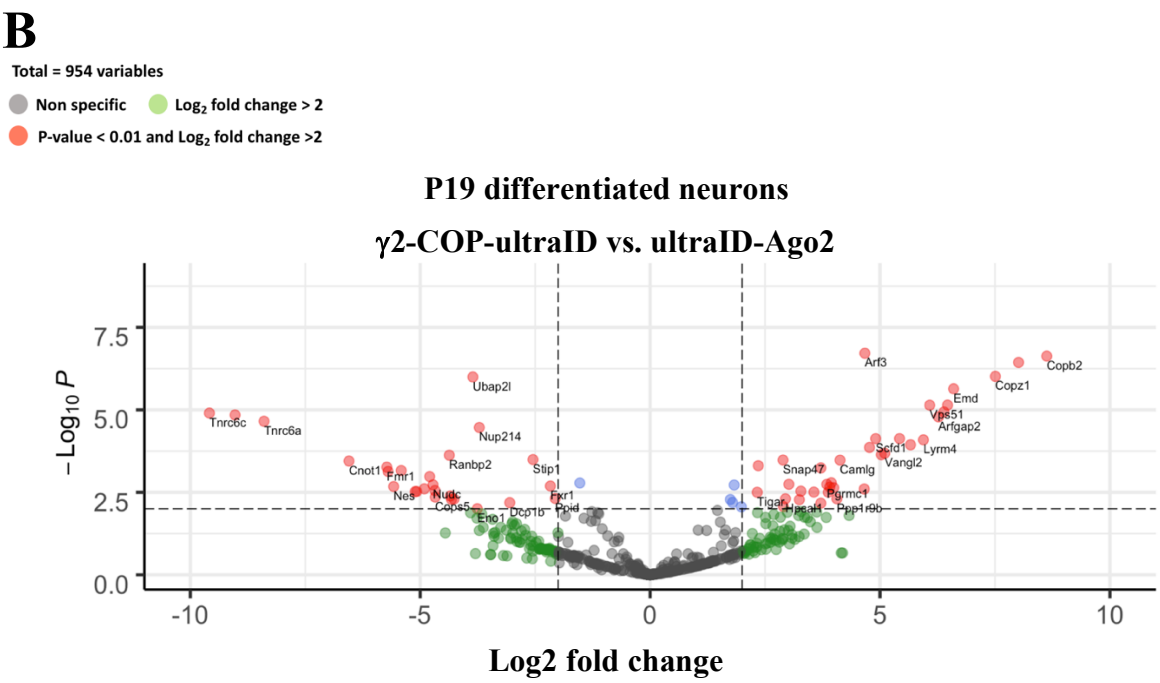

Figure 26. Volcano plots showing the differential abundance of isolated biotinylated proteins in P19 differentiated neurons.

The differential protein abundance was calculated after LC-MS/MS analysis of ultraID samples in three biological replicates for each cell line. The thresholds for significance (P-value < 0.01 and |log2 fold change|>2) are indicated by the dashed lines. Graph (A) shows a statistically significant enrichment of biotinylated proteins by γ1-COP-ultraID over biotinylated proteins by ultraID-Ago2 in P19 differentiated neurons. Points on the top-right quadrant illustrate significantly expressed interactome of γ1-COP while significantly expressed interactome of Ago2 is present on the top-left in P19 differentiated neurons. Detailed information is listed in **Table 8**. Graph B shows statistically significant enrichment of biotinylated proteins by γ2-COP-ultraID over the biotinylated proteins by ultraID-Ago2 in P19 differentiated neurons. Points on the top-right quadrant illustrate significantly expressed γ2-COP interactome, whilst significantly expressed interactome of Ago2 in P19 differentiated neurons is shown on the top-left. Detailed information is listed in **Table 9**.

Table 8. Significantly enriched genes in γ1-COP-ultraID over ultraID-Ago2 in P19 differentiated neurons with P-value<0.01. iBaq hits were indicated with red colour.

Copa	Copg2	Copz1	Rab3gap2	Qtrt1	Aspscr1	Ube3c	Rtn4
Arf3	Arcn1	Vps51	Arfgap2	Tmem165	Arfgap3	Tigar	Vangl2
Copg1	Cttn	Golga5	Scyl1	Gcc1	Zwint	Arfgap1	Copz2
Copb2	Emd	Txnl1	Scyl3	Lman1	Hpcal1	Lyrm4	Srp54
Anxa1	Camlg	Ppp1r9b	Gart	Lrch2	Arfgef2	Pebp1	Ckap5
Tceb2	Pgrmc1	Gdi2	Atp7a	Ttpal	Cep170	Wwox	Pgd
Gcc2	Map2	Dcx	Ywhaz	Pcdha4	Prr11	Mapt	Tcf25
Anxa5	Ubfd1	Ist1	Larp1	Pgrmc2	Cct6a	Ywhae	Pfdn2
Rab3gap1	Tubb2b	Rab7a	Ufsp2	Ykt6	Golga3	Birc6	Gorab
Acly	Pclo	Sec22b	Zdhhc13	Stx5	Gosr1	Slc30a5	Ccdc88a
Tmf1	Golga4	Cog1	Scfd1				

Table 9. Significantly enriched genes in γ2-COP-ultraID over ultraID-Ago2 in P19 differentiated neurons with P-value<0.01. iBaq hits were indicated with red colour.

Copa	Arcn1	Rab3gap2	Arfgap3	Camlg	Pgrmc1	Vars	Lrch2
Copg2	Copz1	Arfgap2	Scyl1	Qtrt1	Tmem165	Tceb2	Cog1
Copb1	Emd	Txnl1	Vangl2	Scyl3	Lman1	Tigar	Pgrmc2
Arf3	Golga5	Scfd1	Gcc1	Arfgap1	Gcc2	Ppp1r9b	Hpcal1
Copb2	Vps51	Lyrm4	Snap47	Aspscr1	Gart	Iqsec3	Gramd1a
Glud1	Slc30a5	Zdhhc13	Golga4	Gosr1	Stx5	Arfs	Wwox
Copg1							

Table 10. Significantly enriched genes in γ1-COP-ultraID over ultraID-Ago2 in P19 differentiated neurons with P-value<0.05. iBaq hits were indicated with red colour.

Copa	Copg2	Copz1	Rab3gap2	Qtrt1	Aspscr1	Ube3c	Rtn4
Arf3	Arcn1	Vps51	Arfgap2	Tmem165	Arfgap3	Tigar	Vangl2
Copg1	Cttn	Golga5	Scyl1	Gcc1	Zwint	Arfgap1	Copz2
Copb2	Emd	Txnl1	Scyl3	Lman1	Hpcal1	Lyrm4	Srp54
Anxa1	Camlg	Ppp1r9b	Gart	Lrch2	Arfgef2	Pebp1	Ckap5
Tceb2	Pgrmc1	Gdi2	Atp7a	Ttpal	Cep170	Wwox	Pgd
Gcc2	Map2	Dcx	Ywhaz	Pcdha4	Prr11	Mapt	Tcf25
Anxa5	Ubfd1	Ist1	Larp1	Pgrmc2	Cct6a	Ywhae	Pfdn2
Rab3gap1	Tubb2b	Tacc2	Cdc42bpb	Tmf1	Birc6	Efhd2	Q8C3W1
Stmn1	Tmed10	Dab2ip	Mettl6	Golga2	Golga3	Hist1h2ah	Prkar2a
Atp6v1f	Cnn3	Tmem263	Slc30a5	Kif1b	Map1b	H3f3a	Npm1
Golga4	Arhgdia	Cfdp1	Ap2a2	Chmp5	Rab7a	Ufsp2	Ykt6
Gorab	Acly	Pclo	Sec22b	Zdhhc13	Stx5	Gosr1	Ccdc88a
Cog1	Scfd1						

Table 11. Significantly enriched genes in γ2-COP-ultraID over ultraID-Ago2 in P19 differentiated neurons with P-value<0.05. iBaq hits were indicated with red colour.

Copa	Arcn1	Rab3gap2	Arfgap3	Camlg	Pgrmc1	Vars	Lrch2
Copg2	Copz1	Arfgap2	Scyl1	Qtrt1	Tmem165	Tceb2	Cog1
Copb1	Emd	Txnl1	Vangl2	Scyl3	Lman1	Tigar	Pgrmc2
Arf3	Golga5	Scfd1	Gcc1	Arfgap1	Gcc2	Ppp1r9b	Hpcal1
Copb2	Vps51	Lyrm4	Snap47	Aspscr1	Gart	Tacc2	Pgd
Srp54	Stx5	Copz2	Dcx	Psmd11	Mettl6	Uba52	Eps15l1
Ywhaz	Ccdc88a	Anxa1	Wwox	Gosr1	Larp1	Gramd1a	Pclo
Pebp1	Iqsec3	Glud1	Slc30a5	Zdhhc13	Golga4	Arfs	Copg1

2.24 Different membrane-associated interactome of γ1-COP and γ2-COP in P19 differentiated neurons

As described in the P19 undifferentiated cells, BFA was applied to prevent the recruitment of γ-COPs to the Golgi membrane [230,231]. In the following experiments, to identify the transient contacts of γ-COPs on the Golgi membrane in P19 differentiated neurons, the differential abundance of proteins isolated from γ-COPs-ultraID over their corresponding BFA-treated samples was analysed and depicted in the following volcano plots (**Figure 27 A and B**). For this analysis, the pCutoff for p value was set to 0.01 and FCcutoff for fold change set to ±2, as presented in the following volcano plots. The Venn diagram (**Figure 27 C, Tables 12-14)** overlaps the proximity proteomic data of γ1-COP on Golgi membrane (**Figure 27 A, Table 12**) with the proximity proteomic data of γ2-COP on Golgi membrane (**Figure 27 B, Table 13**). Few proteins were detected with these criteria as membrane-associated contacts in P19 differentiated neurons. As it is expected that Arfs and ArfGAPs were identified as membrane interactome of γCOPs. The Golgi tether golgin-84 (Golga5) and Golgi-associated protein Vangl2[255] involved in neural tube closure during embryonic development[256] were also identified as the membrane-associated proteins of both γ1- and γ2-COP. With a relaxed threshold of a maximal p value set to 0.05 and an FCcutoff for fold change set to ±2, more membrane-associated proteins were identified in the interactors of different γ-COP paralogues, all of them are known Golgi proteins **(Tables 15-17)**. Hence, as observed in the differentiated neurons, the proximity-dependent biotinylation approach is efficient in defining a transient interactome of coatomer at the membrane.

A

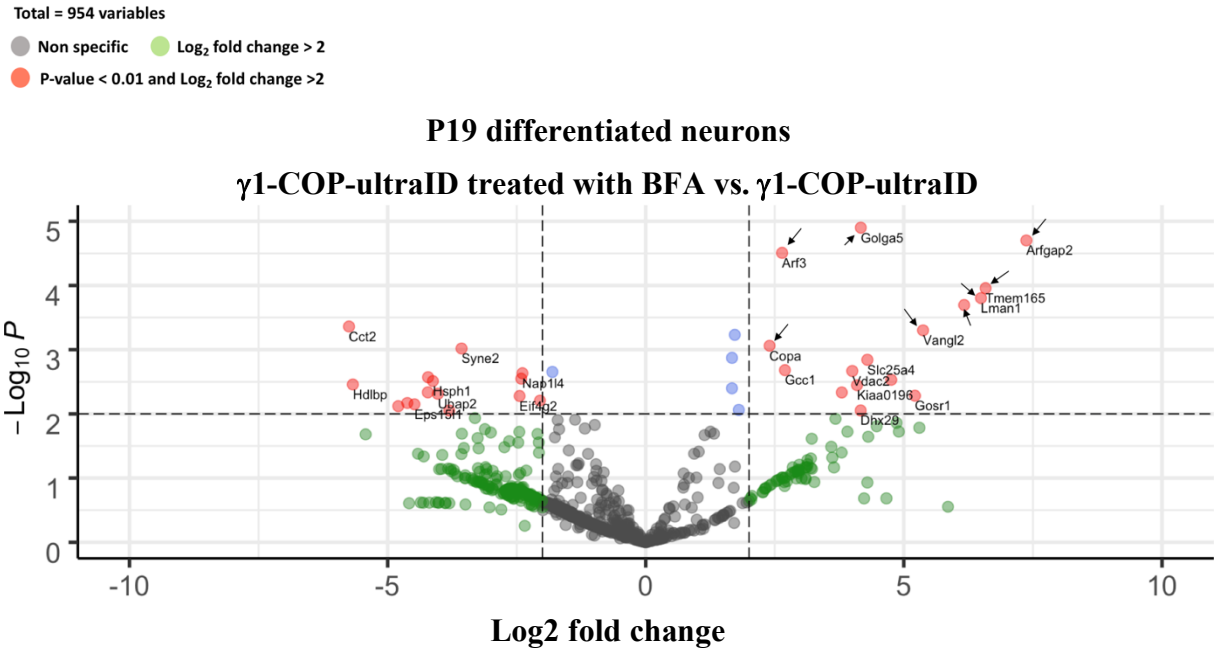
Total = 954 variables
Non specific
Log2 fold change > 2
P-value < 0.01 and Log2 fold change >2
P19 differentiated neurons
γ1-COP-ultraID treated with BFA vs. γ1-COP-ultraID
– Log10 P
Log2 fold change
Golga5
Arf3
Arfgap2
Tmem165
Lman1
Vangl2
Cct2
Syne2
Copa
Slc25a4
Vdac2
Gcc1
Kiaa0196
Gosr1
Hdlbp
Hsph1
Nap1l4
Ubap2
Eif4g2
Dhx29

B

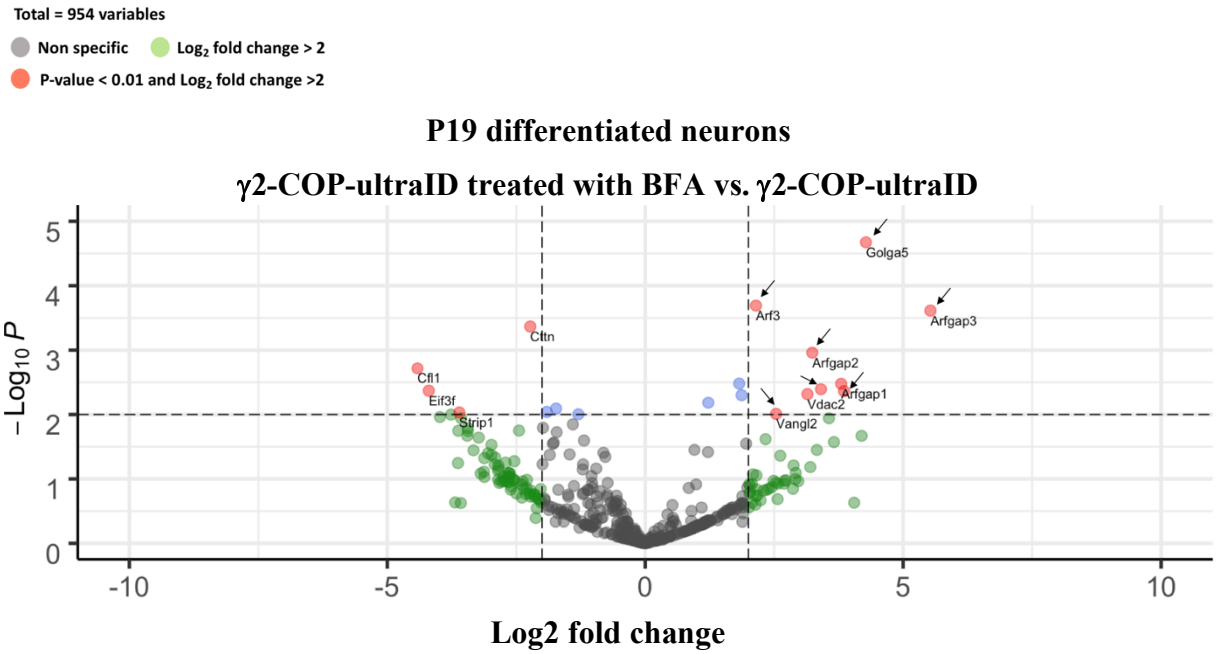
Total = 954 variables
Non specific
Log2 fold change > 2
P-value < 0.01 and Log2 fold change >2
P19 differentiated neurons
γ2-COP-ultraID treated with BFA vs. γ2-COP-ultraID
– Log10 P
Log2 fold change
Golga5
Arf3
Arfgap3
Cttn
Arfgap2
Cfl1
Arfgap1
Eif3f
Vdac2
Strip1
Vangl2

C

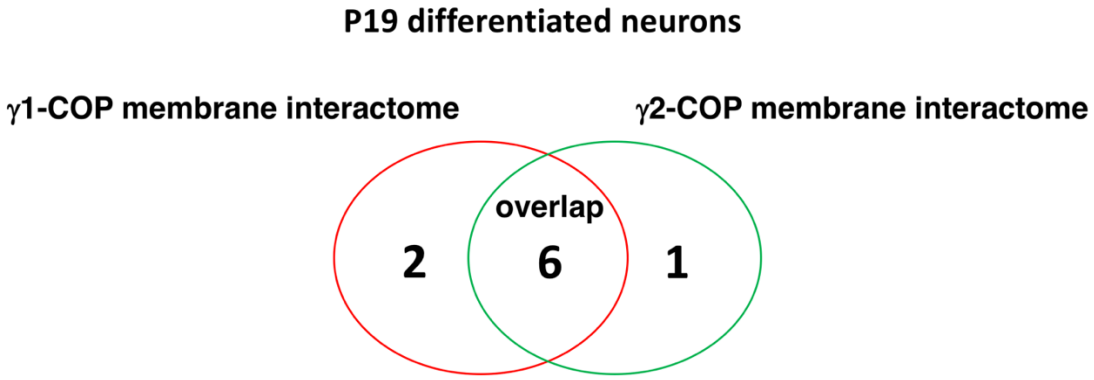

Figure 27. Volcano plots and venn diagram depicting Golgi membrane-associated γ-COP interactome in P19 differentiated neurons.

The differential protein abundance was calculated after LC-MS/MS analysis of ultraID samples in three biological replicates for each cell line. Significance thresholds (dashed lines) were set to P-value < 0.01 and |log2 fold change|>2. Graph (A) shows enrichment of biotinylated proteins in the γ1-COP-ultraID sample over the BFA-treated γ1-COP-ultraID sample. Proteins that had been analysed as significant over the Ago2 negative control datasets are indicated in arrows. Graph (B) Same as Graph (A) for the γ2-COP-ultraID samples. Graph (C) is a Venn diagram of the identified membrane-associated proximal proteins to γ1-COP and/or γ2-COP. Only those proteins that had been analysed as significant over the Ago2 negative control datasets were considered. Two membrane-associated proteins of γ1-COP, one membrane-associated protein of γ2-COP and six membrane-associated proteins of both γ-COPs, were detected in the P19 differentiated neurons dataset. Detailed information is listed in **Tables 12-14**.

Table 12. Venn figure indicating γ1-COP membrane-associated interactome in P19 differentiated neurons with P-value<0.01.

Gene name	Protein name	GO molecular Function	localization
Tmem165	Transmembrane protein 165	Golgi calcium ion transport	Golgi apparatus membrane
		calcium ion transmembrane transport	
Copa	Coatomer subunit alpha	vesicle-mediated transport	Golgi apparatus

Table 13. Venn figure indicating γ2-COP membrane-associated interactome in P19 differentiated neurons with P-value<0.01.

Gene name	Protein name	GO molecular Function	localization
Arfgap1	ADP-ribosylation factor GTPase-activating protein 1	GTPase activator activity	Golgi apparatus

Table 14. Venn figure indicating overlapped membrane-associated interactome between γ1-COP-ultraID and γ2-COP-ultraID in P19 differentiated neurons with P-value<0.01.

Gene name	Protein name	GO molecular Function	localization
Arfgap2	ADP-ribosylation factor GTPase-activating protein 2	GTPase activator activity	Golgi apparatus membrane
Lman1	Protein ERGIC-53-like	endoplasmic reticulum to Golgi vesicle-mediated transport	Golgi organization
Arfgap3	ADP-ribosylation factor GTPase-activating protein 3	GTPase activator activity	Golgi apparatus membrane
Vangl2	Vang-like protein 2	apical protein localization	membrane
Golga5	Golgin subfamily A member 5	Golgi vesicle transport	Golgi apparatus membrane
		Rab GTPase binding	
Arfs	ADP-ribosylation factor	GTP binding	Golgi apparatus

Table 15. Venn figure indicating γ1-COP membrane-associated interactome in P19 differentiated neurons with P-value<0.05.

Gene name	Protein name	GO molecular Function	localization
Tmf1	TATA element modulatory factor	androgen receptor binding	Golgi apparatus membrane
		DNA binding	
		nuclear receptor transcription coactivator activity	
Birc6	Baculoviral IAP repeat-containing protein 6	apoptotic process	Golgi apparatus membrane
		cell cycle	
		regulation of cell population proliferation	
		protein ubiquitination	
Tmem263	Transmembrane protein 263	membrane protein	membrane
Slc30a5	Zinc transporter 5	zinc ion transmembrane transporter activity	Golgi apparatus
Golga2	Golgin subfamily A member 2	microtubule binding	cis-Golgi network membrane
		positive regulation of axonogenesis	
		Golgi localization	
		positive regulation of protein glycosylation	
Gcc2	GRIP and coiled-coil domain-containing protein 2	microtubule organizing center organization	Golgi apparatus k membrane
		retrograde transport	
		protein localization to Golgi apparatus	
Tmed10	Transmembrane emp24 domain-containing protein 10	COPI-coated vesicle budding	Golgi apparatus membrane
		endoplasmic reticulum to Golgi vesicle-mediated transport	
		Golgi organization	
Golga4	Golgin subfamily A member 4	GTPase binding	Golgi apparatus membrane and cytopalsm
		positive regulation of axon extension	
		Golgi to plasma membrane protein transport	
Gcc1	GRIP and coiled-coil domain-containing protein 1	small GTPase binding	Golgi apparatus
Copa	Coatomer subunit alpha	vesicle-mediated transport	Golgi apparatus

Table 16. Venn figure indicating γ2-COP membrane-associated interactome in P19 differentiated neurons with P-value<0.05.

Gene name	Protein name	GO molecular Function	localization
Stx5	Syntaxin-5	SNAP receptor activity	Golgi apparatus membrane
		SNARE binding	
		vesicle fusion with Golgi apparatus	
Arfgap1	ADP-ribosylation factor GTPase-activating protein 1	GTPase activator activity	Golgi apparatus
Wwox	WW domain-containing oxidoreductase	skeletal system morphogenesis	Mitochondrion, Nucleus and Cytoplasm
		oxidoreductase activity	
		enzyme binding	
Cog1	Conserved oligomeric Golgi complex subunit 1	intra-Golgi vesicle-mediated transport	Golgi apparatus membrane
		protein transport	

Table 17. Venn figure indicating overlapped membrane-associated interactome between γ1-COP-ultraID and γ2-COP-ultraID in P19 differentiated neurons with P-value<0.05.

Gene name	Protein name	GO molecular Function	localization
Arfgap2	ADP-ribosylation factor GTPase-activating protein 2	GTPase activator activity	Golgi apparatus membrane
Tmem165	Transmembrane protein 165	metal ion transmembrane transporter activity	Golgi apparatus membrane
Lman1	Protein ERGIC-53-like	endoplasmic reticulum to Golgi vesicle-mediated transport	Golgi organization
Arfgap3	ADP-ribosylation factor GTPase-activating protein 3	GTPase activator activity	Golgi apparatus membrane
Golga5	Golgin subfamily A member 5	Golgi vesicle transport	Golgi apparatus membrane
		Rab GTPase binding	
Arfs	ADP-ribosylation factor	GTP binding	Golgi apparatus
Vangl2	Vang-like protein 2	apical protein localization	Cell membrane
			Golgi-associated protein
Gosr1	Golgi SNAP receptor complex member 1	SNAP receptor activity	Golgi apparatus
		endoplasmic reticulum to Golgi vesicle-mediated transport	
		regulation of vesicle targeting	

2.25 Identification of the different interactome between γ1-COP and γ2-COP in P19 differentiated neurons

Next, we directly compared the datasets from the γ1-COP-ultraID and γ2-COP-ultraID. In the following volcano plots, statistically significant enrichment of proteins in the interactome of γ1-COP-ultraID over γ2-COP-ultraID in P19 differentiated neurons was analysed. A pCutoff for p value was set to 0.01 and an FCcutoff for fold change set to ±2 (**Figure 28 A**). As described above for the P19 undifferentiated cells, only those proteins that were deemed at significant over the ultraID-Ago2 control dataset were considered to identify the differential interactome of the two different γ-COP paralogues (**Figure 28 B**). The area I in **Table 18** are the proteins that specifically interact with γ1-COP. The area II in **Table 19** represents the proteins that specifically interact with γ2-COP, no protein was identified in this category. Proteins with functions related to neuron generation were identified as specific proximal

proteins to γ1-COP enriched proximity proteins. This includes the copper-transporting ATPase 1(Atp7a), cytoskeleton-associated protein 5 (Ckap5), IST1 homolog (Ist1) and Src substrate cortactin (Cttn).

With relaxed significance threshold of P-value < 0.05 and FCcutoff for fold change to ±2 (**Tables 20 and 21**), more candidates were identified with proteins that play a role on synaptic vesicle traffic, such as Kinesin-like protein KIF1B and Rab3 GTPase-activating protein catalytic subunit. Some other γ1-COP enriched proximity proteins are related to chemical synaptic transmitters and neuron migration. This includes cAMP-dependent protein kinase type II-alpha regulatory subunit, Tubulin beta-2B chain and 14-3-3 protein epsilon. In addition, proteins such as stathmin, and Microtubule-associated protein 1B promote the axon extension in the γ1-COP enriched proximity proteins dataset.

As previously stated, the ultraID method could identify the proximal proteins within 10 nm to result in the identification of both directly interacted proteins and neighbouring proteins. Therefore, the identification of proteins related to neurogenesis that are enriched in the γ1-COP dataset may either indicate the preferential interaction of γ1-COP-containing coatomer with certain cargo proteins (e.g. Atp7a) or the preferential localization of γ1-COP-containing coatomer near sites of membrane protrusion during the neuronal differentiation of P19 cells.

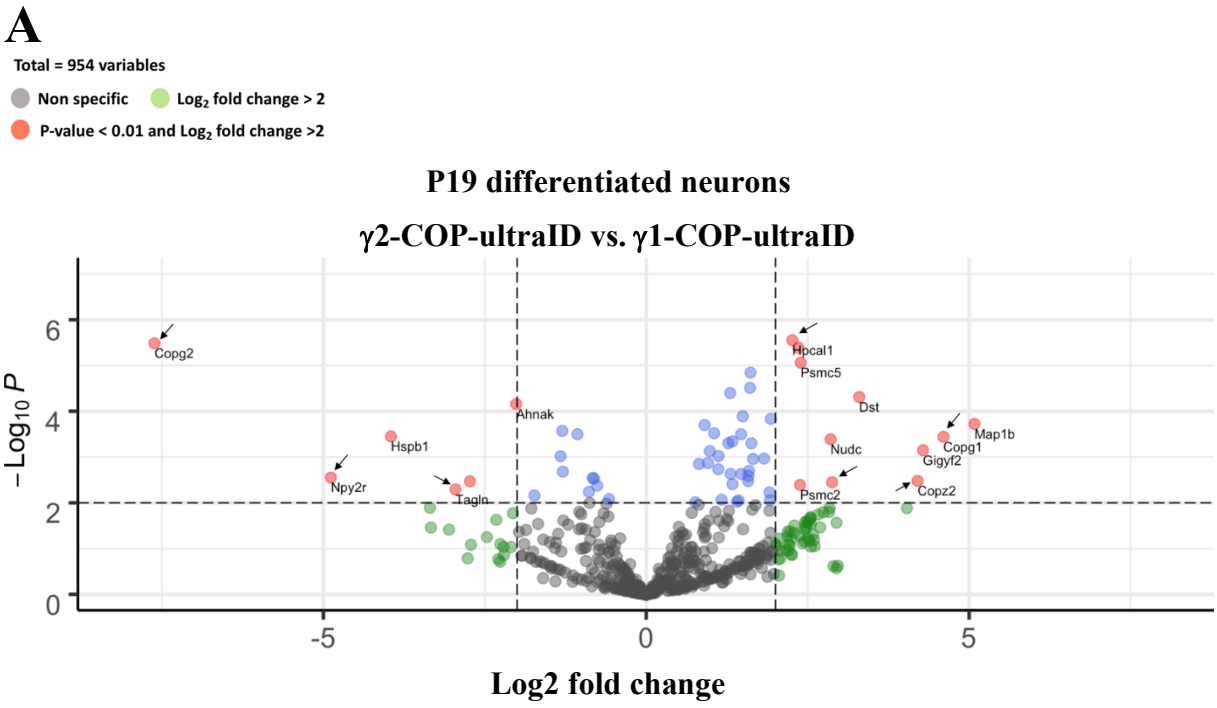

B

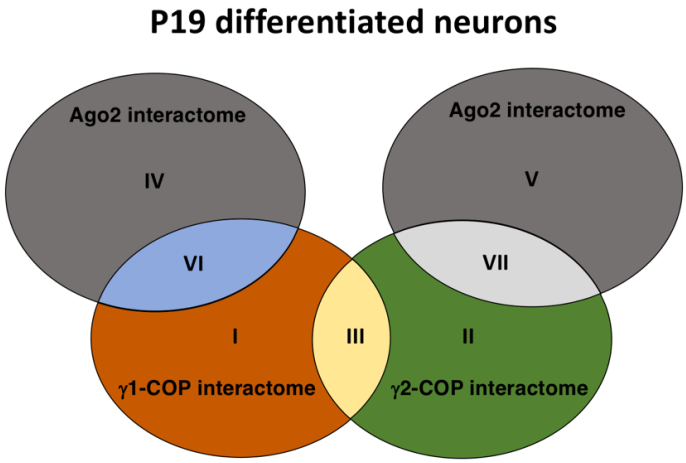

Figure 28. Volcano plots and venn diagram depicting differential interactomes between γ1-COP and γ2-COP in P19 differentiated neurons.

(A) Volcano plot showing the differential abundance of proteins detected in the γ1-COP-ultraID and γ2-COP-ultraID datasets. Significance thresholds (dashed lines) were set to P-value < 0.01 and |log2 fold change|>2. Dots on the top-right quadrant illustrate significantly enriched hits for γ1-COP while enriched hits for γ2-COP are on the top-left. Proteins that had been analysed as significant over the Ago2 negative control datasets are indicated in arrows. (B) Venn figure displaying different categories of identified proteins. Only those proteins that had been analysed as significant over the Ago2 negative control datasets were considered. Area I contains the proteins significantly enriched in the γ1-COP samples compared to the γ2-COP and Ago2 samples **(Table 18 and 20).** Area II contains the proteins significantly enriched in the γ2-COP compared samples compared to the γ1-COP and Ago2 samples **(Table 19 and 21).** Area III contains the overlapped interactome of γ1-COP and γ2-COP. Area IV contains the proteins significantly enriched in the Ago2 samples compared to the γ1-COP samples. Area V contains the proteins significantly enriched in the Ago2 samples compared to the γ2-COP samples. Area VI displaying the overlapped interactome of γ1-COP and Ago2. Area VII displaying the overlapped interactome of γ2-COP and Ago2.

Table 18. The significantly enriched proteins in γ1-COP-ultraID samples in P19 differentiated neurons (Part I in the Venn figure) with P-value < 0.01.

Gene name	Protein name	GO molecular Function
Copg1	Coatomer subunit gamma-1	coatomer subuunits
Ttpal	Alpha-tocopherol transfer protein-like	phosphatidylinositol bisphosphate binding
Atp7a	Copper-transporting ATPase 1	central nervous system neuron development
		neuron projection morphogenesis
		chaperone binding
		copper ion transmembrane transporter activity
Pcdha4	Protocadherin alpha-4	calcium ion binding
		cell adhesion
Ckap5	Cytoskeleton-associated protein 5	central nervous system myelin formation
		dendritic spine maintenance
		long-term synaptic potentiation
		microtubule plus end polymerase
Tmem165	Transmembrane protein 165	Golgi calcium ion transport
		cellular calcium ion homeostasis
Ist1	IST1 homolog	cytoskeleton-dependent cytokinesis
Cttn	Src substrate cortactin	regulation of axon extension
		dendritic spine maintenance
		actin cytoskeleton reorganization

Table 19. The significantly enriched proteins in γ2-COP-ultraID samples in P19 differentiated neurons (Part II in the Venn figure) with P-value < 0.01. – Null

Table 20. The significantly enriched proteins in γ1-COP-ultraID samples in P19 differentiated neurons (Part I in the Venn figure) with P-value < 0.05.

Anxa1	Annexin A1	calcium-dependent phospholipid binding
		calcium-dependent protein binding
		calcium ion binding
		phospholipid binding
Cttn	Src substrate cortactin	actin filament binding
		Arp2/3 complex binding
		profilin binding
		proline-rich region binding
Ist1	IST1 homolog	cytoskeleton-dependent cytokinesis

Gene name	Protein name	GO molecular Function
Copg1	Coatomer subunit gamma-1	coatomer subuunits
Copz2	Coatomer subunit zeta-2	
Ttpal	Alpha-tocopherol transfer protein-like	phosphatidylinositol bisphosphate binding
Tmem263	Transmembrane protein 263	membrane protein
Anxa5	Annexin A5	calcium-dependent phospholipid binding
		peptide hormone binding
		receptor tyrosine kinase binding
Pcdha4	Protocadherin alpha-4	calcium ion binding
		identical protein binding
Kif1b	Kinesin-like protein KIF1B	ATP-dependent microtubule motor activity
		ATPase activity
		anterograde axonal transport
		microtubule binding
Pfdn2	Prefoldin subunit 2	protein folding chaperone
		unfolded protein binding
Ubfd1	Ubiquitin domain-containing protein UBFD1	Expressed in embryo
Dab2ip	Disabled homolog 2-interacting protein	SH3 domain binding
		vascular endothelial growth factor receptor 2 binding
		death receptor binding
		GTPase activator activity
Rab3gap1	Rab3 GTPase-activating protein catalytic subunit	brain development
		establishment of protein localization to endoplasmic reticulum membrane
		Rab GTPase binding
		regulation of short-term neuronal synaptic plasticity
		regulation of synaptic vesicle priming
		synaptic vesicle transport
Prkar2a	cAMP-dependent protein kinase type II-alpha regulatory subunit	ubiquitin protein ligase binding
		modulation of chemical synaptic transmission
		cAMP-dependent protein kinase regulator activity
		protein domain specific binding
Tubb2b	Tubulin beta-2B chain	embryonic brain development
		neuron migration
		positive regulation of axon guidance
		microtubule cytoskeleton organization
Efhd2	EF-hand domain-containing protein D2	calcium ion binding

Golga3	Golgin subfamily A member 3	cell differentiation
		multicellular organism development
		spermatogenesis
Atp6v1f	V-type proton ATPase subunit F	ATPase-coupled ion transmembrane transporter activity
		proton-transporting ATPase activity
Ywhae	14-3-3 protein epsilon	hippocampus development
		cerebral cortex development
		neuron migration
		regulation of postsynaptic membrane neurotransmitter receptor levels
		protein localization to nucleus
Stmn1	Stathmin	axonogenesis
		brain development
		neuron projection development
		mitotic cytokinesis
		regulation of microtubule polymerization or depolymerization
Ckap5	Cytoskeleton-associated protein 5	central nervous system myelin formation
		dendritic spine maintenance
		establishment or maintenance of microtubule cytoskeleton polarity
		long-term synaptic potentiation
		microtubule polymerization
		mitotic spindle organization
Cfdp1	Craniofacial development protein 1	cell adhesion
		multicellular organism development
		negative regulation of fibroblast apoptotic process
		regulation of cell population proliferation
		regulation of cell shape
Tmem165	Transmembrane protein 165	Golgi calcium ion homeostasis
		protein N-linked glycosylation
Lman1	Protein ERGIC-53	endoplasmic reticulum organization
Map1b	Microtubule-associated protein 1B	axon extension
		positive regulation of neuron differentiation
		mitochondrion transport along microtubule
		synapse assembly
		response to vitamin A
		microtubule binding

Table 21. The significantly enriched proteins in γ2-COP-ultraID samples in P19 differentiated neurons (Part II in the Venn figure) with P-value < 0.05.

Gene name	Protein name	GO molecular Function
Vars	Valine--tRNA ligase	ATP binding

3. Discussion

COPI transport vesicles are coated with coatomer which is made of 7 subunits (α,β,β',δ,ε,γ, and ζ-COP). In mammals, the paralogues of gene Copg1 and Copz1 were designated Copg2 and Copz2[73,74]. Since their discovery, the potential specific functions mediated by the distinct

paralogues have yet to be determined[45,81,103,257]. Recombinant coatomer complexes containing either γ1-COP or γ2-COP have similar efficiency on the in vitro generation of COPI vesicles from permeabilised HeLa cells[258] and purified Golgi membranes[259]. Additionally, according to a previous study, the proteomes of COPI vesicles generated from γ1-COP or γ2-COP-containing coatomer were indistinct in vitro[258], which suggested γ1-COP and γ2-COP are functionally redundant. Our own previous study showed that the depletion of γ1-COP can disrupt neurite extension in neurons derived from pluripotent cells, whereas the neurite outgrowth was not affected by the removal of γ2-COP.

During our research, we used either the coding sequence of GFP or γ1-COP-GFP to construct P19 GFP KI or γ1-COP-GFP KI cell lines, to verify the paralogue-specific function of γ1-COP during neuronal differentiation in P19 cells. We observed that the neurites failed to extend in GFP KI while γ1-COP-GFP KI could rescue the outgrowth of neurites (**Figure 9**). Additionally, when evaluating the effect on the disruption of γ1-COP, we constructed γ2-COP-GFP KI cell lines (in which the whole Copg1 locus is replaced with the coding sequence of γ2-COP-GFP). This was done in order to determine whether the phenotype of γ1-COP KO cells is the result of a missing specific function mediated by γ1-COP, or is due to a reduced combined expression of the γ-COP protein irrespective of the paralogous identity. Our findings demonstrated that both γ1-COP and γ2-COP, when expressed from the Copg1 locus, can rescue the disruption of tight embryoid body formation compared to the γ1-COP-missing cells (**Figure 8**). This indicates that during early stages of P19 cells neuronal differentiation, common functions shared by γ1-COP and γ2-COP ensure a correct EB formation. These common functions are regulated by quantity balance of the proper expression of either paralogous γ-COP. By contrast, the data from the analysis of neurite extension in late-stage differentiation, suggests a unique function for γ1-COP in stimulating efficient neurite outgrowth. Indeed, in this case the expression of γ2-COP from the Copg1 locus could only partially rescue the absence of γ1-COP.

Previous data shows that the impaired generation of COPI transport vesicles results in disruption of dendritic growth in cultured hippocampal neurons[260,261]. Furthermore, decreased dendritic growth is caused by mutations of components of COPII transport vesicles[262] in experiments using flies. According to the analysis of apoptosis (**Figure 4A**), higher apoptotic activity is not evident in either γ1-COP or γ2-COP absence cells. Moreover, our data (**Figure 4B and C**) suggests that depletion of γ1-COP or γ2-COP does not result in increased ER stress. Thus, it does not appear that the phenotype of γ1-COP KO cells is the result of

pleiotropic effects caused by a decreased viability/fitness of the cells. To explain the mechanism underlying the role of γ1-COP in promoting neurite extension, two hypotheses are proposed: The first hypothesis is that γ1-COP contains some specific regions important for the process of neuronal differentiation. The second is that γ1-COP interacts with some specific cargo proteins to promote neuronal polarisation. To test our hypotheses, we started to construct the chimeric γ-COP cells (where the whole Copg1 locus is replaced with coding sequence of either the γ1-COP trunk combined with γ2-COP appendage or the γ2-COP trunk combined with γ1-COP appendage) to find a potential functional region which can facilitate neurite extension. Both chimeras supported the generation of the tight embryoid bodies **(Figure 14)**, which supports our previous conclusion that γ2-COP can take over the role of γ1-COP in γ1-COP deletion cells when expressed at sufficient levels. By contrast, the case in the process of neuronal differentiation is more complicated. We found that in cells that expressed either chimeric γ-COP protein from the Copg1 locus, the average length of extended neurites was significantly shorter than that measured in γ1-COP-expressing cells (**Figure 15**). This would suggest that there is not a discrete motif located either in the trunk or appendage domain of γ1-COP that explains its function during neuronal polarisation. Conversely it is possible that specific γ1-COP sequences distributed over the full length γ1-COP protein are responsible for its specific function.

A proximity-dependent biotinylation approach was applied, using the novel ultraID enzyme and MS analysis (**Figure 16**), to search potential binding partners of γ1-COP in order to clear its role during neuronal polarisation. As previously explained, Ago2 was chosen as a negative control to filter out random background biotinylation, since it is unrelated to the COPI pathway in function but shows at a partial localisation to the ER and Golgi[228,229] (**Figure 17**). Additionally, cells treated with BFA (an inhibitor of the guanine exchange factor GBF1 that activates Arf prior to the recruitment of coatomer to Golgi membranes) were used as a control to facilitate the identification of the membrane-associated interactome of γ-COPs (**Figure 17**). The approach was successful as, from the membrane-bound interactome data with p value < 0.01 and FCcutoff for fold change to ±2 in P19 undifferentiated cells, the majority of membrane-associated interactors of γ1- and γ2-COP are known Golgi membrane resident proteins **(Figure 22 A-C and Tables 3-5)**. Examples include Arfs, ArfGAPs[11], Golgins[232] and SNAREs. As discussed in the results, the 21 proteins significantly enriched in the γ1-COP interactome, and the 17 proteins in the γ2-COP interactome **(Figure 22 A-C and Tables 3-5)** were all found to be Golgi associated proteins. Strikingly, some trans-Golgi resident golgins including Gcc1/2 and Golga4, normally involved in tethering vesicles containing cargos from

endosomes, were also found in the datasets. In accordance with the recent observation of a COPI-mediated traffic from endosomes to TGN in yeast[113], it calls for further exploring the role of the COPI-mediated routes in endosomal trafficking in mammals that was suggested by several reports more than 20 years ago[263,264]. When comparing the membrane-associated interactome between the two datasets of distinct γ-COP paralogues, only few differences were found. Notably, we found that ERGIC-53, a protein that constitutively cycles between the ER and the cis-Golgi, was exclusively found in the membrane-associated interactome of γ1-COP in P19 undifferentiated cells. This data supports the previous observation of a differential cellular localisation of the different γ-COP containing coatomers with γ1-COP coatomer being preferentially at the cis-Golgi [189]. Indeed, ERGIC-53 is found mostly at the ERGIC, with a small amount detected at the cis-most Golgi cisterna, but never beyond[265].

Additionally, using ultraID to probe the membrane interactome of γ-COPs in P19 differentiated neurons with thresholds set to p-value < 0.01 and FCcutoff for fold change to ±2, 8 proteins were identified in the γ1-COP-specific interactome, and 7 proteins in γ2-COP-specific interactome **(Figure 27 A-C and Tables 12-14).** However, the membrane-associated interactomes of γ1-COP and γ2-COP were also mostly identical in differentiated neurons. Interestingly, the interactomes of γ1-COP and γ2-COP seemed to remodel upon differentiation. For example, ERGIC-53 was found to specifically interact with γ1-COP in undifferentiated cells but was observed in the membrane-associated interactome of both γ1-COP and γ2-COP in neurons. This suggests that in neurons both γ1-COP and γ2-COP are active in the early secretory pathway between Golgi and ERGIC. This might imply that the concentration gradient of the γ-COP paralogues changes during differentiation. The organellar redistribution and morphology change during P19 cells differentiation may also result in the differential localisation of the different γ-COP containing COPI transport vesicles. Moreover, in P19 differentiated neurons, when we set the p value < 0.05 and FCcutoff for fold change to ±2, the proteins identified by the ultraID approach are all Golgi associated proteins (**Tables 15-17**). This confirms that using ultraID approach allowed us to determine a membrane-associated interactome of coatomer that indicates its expected proximal landscape in P19 differentiated neurons. In summary, the strategy proved to be successful as the final datasets contained only Golgi-associated proteins.

When considering the interactomes of γ1-COP and γ2-COP in non-BFA-treated undifferentiated P19 cells only a few differences could be found (**Figure 23 A-B and Table 6-7**). Remarkably, we observed that whereas both ζ1-COP and ζ2-COP interact with γ1-COP,

ζ2-COP was not found to interact with γ2-COP. These findings suggest that only three versions of the coatomer complex exist in undifferentiated P19 cells containing either γ1/ζ1, γ1/ζ2 or γ2/ζ1. This concurs with previous quantification of the relative abundance of the different isotypic coatomer complexes in other cell types, that found that the γ2/ζ2-coatomer was either absent or made, at most, 5% of the total amount of coatomer[75,189]. Recombinant γ2/ζ2-coatomer can be prepared with the same efficiency as the other isotypic coatomer complexes and also demonstrates the same efficiency in producing COPI vesicles in vitro assays[259]. Hence the absence of γ2/ζ2-coatomer in many cell lines may just reflect the lower abundance of both γ2-COP and ζ2-COP compared to γ1-COP and ζ1-COP. It may also suggest that ζ2-COP rather than, or in combination with, γ1-COP may play a key role that cannot be performed by its paralogue during P19 cells neuronal differentiation[75]. Although, in the following proteomics datasets coming from P19 differentiated neurons, we found ζ2-COP associated with both γ1-COP and γ2-COP, it would be interesting to analyse whether a higher level of γ2/ζ2-coatomer combination is detectable in γ1-COP KO cells. If not, this would strongly suggest that ζ2-COP may be most significant during P19 neuronal differentiation.

Compared with the microscopy results from undifferentiated (**Figure 20 A-C and Figure 25 A-C**), we can observe in the differentiated neurons, the localisation of γ-COPs and biotinylated proteins, not only in the cell bodies of neurons but also in the axon hillock (the swelling part start from the axon)[266]. From the literature, it is demonstrated that in primary neurons COPI vesicles are transported along the neurite towards the axonal growth cone where coatomer can be detected[267]. Additionally, redistribution of organellar occurs in neurons. Although a Golgi apparatus cannot be detected in the large majority of dendrites, the neuronal ER distributes throughout the entire cell body to synaptic terminals and thus offers the possibility that COPI mediating retrograde traffic might be detected within neurites[267]. Another possibility is that the intermediate compartment (IC), excluded from dendritic spines and shaft, recruits COPI coats to function in retrograde transfer cargos and escaped ER proteins back to ER[268]. This supports the theory that COPI mediating retrograde traffic might be detected within neurites. There is additional indirect evidence of an active COPI-mediated route in neurites, KDEL receptors, which recycle resident luminal ER proteins with a KDEL signal sequence from the cis-Golgi back to the ER via COPI vesicles, were found to localise to axons[124,269]. Hence, there are multiple lines of evidence that in neurons, COPI vesicles not only mediate transport routes in the cell body but also longer-range trafficking within neurites. This possibly explains the microscopy data in differentiated cells and also the proteomic datasets obtained from P19 neurons.

Indeed, it is reported that about 13% of axonal proteins originated from the secretory pathway are involved in Golgi apparatus[270]. On examining the MS data of γ-COP interactome in P19 differentiated neurons with p value < 0.01 and FCcutoff for fold change to ±2 **(Figure 28 A and B, Tables 18 and 19**), we found that some proteins are involved in the neurite outgrowth significantly enriched in the γ1-COP interactome. This includes a series of proteins including Copper-transporting ATPase 1(Atp7a), Cytoskeleton-associated protein 5 (Ckap5), IST1 homolog (Ist1) and Src substrate cortactin (Cttn). For example, Atp7a is reported to interact with the Golgi-localised COG (conserved oligomeric Golgi complex) tethering complex in order to regulate copper-induced neurodegeneration and synapse development[271]. With a P-value < 0.05 and FCcutoff for fold change to ±2 **(Figure 28 B and Table 20 and 21)** more neurogenesis-related proteins were found significantly enriched in the γ1-COP interactome. These include Kinesin-like protein KIF1B (KiF1b), Rab3 GTPase-activating protein catalytic subunit (Rab3gap1), 14-3-3 protein epsilon (Ywhae), Stathmin1 (Stmn1), Tubulin beta-2B chain (Tubb2b) and Microtubule-associated protein 1B (Map1b). KiF1b is a motor protein mediating transport of axonal vesicles. A strong homology to KiF1b, KiF1c directly interacted with 14-3-3 proteins involved in traffic of vesicles from the Golgi back to ER[272,273]. KiF1b β isoform binding to RAB3 through the adaptors DENN/MADD (Rab3-GEP, Rab3-guanine exchange factor) plays a role on conveying synaptic vesicle precursors to axon terminal for both neurotransmitters and synaptic plasticity[274]. The activity of Rab3 proteins is mediated by Rab3GEP, Rab3GAP and RabGDI (GDP dissociation inhibitor). The first two regulators define the cycle of active-GTP to the inactive-GDP form. Rab3GAP directly combining with Rab3GEP specifically modulates RAB3 activity within axons[249,275-278]. Stathmin1, containing a C-terminal binding with tubulin in a phosphorylation dependent way to regulate microtubule dynamics, plays an essential role on neuronal differentiation[279]. Tubb2b, a tubulin gene responsible for neuronal migration, is a cytoskeleton component in both dendrites and the axon[280]. MAP1B are the main microtubule associated proteins (MAPs) found in axons[281,282]. Microtubules serve as a rail on motor proteins to transport proteins such as kinesin proteins[283]. In fact, previous data supports that γ2-COP containing COPI vesicles are localised within the axon towards the growth cone in primary neurons[186] and the α-subunit of COPI vesicles was detected with partial co-localisation with the survival motor neuron (SMN), SMN can be co-immunoprecipitated with α-COP protein, indicating a direct interaction between α-COP and SMN for the regulation of long-distance traffic in neurites and growth cones[186]. This may suggest that both γ1-COP and γ2-COP containing COPI vesicles may be involved in long-distance transport at the growth cone. However, since we detected

several neurobiogenesis-related proteins that are more enriched in the γ1-COP interactome, it may suggest that γ1-COP is more often in close proximity to these proteins that are important for axon formation and maintenance. This might indicate that γ1-COP-containing coatomer is the coatomer subtype that is preferentially involved in long-range trafficking.

In conclusion, the key findings from the data in this study suggest that γ1-COP play a specific role during neuronal polarisation. By applying an ultraID approach to determine membrane-bound interactome of coatomers, the regulators of the recruitment of coatomer to membranes as well as SNAREs and Golgi tethers were detected as expected. In P19 non-differentiated cells, the datasets revealed that a striking feature is the absence of a γ2/ζ2-coatomer. More γ1-COP-specific interactions in differentiated neurons appear to take place and involve proximity to proteins involved in neuronal polarisation. These proteins will therefore be of prime interest for future studies aimed at understanding how γ1-COP may regulate neuronal polarisation.

4. Materials and Methods

4.1 Materials

4.1.1 Primers and oligos

Table-M1: Oligo

DNA oligo name	Sequence
Oligo crRNAs assay sense strand	AGATTTCAACATGGTGTCAGCGGTAGCTAATTTCTACTAAGTGTAGATTTAACACAGTGGTCTGGGGAAGGGTTTT
Oligo crRNAs assay anti-sense strand	AAAACCCTTCCCCAGACCACTGTGTTAAATCTACACTTAGTAGAAATTAGCTACCGCTGACACCATGTTGAA
Oligo crRNA-2 targets sense strand	CCCCTTCCCCAGACCACTGTGTTAAGAAAGACGT
Oligo crRNA-2 targets anti-sense strand	CTTTCTTAACACAGTGGTCTGGGGAAGGGGAGCT
Oligo AatII-SacI sense strand	GATCCTACCCATACGATGTTCCAGATTACGCTTGA
Oligo AatII-SacI anti-sense strand	TCAAGCGTAATCTGGAACATCGTATGGGTAG

Table-M2: Primers

Primer Name	Sequence
XY11 forward	cgcctggagtcgacggccggGGCGGGCGGGAGTACGGA
XY11 reverse	tattgcggccatgctgcagcTAAAAAAAAAAATCTGTATTGACTCTTGATTGTCTCTTAACAC
XY12 forward	cgctgacaccATGTTGAAGAAGTTCGACAAGAAG
XY12 reverse	aacttcttcaacatGGTGTCAGCGGTAGCTCCACG
XY13 forward	tgacaagtagAGGTGGCCTAAGCCCCAC
XY13 reverse	taggccacctCTACTTGTCATCGTCGTCCTTG
XY14 forward	cgctgacaccATGATTAAGAAGTTCGACAAGAAGGA
XY14 reverse	ttcttaatcatGGTGTCAGCGGTAGCTCCACG
XY15 forward	acagccggagAAGTTGGCTCCTTCCAGG
XY15 reverse	gagccaacttCTCCGGCTGTTTGACTGC
XY16 forward	taagccagagAAGGTAGCAGCCACACGG
XY16 reverse	ctgctaccttCTCTGGCTTAGGAGTCAC
XY18 forward	cgctgacaccATGGTGAGCAAGGGCGAG
XY18 reverse	ttgctcaccatGGTGTCAGCGGTAGCTCCACG
XY35 forward	gtgggctccgcctccggtttACTGCAGGCTAGTGGTGG
XY35 reverse	ttgtagtctgccggtggcttCTACTTCTCCTTGAACTTCTTCAGG
XY36 forward	gtgggatccgcctccggtttACTGCAGGCTAGTGGTGG
XY37 reverse	gccgctcgagCTTCTCCTTGAACTTCTTCAG
XY38 forward	cagggagaagCTCGAGCGGCCGC
XY38 reverse	tattgcggccatgctgcagcTCAAGCAAAGTACATGGTGCGCAGAG
XY 39 forward	cgcctggagtcgacggccggATGGAACAAAAACTCATCTCAGAAGAGG
P-XY 01 forwrd	GGCGGGCGGGAGTACGGAA
P-XY 01 reverse	TAAAAAAAAAAATCTGTATTGACTCTTGATTGTCTCTTAACACAGTGGTCTGGGG

4.1.2 Plasmids and cassette

Table-M3: Plasmids

Constructed Plasmid or Cassette	Description	Manufacturer
pJB354	Doxycycline induction gene expression within PiggyBac (PB) transposon plasmid containing γ1-COP coding sequence and GFP	Generated in Béthune's Lab

pJB354-left HA-γ1-COP-GFP-right HA	Doxycycline induction gene expression within PiggyBac (PB) transposon plasmid containing PCR cassette for γ1-COP KI cell line generation	Generated in Béthune's Lab
pJB354-left HA-γ2-COP-GFP-right HA	Doxycycline induction gene expression within PiggyBac (PB) transposon plasmid containing PCR cassette for γ2-COP KI cell line generation	Generated in Béthune's Lab
pJB354-left HA-GFP-right HA	Doxycycline induction gene expression within PiggyBac (PB) transposon plasmid containing PCR cassette for GFP KI cell line generation	Generated in Béthune's Lab
pJB354-left HA-γ1-2-COP-GFP -right HA	Doxycycline induction gene expression within PiggyBac (PB) transposon plasmid containing PCR cassette for γ1-2-COP KI cell line generation	Generated in Béthune's Lab
pJB354-left HA-γ2-1-COP-GFP -right HA	Doxycycline induction gene expression within PiggyBac (PB) transposon plasmid containing PCR cassette for γ2-1-COP KI cell line generation	Generated in Béthune's Lab

pY109 (lenti-LbCpf1)	Plasmid containing Lenti virus delivery of LbCpf1 and puromycin resistance gene	Addgene
pY109-crRNAs assay	Plasmid containing Lenti virus delivery of LbCpf1, crRNAs array and puromycin resistance gene	Generated in Béthune's Lab
pY109_2-crRNAs array	Plasmid containing Lenti virus delivery of LbCpf1 and crRNAs array without puromycin resistance gene	Generated in Béthune's Lab
pMB1610 pRR-Puro (pMB1610)	Recombination reporter plasmid pMB1610 responsible for a divided puromycin resistance approach to cell selection as its cutting target sequence resulting in Homology-directed repair (HDR)[284] to assist with CRISPR cell lines selection by puromycin treatment	Addgene
pMB1610 pRR-Puro-crRNA2 targets	Recombination reporter plasmid containing crRNA2 targets responsible for a divided puromycin	Generated in Béthune's Lab

	resistance approach to cell selection as its cutting target sequence resulting in Homology-directed repair (HDR)[284] to assist with CRISPR cell lines selection by puromycin treatment	
pJB357	Doxycycline induction gene expression within PiggyBac (PB) transposon plasmid containing γ2-COP coding sequence and GFP	Generated in Béthune's Lab
pJB441	Plasmid containing myc and ultraID coding sequence	Generated in Béthune's Lab
pSF3-BirA R118G-hAgo-2	Plasmid containing Ago2 coding sequence	Generated in Béthune's Lab
indPB4-γ1-COP-ultraID	Doxycycline induction gene expression within PiggyBac (PB) transposon plasmid containing γ1-COP coding sequence, myc and ultraID	Generated in Béthune's Lab
indPB4-γ2-COP-ultraID	Doxycycline induction gene expression within PiggyBac (PB) transposon plasmid containing γ2-COP coding sequence, myc and ultraID	Generated in Béthune's Lab

indPB4-ultraID-Ago2	Doxycycline induction gene expression within PiggyBac (PB) transposon plasmid containing myc, ultraID, Ago2 coding sequence	Generated in Béthune's Lab

4.1.3 Chemicals, kits and enzymes

Table-M4: Chemicals used in this study with their respective product number and manufacturer

Product name	Catalogue Number	Company
1,2-Cyclohexanedione	C101400	Sigma
2-Mercaptoethanol	M6250	Sigma
2-Propanol	33539	Sigma
Acrylamide/Bis-acrylamide (30% solution)	A3699	Sigma
Agar	2235	neoFroxx
Agarose, universal	732-2789P	VWR
Albumin Fraction V (BSA)	8076.2	Carl Roth
Ammonium bicarbonate	A3689	AppliChem
Ammonium peroxydisulfate	9592.2	Carl Roth
Biotin	B4501	Sigma
Bradford reagent (5X)	39222.03	Serva
cOmplete protease inhibitor cocktail tablets, EDTA-free	118735-80001	Roche Diagnostics
Disodium hydrogen phosphate dodecahydrate ($Na_2HPO_4 \cdot 12H_2O$)	28028.298	VWR
Dithiothreitol (DTT)	A2948	AppliChem
EDTA, disodium salt dihydrate	A3553	AppliChem
Ethanol, absolute	20821.33	VWR
Formaldehyde solution (16% w/v)	28906	Thermo-Scientific

Formic Acid	20318.297	VWR
GeneRuler 1 kb Plus DNA ladder	SM1331	Thermo-Scientific
Glycerol	G/0605/15	Fisher Scientific
Glycine	LC-4522.2	neoFroxx
HEPES PUFFERAN	9105.4	Carl Roth
Lithium chloride	12083	Grüssing
Methanol	20847.307	VWR
Milk powder	T145.2	Carl Roth
Mowiol 4-88	81381	Sigma
Mycoplasma Removal Agent	BUF035	Bio-Rad
Nonidet P-40 Substitute	74385	Sigma
Protein ladder(11-245 kDa)	1123YL-500	neoFroxx
Sodium chloride	LC-5932.1	neoFroxx
Sodium cyanoborohydride solution (5.0M in 1M NaOH)	296945	Sigma
Sodium deoxycholate	30970	Sigma
Sodium dihydrogen phosphate dihydrate ($NaH_2PO_4 \cdot 2H_2O$)	12133	Grüssing
SDS salt in pellets	20765.03	Serva
SDS solution (20%)	5030	Sigma
Sodium hydroxide (NaOH)	30620	Sigma
Streptavidin Sepharose High Performance	Lot 10280314 GE17-5113-01	GE Healthcare
TEMED	T9281	Sigma
TRIS PUFFERAN	4855.2	Carl Roth
Triton X-100	X100	Sigma
Tween 20	9127.1	Carl Roth
Q5 High-Fidelity Master Mix (2X)	M0492S	NEB

Table-M5: Kits used in this study with their respective product number and manufacturer

Product name	Catalogue Number	Company
FastGene Gel PCR Extraction Kit	FG-91302	Nippon Genetics
GenElute HP Plasmid Midiprep Kit	NA0200	Sigma
GenElute HP Plasmid Miniprep Kit	NA0160	Sigma
Quick Ligation Kit	M2200S	NEB
QIAamp DNA Mini Kit	51304	Qiagen
FAM-FLICA® Caspase Assays	Caspase-3/7 FAM-DEVD-FMK (653)	Bio-Rad

Table-M6: Enzymes used in this study with their respective product number and manufacturer

Enzyme	Catalogue Number	Company
EcoRI-HF	R3101S	NEB
FseI	R0588S	NEB
MluI-HF	R3198S	NEB
NotI-HF	R3189S	NEB
PmeI	R0560S	NEB
AvrII	R0174S	NEB
BsmbI	R0739	NEB
BamHI HF	R3136S	NEB
AatII	R0117S	NEB
SacI	R3156	NEB
BsrGI-HF	R3575S	NEB

4.1.4 Medium, buffer and supplements for Prokaryotic strains culture

Table-M7: Prokaryotic strains

Strain Species	Company	Application

DH5α E.Coli	Invitrogen	Cloning

Table-M8: Prokaryotes culture medium

Name	Ingredients	Manufacturer	Catalogue Number
LB Medium	Bacto Tryptone 1% (w/v)	BD	211705
	Bacto Yeast 0.5% (w/v)	Roth	2363.3
	NaCl 1% (w/v)	Sigma	31434
	Adjusted to pH 7.0	-	-
LB Agar	LB Medium	-	-
	Agar 1.5% (w/v)	Fluka	05040
LB Plates	LB Agar	-	-
	Ampicillin 100 µg/mL	Sigma	A9518
SOB	Bactotryptone 2% (w/v)	BD	211705
	Bactoyeast 0.5% (w/v)	Roth	2363.3
	Adjusted to pH 6.7-7	-	-
	NaCl 10 mM	Sigma	31434
	KCl 2.5mM	AppliChem	A3582
	MgCl2 10 mM	AppliChem	A3618
	MgSO4 10 mM	Millipore	1.05886
SOC	SOB medium	-	-
	Glucose 20mM	Sigma	158968

Table-M9: Other chemical stuff for prokaryotes culture

Name	Manufacturer	Catalogue number	Concentration
Ampicillin	Sigma	A9518	100 µg/mL

LB, LB-Agar and SOB medium were autoclaved prior to use.

4.1.5 Cell lines

Table-M10: Eukaryotic strains

Constructed cell line	Species	Target cell line	Manufacturer
-	Mouse	P19 WT	Sigma (95102107)

P19 Copg1$^{-/-}$	Mouse	P19 WT	Generated in previous study in Bethune's Lab
P19 Copg2$^{-/-}$	Mouse	P19 WT	Generated in previous study in Bethune's Lab
γ1-COP-GFP KI	Mouse	P19 WT	Generated in this study in Bethune's Lab
GFP KI	Mouse	P19 WT	Generated in this study in Bethune's Lab
γ2-COP-GFP KI	Mouse	P19 WT	Generated in this study in Bethune's Lab
γ1-2-COP-GFP KI	Mouse	P19 WT	Generated in this study in Bethune's Lab
γ2-1-COP-GFP KI	Mouse	P19 WT	Generated in this study in Bethune's Lab
T-Copg1-ultraID#2	Mouse	P19 Copg1$^{-/-}$	Generated in this study in Bethune's Lab
T-Copg2-ultraID#2	Mouse	P19 Copg2$^{-/-}$	Generated in this study in Bethune's Lab
T-ultraID-Ago2	Mouse	P19 WT	Generated in this study in Bethune's Lab

4.1.6 Medium, buffer and supplements for cell culture

Table-M11: Chemicals for cell culture

Name	Company	Catalogue number	Concentration
Alpha-MEM	Sigma	M4526	88% (v/v)
Fetal Bovine Serum (FBS)	BioWest	S181B	10% or 5%(v/v)
L-Glutamine 200mM (100X)	Gibco	25030-024	2 mM (1% (v/v))
Penicillin-Streptomycin	Gibco	15140-122	1%(v/v)
Hygromycin B	Sigma	H0654	150 μg/mL
Retinoic Acid	Sigma	R-2625	0.5 μM
AraC	Sigma	C1768	10 μM
Tunicamycin	Sigma	SML1287	5 mg/mL in DMSO

Staurosporine	Sigma	S6942	1mM in DMSO
D-PBS	Sigma	D8537	1X
Trypsin-EDTA (1X)	Gibco	25300-054	0.05%
TrypLE Express Stable Trypsin Replacement Enzyme	Gibco	12605-010	1X
DMSO	Sigma	D2438	10%(v/v) in FBS
Cell dissociation buffer	Gibco	13151014	5%(v/v) in Alpha-MEM
Poly-L/D-Lysine	Sigma	P0899	0.1mg/ml
DNAseI	Applichem	A3778	50µg/ml
Doxycycline hyclate	AppliChem	A2951	5ng/ml
Ampicillin	Sigma	A9518	100 µg/mL
Jet-Prime	Polyplus transfection	114-01	-

4.1.7 Buffer and chemical stuff

Table-M12: Buffers

Buffers or solutions	**Ingredients**
Tris Acetate - EDTA (TAE)	40 mM Tris (pH 8) 40 mM Acetic Acid 1mM EDTA (pH 8)
phosphate buffer saline (PBS)	126mM NaCl 89mM Na_2HPO_4 23mM NaH_2PO_4
0.1% PBST	1X PBS + 0.1% Tween 20(v/v)
Buffer for antibody dilutions	2% BSA in 0.1%PBST
SDS PAGE running buffer	25 mM Tris 192 mM glycine 0.1% SDS
Wet transfer buffer for WB	25 mM Tris 192 mM glycine 20% methanol

stacking gel for SDS PAGE	5% acrylamide 130 mM Tris-HCl (pH 6.8) 0.1% SDS 0.1% ammonium persulfate 0.1% tetramethylethylenediamine (TEMED)
separating gel for SDS PAGE	12% or 8% acrylamide 375 mM Tris-HCl (pH 8.8) 0.1% SDS 0.1% ammonium persulfate 0.04% TEMED
blocking solution for WB	5% skimmed milk powder in PBS
Mowiol mounting medium	6.0g glycerol (100%) 2.4g Mowiol 4-88 6.0 ml milliQ water 12 ml Tris-HCl (0.2M, pH 8.5)
RIPA lysis buffer for WB	25mM Tris-HCl (pH 7.4) 150mM NaCl 1mM dithiothreitol (DTT) 1X Protease Inhibitor Cocktail (PI)
Lysis buffer for MS	50 mM Tris pH 7.4 500 mM NaCl 0.4% SDS 5 mM EDTA (PH8.0) 1 mM DTT 1X Protease Inhibitor Cocktail (PI)
equilibration buffer	50mM Tris-HCl pH 8.0 150mM NaCl 0.1% SDS 0.5% sodium deoxycholate 1% Triton X-100 1mM DTT
wash buffer 1	2% SDS in HPLC grade water

wash buffer 2	0.1% sodium deoxycholate 1% Triton X-100 500mM NaCl 1mM ethylenediaminetetraacetic acid (EDTA) 50mM HEPES (pH 7.4)
wash buffer 3	10mM Tris-HCl (pH 8.0) 250mM LiCl 1mM EDTA 0.5% NP-40 0.1% sodium deoxycholate
wash buffer 4	50mM NH4HCO3
5XSDS loading dye	5% β-mercaptoethanol 0.02% bromophenol blue 10% SDS 30% glycerol 250mM Tris-HCl (pH 6.8)

4.1.8 Antibodies

Table-M13: Primary antibodies

Antibody	**Host**	**Company (catalogue number)**	**Application and dilution**
anti-γ1-COP	Rabbit	Wieland group (BZH, Heidelberg)	WB, 1:800
anti-γ2-COP	Rabbit	Wieland group (BZH, Heidelberg)	WB, 1:800
anti-ß-Tubulin (TujI/TUBB3)	Mouse	Biolegend (MMS435P25)	IF, WB, 1:1000
anti-α-COP (1409B)	Rabbit	Wieland group (BZH, Heidelberg)	WB, 1:4000
anti-GAPDH	Mouse	Proteintech (60004-1-Ig)	WB, 1:15000
anti-GRP78	Rabbit	Proteintech (T5168)	WB, 1:1000
anti-CHOP	Rabbit	Proteintech	WB, 1:200

		(15204-1-AP)	
anti-myc (71D10)	Rabbit	Cell Signaling Technology (#2278S)	IF,1:400
anti-GM130	Mouse	BD Biosciences	IF,1:500

Table-M14: Secondary antibodies

Secondary antibody	**Host**	**Company (catalogue number)**	**Application and dilution**
anti-mouse IgG IRDye 800CW	goat	LI-COR (926-32210)	WB, 1:15000
anti-mouse IgG Alexa Fluor 680	goat	Thermo Scientific (A21057)	WB, 1:10000
anti-rabbit IgG IRDye 800CW	goat	LI-COR (926-32211)	WB, 1:15000
anti-rabbit IgG IRDye 680CW	goat	LI-COR (926-68071)	WB, 1:15000
anti-mouse Alexa 647	donkey	Invitrogen (A28175)	IF, 1:1000
anti-mouse Alexa 546	goat	Invitrogen (A11030)	IF, 1:1000
anti-rabbit Alexa 488	goat		IF, 1:1000
Streptavidin-Alexa Fluor 647	-	Jackson ImmunoResearch (016-600-084)	IF, 1:1000
Streptavidin-DyLight680	-	Invitrogen (21848)	IF, 1:1000

4.1.9 Equipment

Table-M15: Equipment

Equipment	**Manufacturer**
Bioruptor Next Gen	Diagenode
FlexCycler2 PCR Thermal Cyclers	Analytik Jena
NanoDrop ND-1000 Spectrophotometer	NanoDrop Technologies
Nikon Eclipse TS 100 Inverted Microscope	Nikon

Odyssey Clx Imaging System	LI-COR
Steri-Cycle CO2 Incubator	Thermo Fisher Scientific
SteriMax smart Infrared Loop Sterilizer	WLD-TEC
TC 20 Automated Cell Counter	Bio-Rad
Ti-HCS widefield microscope	Nikon
Nikon VoX-Ti spinning disk confocal microscope	Nikon

4.2 Molecular Biological Methods

4.2.1 Plasmids and PCR cassette constructs

In this thesis, two groups of plasmids, or PCR cassettes, were constructed to generate CRISPR knock-in cell lines and cell lines for the doxycycline-induced expression of ultraID-tagged proteins (indicated as CRISPR group and ultraID group respectively). In the CRISPR group, the newly synthesis DNA constructs include CRISPR donor PCR cassettes, Py109-crRNAs assay, Py109_2-crRNAs array and pMB1610-crRNA2 targets. Before CRISPR donor PCR cassettes were amplified, they were cloned to the pJB354 vector to store as a PCR template (**Table 22**).

The features of pY109 (lenti-LbCpf1) vector contain Lenti-virus delivery of Cas12a/Cpf1 gene and a BsmBI cloning cassette for insertion of Cas12a/Cpf1 guide RNAs under a U6 promoter control. The CHOPCHOP tool was adopted to select two crRNAs that target the 5'UTR and 3'UTR regions in the Copg1 gene[285] and that were cloned as a dual crRNA expression array (Oligo crRNAs array) between the BsmbI sites of the pY109 (lenti-LbCpf1) plasmid [286] to construct the plasmid Py109-crRNAs array, as presented in **Table 23**. Additionally, the Oligo AatII and SacI were cloned into the pY109-crRNAs array vector in order to remove the puromycin selection gene to construct the plasmid Py109_2-crRNAs array (**Table 24**) for the subsequent CRISPR knock-in cell line generation. The recombination plasmid pMB1610 pRR-Puro (pMB1610) carries a split puromycin resistance cassette that can re-assemble in a functional puromycin resistance cassette when the split cassette is cleaved by a Cas protein and repaired by Homology-directed repair (HDR), this reporter plasmid allows selected those cells in which Cas-mediated cleavage and HDR occured[284]. The target sequence of crRNA2 was inserted between the two puromycin resistance split cassettes in pMB1610 to construct plasmid pMB1610-crRNA2 targets (**Table 25**), then, once the crRNA2-guided Cas12a induced the DNA strand break, a functional puromycin resistance

occurred via HDR. The insert was ligated into the corresponding plasmid vector through a quick ligase, as seen in **Table 23-25**.

Table 22 shows that all the fragments assembled together and cloned into the coresponding plasmid vector using NEBuilder HiFi DNA Assembly Master Mix (NEB) to construct the plasmid for the following generation of stable cell lines. The vector was generated by digestion with restriction enzymes. The homology arms (HA) were amplified using genomic DNA from the P19 WT cells. Genomic DNA was extracted using the QIAamp DNA Mini Kit, as according to the manufacturer's instructions. All the γ-COPs and GFP fragments were amplified based on pJB354 and pJB357 containing a full length γ1-COP-GFP coding sequence and full length γ2-COP-GFP coding sequence as a PCR template. Finally, the repair templates for HDR were all amplified to produce CRISPR donor PCR cassettes for the subsequent generation of CRISPR knock-in cell lines.

In the ultraID group, the newly synthesis plasmids contain indPB4-γ1-COP-ultraID, indPB4-γ1-COP-ultraID and indPB4-ultraID-Ago2. In order to introduce ultraID at the C-terminal of the two different γ-COP paralogues, the NEBuilder HiFi DNA Assembly Master Mix (NEB) was used to assemble a myc-ultraID cassette into the vectors of either pJB354-2 or pJB357-2 (**Table 26**). pJB354 and pJB357 vectors harbours the genes necessary for a doxycycline-dependent induction of gene expression within a PiggyBac (PB) transposon cassette. Additionally, the Ago2 tagged with ultraID at the N-terminal was assembled to the vector of pJB354-1 as a control plasmid (**Table 26**). Myc-ultraID fragment was then amplified based on pJB441. The Ago2 fragment was amplified based on pSF3-BirA R118G-hAgo-2. All the plasmids information are listed in **Material 4.1.2**.

Table 22: Donor PCR cassettes for generating CRISPR knock-in cell lines

Plasmid vector	Inserts				Constructed Plasmids	PCR cassettes	Generated cell line
	Fragment-C1	Fragment-C2	Fragment-C3	Fragment-C4			
pJB354 vector-1	HA-1 left	Copg1-GFP	HA right	null	pJB354-left HA-γ1-COP-GFP-right HA	left HA-γ1-COP-GFP-right HA	γ1-COP-GFP KI
pJB354 vector-1	HA-2 left	Copg2-GFP	HA right	null	pJB354-left HA-γ2-COP-GFP-right HA	left HA-γ2-COP-GFP-right HA	γ2-COP-GFP KI
pJB354 vector-1	HA-G left	GFP-HA right	null	null	pJB354-left HA-GFP-right HA	left HA-GFP-right HA	GFP KI
pJB354 vector-1	HA-1 left	Copg1 trunk	Copg2 appendage-GFP	HA right	pJB354-left HA-γ1-2-COP-GFP-right HA	left HA-γ1-2-COP-GFP-right HA	γ1-2-COP-GFP KI
pJB354 vector-1	HA-2 left	Copg2 trunk	Copg1 appendage-GFP	HA right	pJB354-left HA-γ2-1-COP-GFP-right HA	left HA-γ2-1-COP-GFP-right HA	γ2-1-COP-GFP KI

HA left = homology arms at 5' UTR in Copg1 locus (75bp)

HA right = homology arms at 3'UTR in Copg2 locus (55bp)

Table 23: Py109-crRNAs assay plasmids containing a Cas12a/Cpf1 gene and crRNA arrays for the generation of CRISPR knock-in cell lines

Plasmid vector	Inserts	Constructed Plasmids	Generated cell line
pY109 (lenti-LbCpf1) vector	Oligo crRNAs array (the annealing oligo of crRNA1 and crRNA2)	pY109-crRNAs array	CRISPR knock-in cell lines

Table 24: Py109_2-crRNAs array plasmid originating from Py109-crRNAs assay plasmid formed by puromycin selection gene deletion for the generation of CRISPR knock-in cell lines

Plasmid vector	Inserts	Constructed Plasmids	Generated cell line
pY109-crRNAs array vector	Oligo AatII-SacI	pY109_2-crRNAs assay	CRISPR knock-in cell lines

Table 25: Recombination reporter plasmid (pMB1610-crRNA2 targets) to assist with CRISPR cell line selection via puromycin treatment

Plasmid vector	Inserts	Constructed Plasmids	Generated cell line
pMB1610 vector	Oligo crRNA2 targets	pMB1610-crRNA2 targets	CRISPR knock-in cell lines

Table 26: Doxycycline induction gene expression within a PiggyBac (PB) transposon plasmid for the generation of protein coding gene tag ultraID cell lines

Plasmid vector	Inserts		Constructed Plasmids	Generated cell line
	Fragment-u1	Fragment-u2		
pJB354 vector-2	ultraID	null	indPB4-γ1-COP-ultraID	T-Copg1-ultraID#2
pJB357 vector-2	ultraID	null	indPB4-γ2-COP-ultraID	T-Copg2-ultraID#2
pJB354 vector-1	ultraID	Ago2	indPB4-ultraID-Ago2	T-ultraID-Ago2

4.2.2 Restriction digestion

For the following Gibson assembly or ligation experiment, 2.5µg of plasmid DNA was digested in a recommended buffer for a period of 1.5-2 h, with restriction enzymes purchased from NEB. Prior to DNA sequencing, samples were usually pre-selected through a preparative restriction digestion using 750µg of plasmid. The restriction digest protocols for the subsequent cloning are described in **Supplementary Table 1** at the end of the thesis.

4.2.3 Oligo annealing

In order to clone the Py109-crRNAs assay plasmids, the annealing of a crRNAs assay (Oligo crRNAs array) was incubated at 95°C for 5 mins, after which the temperature was decreased to 25°C at a rate of 0.1°C per sec. After this, the assay was kept at room temperature for subsequent ligation. In addition to the above annealing protocol, other reactions to form the Py109-crRNAs assay and Py109_2_crRNA assay plasmids were carried out at 95°C for 5 mins, according to an incubation at a decreased temperature of 37°C for a period of 1h. All the reactions were performed as follows in **Supplementary Table 2** at the end of the thesis, and all the oligo sequences are listed in **Material 4.1.1**.

4.2.4 Polymerase chain reaction (PCR)

To purify all the DNA fragments for the following experiment, the PCR reactions were all performed using a Q5 High Fidelity DNA Polymerase (NEB), as well as primers (0.5μM) and a template DNA(<1ug) in the thermal cycler FlexCycler2 (Analytic Jena). The denature temperature was usually set to 98°C, while an elongation was performed at a temperature of 72°C. The elongation time was calculated based on the assumption that 1 kilobase of DNA was replicated over 20-30s. In the P19 cells meanwhile, the PCR reactions were all performed using Taq DNA Polymerase (NEB), primers (0.2μM), dNTPs (200μM) and template DNA(<1ug) in a thermal cycler FlexCycler2 (Analytic Jena). This was done in order to map whether the desired inserts were successfully knocked in the Copg1 locus. The denature temperature was 95°C and the elongation temperature was 68°C. The polymerase extension speed was 60s per kilobase. All the annealing temperatures were individually determined, and calculated using the online NEB tool. The PCR protocols are described in **Supplementary Table 3** at the end of the thesis and all the primer sequences are listed in **Material 4.1.1**

4.2.5 Agarose Gel Electrophoresis

Agarose gels were prepared using 1-2 % (w/v) agarose dissolved in TAE buffer depending on product size, with the addition of 1:150000 diluted Red Safe TM stain (iNtRON Biotechnology). DNA samples were mixed with 6× Purple loading Dye (NEB) before loading. 1kb plus DNA ladder GeneRuler^{TM} (NEB) was used to identify the size of the DNA prior to electrophoresis. Agarose gels were inspected with Bio-Rad GelDoc system under UV

irradiation. To cut excise bands for DNA extraction, LED Iluminator (INTAS) was used to prevent UV-induced DNA mutations.

4.2.6 Gel Extraction and PCR product Purification

The required digested plasmids vector and PCR fragments were routinely purified through gel extraction using a Gel extraction or PCR purification kit (FastGene) according to the manufacturer's manuals.

4.2.7 Ligation

30-100 ng of plasmid DNA was mixed with up to 3 to 6-fold molar insert in the Quick ligation buffer and Quick ligase (NEB). The reaction was then incubated for 15-20 min at room temperature.

4.2.8 Gibson assembly

50-100 ng of plasmid DNA was mixed with up to 1 to 9-fold molar insert together with the NEBuilder HiFi DNA Assembly Master Mix (NEB). Following this, the reaction was incubated for a period of 45 min to 1h at a temperature of 50°C.

4.2.9 Transformation of E. coli

50 µl of chemically competent DH5α strain cells were mixed with 2-5µl of Gibson assemble reaction product, and the mixture was incubated for 30-45 min on ice. Heat shock was performed for 45 sec. at 42°C, which was followed by incubation back on ice for 2 min. The pre-warmed SOC medium (250-950µl) was added to the mixture, and transferred to a shaking thermal block at 37°C under agitation for 1h. The transformed cells (20µl to 200µl) were streaked onto the Ampicillin resistance LB plates, and transferred at 37°C overnight. 4-6 colonies were picked in each construct.

4.2.10 Plasmids purification and Determination of DNA concentration

Plasmids were isolated using the Plasmid Mini or Midi Kit GeneElute HP (Sigma) following the protocol of the manufacturer. The concentration of samples was detected with ND-1000 spectrophotometer from PeqLab (Erlangen, Germany).

4.2.11 Plasmids Precipitation

For subsequent stable cell lines construction, ethanol precipitation was performed. DNA samples were mixed with 3 volumes of cold 100 % ethanol and 0.1 volume of 3 M sodium acetate. The mixture was incubated at -20°C for 30 min, and then centrifuged at 17,000 g for 30min at 4°C. The pellet was washed once with cold 70 % (v/v) ethanol, and centrifuged at 17,000 g for 15min at 4°C. The precipitated DNA in the pellet was aired dry in cell culture hood for 10 min, and resuspended in desired volume of sterile elution buffer.

4.3 Cell biology methods

4.3.1 Cell culture

P19 cells were cultured in P19 growth medium containing alpha MEM which was supplemented with 10 % heated inactivation of fetal bovine serum (FBS), 1% Pen/Streptomycin and 1% Glutamine, at 37°C with 5% CO_2. Once the cells reached 80 % confluence, they would be dissociated through the addition of Trypsin/EDTA (Sigma, Germany), and split in the ratio of 1:10 in a new 10cm or 15cm cell culture dish every two days. Mycoplasma PCR detection kit (Mycoscope, Genlatis) was regularly utilized to detect the contamination of mycoplasma.

4.3.2 Heat inactivation of serum

500ml of FBS was thawed in a fridge at 4°C overnight. In the following day, the thawing was completed in water bath at 37°C with inverted mixing every 10 min, and to equilibrate the temperature of 37°C, an additional incubation of 15 min. is necessary once serum is totally thawed. Then, the temperature was increased to 56°C, and serum was kept for 65 mins with inverted mixing every 10 min.

4.3.3 Generation of stable cell lines

4.3.3.1 Construction of CRISPR knock-in cell lines

CRISPR knock-in cell lines were established in this thesis in order to specifically express γ1-COP-GFP, GFP, γ2-COP-GFP, γ1-2-COP-GFP and γ2-1-COP-GFP from the Copg1 locus-designated P19 γ1-COP-GFP KI cell line, GFP KI, γ2-COP-GFP KI, γ1-2-COP-GFP KI and γ2-1-COP-GFP KI, respectively. The schematic figures of CRISPR cell line generation were shown in **Figure 5 and 11**. One day before transfection, 200,000 cells per well were seeded in six-well plate. The CRISPR-Cas12a/Cpf1 gene editing strategy was applied by the co-transfection of 1μg donor template with the homology arm (CRISPR donor PCR cassettes list in Table 22), 1.5μg crRNAs array (pY109_2-crRNAs array) and 0.5μg recombination reporter plasmid for selection (pMB1610-crRNA2 targets) of P19WT cells using Jet-PRIME regent. Detailed plasmid construction method on this was proposed in **Method 4.2.1** and **Tables 23-25**. The pMB1610-crRNA2 targets contains two puromycin fragments and target sequence of crRNA2 between the two puromycin fragment[284]. After the sequence of crRNA2 targets was cut by crRNA array guided Cas12a, the functional puromycin resistance was repaired via HDR for cell selection. 24h after transfection, cells were treated with 4μg/ml puromycin supplemented medium for 48h. Then, the selected cells were transferred to a 10 cm dish and after getting 70% confluent, GFP-positive pool was sorted by FACS. Single GFP-positive cells were sorted to 96-well plate from the expansion of GFP-positive pools by FACS to acquire the cells including P19 γ1-COP-GFP KI cell line, GFP KI and γ2-COP-GFP KI. In addition, instead of the single cell screening, γ1-2-COP-GFP KI and γ2-1-COP-GFP KI were obtained by cell colony picking using the GFP-positive pools above selected from FACS. All the clonal cells demonstrated a Golgi-localized GFP signal were remained for subsequent western blot analysis. The clones only expressing the migrated GFP tagged γ1-COP and γ2-COP were kept for verification of bi-allelic insertion by PCR mapping. With these analyses, all the CRISPR cell lines constructed in the thesis were identified as the exogenous bi-allelic insertions. All the cell lines information is listed in **Material 4.1.5**.

4.3.3.2 Construction of a doxycycline inducible ultraID tag gene expression cell lines

In this thesis, CRISPR knock-in cell lines were established to specifically express γ1-COP-GFP,

GFP, γ2-COP-GFP, γ1-2-COP-GFP and γ2-1-COP-GFP from the Copg1 locus-designated P19 γ1-COP-GFP KI cell line, GFP KI, γ2-COP-GFP KI, γ1-2-COP-GFP KI and γ2-1-COP-GFP KI respectively. The schematic figures of CRISPR cell line generation are shown in **Figure 5 and 11**. One day before transfection took place, 200,000 cells per well were seeded in a six-well plate. The CRISPR-Cas12a/Cpf1 gene editing strategy was applied using the co-transfection of a 1μg donor template with a homology arm (the CRISPR donor PCR cassettes are listed in Table 22), a 1.5μg crRNAs array (pY109_2-crRNAs array) and a 0.5μg recombination reporter plasmid for selection (pMB1610-crRNA2 targets) of P19WT cells using a Jet-PRIME regent. The detailed process of this plasmid construction method is shown in **Method 4.2.1** and **Tables 23-25**. The pMB1610-crRNA2 targets contained two puromycin fragments and a crRNA2 target sequence between the two puromycin fragments[284]. After the sequence of crRNA2 targets was cut using a crRNA array guided Cas12a, the functional puromycin resistance was repaired via HDR for cell selection purposes. 24h after transfection, the cells were treated with 4μg/ml puromycin supplemented medium for 48h. Then, the selected cells were transferred to a 10cm dish, and after becoming 70% confluent, a GFP-positive pool was sorted via FACS. Single GFP-positive cells were sorted in a 96-well plate from the expansion of GFP-positive pools via FACS, to acquire the cells including P19 γ1-COP-GFP KI cell line, GFP KI and γ2-COP-GFP KI. In addition, instead of the single cell screening, γ1-2-COP-GFP KI and γ2-1-COP-GFP KI were obtained via cell colony picking using the GFP-positive pools above, which were themselves selected from FACS. All the clonal cells that demonstrated a Golgi-localized GFP signal were kept for subsequent western blot analysis. The clones only expressing the migrated GFP tagged γ1-COP and γ2-COP were kept for verification of bi-allelic insertion via PCR mapping. After the above mentioned analyses, all the CRISPR cell lines constructed in the thesis were identified as exogenous bi-allelic insertions. All the cell line information is listed in **Material 4.1.5**.

4.3.4 Plasmids transfection

P19 cells were seeded at 100,000 cells per well of a 6-well plate. On the next day, transfection was performed with precipitated sterile DNA (2-5μg). In this respect, the DNA was dissolved in 200μl Jet-PRIME buffer by vortex for 10s. After spinning down, Jet-PRIME reagent was mixed with the DNA containing the diluted buffer in the ratio of 1:2 (mass of DNA in the unit of μg: volume of Jet-Prime Reagent in the unit of μl), and incubated for 10 min at room temperature. The transfection mixture with 1.8 ml P19 growth medium was added to the cells

in 6-well plate, and maintained in the incubator at 37°C overnight for subsequent experiments.

4.3.5 Fluorescence-Activated Cell Sorting (FACS)

Detached cells were resuspended in serum free media supplemented with 5% dissociation buffer, and centrifuged at 500g for 5 min. at room temperature. The pellet was resuspended in 500ul-1ml serum free media with 5% dissociation buffer. Cell strainer was applied for cell path-through to remove the cell clumps. GFP positive cell pools were selected by FACS and put into a 10cm dish. After the culture for a few days, Single GFP positive cells in those cell pools were sorted by FACS again, and transferred to 96 plates. Cell colonies were grown, and transferred into a lager plate. Using fluorescence microscopy, the clones that displayed a Golgi-like GFP signal were selected for further screening with western blot.

4.3.6 Cell Colony picking

To collect cell colony, 500 cells were seeded in the 10cm dish. One week or two weeks later, when the diameter of the colony was about 2mm, paper cloning discs soaked with trypsin was placed on the cell colony for 3min. The cells were stuck to the paper, which was dispensed to 500µl fresh P19 growth media in 24 well plates. After dislodging the cells from the paper disc, the well plate was kept in the incubator at 37°C overnight. The next day, prior to feeding the fresh medium to the well, the paper disc was removed. One week later, the cells were transferred to 6 well plates.

4.3.7 Poly-D-Lysine coating

The plate surface was coated with 0.1mg/ml Poly-D-Lysine (1.0 mL/25 cm^2) for 10 minutes. After the removal of the solution, the surface was washed with sterile water twice. Prior to introducing the medium and cells, the plate were allowed to dry for at least 2 hours in the incubator at 37°C.

4.3.8 Hanging drop assay

10,000 cells/ml dilution was treated with 0.5µM RA in P19 induction medium, and loaded at the rate of 20µl per drop to the inside lid of a 10 cm bacterial dish filled with 10 ml PBS to

prevent the drop from drying. Using 10X air objective, the images of separate drops on Day 2 and Day4 were adapted by a Nikon TS100F microscope suited with a CMOS camera (Imaging source, DMK 23UX174).

4.3.9 P19 cells differentiation

A two-step protocol was adopted during the differentiation of P19 cells into neurons. In the first step, 10^6 cells were cultured in P19 induction medium containing 0.5μM RA, thus forming the cell aggregates which we called embryoid body in nonadherent bacterial dish (10cm). After the fresh of two days, P19 induction media was replaced by 0.5μM RA. Two more days later, the embryoid bodies were collected by centrifuging at 1100g for 5min at room temperature, and washed once with serum free αMEM medium (Sigma-Aldrich) media. Then, the pellet was dissociated using 2ml trypsin with 50μg/ml DNAseI to prevent the formation of DNA gel for 10 min. at 37°C. To neutralize the trypsin, 4ml of P19 growth media was added, and the cells were centrifuged at 1100g for 5mins at room temperature. To remove the clumps, the resuspended cells in P19 growth media passed through the BD strainer, and were seeded onto poly-D-lysine coated plate. The cell density was $7.8*10^4/cm^2$. After the plating of 48h, the medium was replaced by P19 growth medium containing 10μM of Ara-C to knock off dividing cells.

4.3.10 COPI formation inhibition and biotinylation induction

The cells were incubated with doxycycline (5 ng/ml) for a period of 24 h-48 h prior to the following induction. To inhibit the COPI formation, the medium was exchanged for the P19 growth medium supplemented with 5 μg/ml Brefdin A (BFA) while the P19 growth medium meanwhile, was adopted for the other samples. After an incubation of 1 h, 50 μM of biotin was added to the cells in all the samples and incubated at 37°C for 4 h. Thereafter, a preparation of western blot, immunostaining or MS sample was performed.

4.3.11 Immunostaining

For neuron differentiation, after RA induction, $7.8*10^4$ cells/well were seeded in poly-D-lysine-coated 8-well μ-slides to complete the differentiation according to P19 differentiation protocol. While, for the undifferentiated ultraID cells, $2*10^4$ cells/well were seeded in 8-well

μ-slides combined with a doxycycline, biotin or BFA induction dependent manner. After differentiation or induction, the cells were carefully washed once with PBS, and incubated with cold methanol for 10 min. at -20 °C for permeabilization and fixing. After that, the cells were washed twice with 2% BSA in PBS, and blocked with 10% BSA in PBS for 45 min at room temperature. The cells were subsequently incubated with specific primary antibody overnight at 4°C. In the following day, the cells were washed for 3 times with 2% BSA in PBS, and incubated with secondary antibodies for 45min at room temperature in the darkness. After being washed for 3 times, the samples were subjected to DAPI (0.1μg/mL in PBS) for 10 min at room temperature in the darkness. Prior to adding Mowiol mounting medium dropwise into the wells, three gentle washes were completed with PBS.

4.3.12 Cellular apoptosis detection

For the validation of the cell lines' apoptosis, a FAM FLICA Caspase-3/7 assay (Cat. no. ICT093; Bio-Rad) was performed in order to detect the caspase activation according to the manufacturer's instructions by a BD FACS Canto flow cytometer. 30X FLICA was incubated with 5*105 cells/ml per sample for 2 h at 37°C. Additionally, Propidium Iodide PI staining was an effective analytical tool to distinguish between living and dead cells.
The following controls were involved in the PMT voltage settings and fluorescent compensation adjustments. The cells were induced with 1 μM of staurosporine for 20 h for the apoptosis positive control. Moreover, ethanol was used to kill the cells, which thereby created PI positive controls.

4.3.13 Fluorescence microscopy techniques

In order to properly observe the neurites extension in CRISPR cell lines, images of the differentiated neurons were taken using a Nikon Ti-HCS widefield microscope fitted with a Nikon DS-Qi2 high-sensitive CMOS monochrome camera. The camera had a resolution of 2404 x 2404 pixel thanks to the use of a Nikon Plan Fluor 10x NA 0.3 phase contrast objective which had a 0.73 μm pixel size. Furthermore, in order to observe the colocalization of the ultraID fusion proteins and biotinylated proteins in ultraID cell lines, images of the undifferentiated cells were taken using a Nikon VoX-Ti spinning disk confocal microscope. This was carried out at the Nikon Imaging Centre in Heidelberg, where the microscope was fitted out with a Yokagawa CSU-X1 confocal scanning unit, a Hamamatsu C9100-02

EMCCD camera with a 1000 x 1000 pixel resolution and a Nikon Plan Apo VC 100x NA 1.4 oil immersion objective with an 8 μm pixel size.

4.4 Biochemical Methods

4.4.1 Cell lysis for western blot

The suspended cells were collected by centrifuging at 1100g for 5mins at room temperature. The sample was washed once by PBS, and the pellet was recovered. Based on the size of cell pellet, appropriate lysis buffer was added on ice. For adherent cells, after the removal of the medium, the cells were rinsed by chilled PBS, and lysis buffer was added on ice. Prior to the transference to EP tube, the cells were lysed using cell scraper. Lysed samples were kept on ice and sonicated (Bandelin SONOREX, TYP: RK31) every 10 min. for 30 sec. (repeated for 3 times). Then, lysates were centrifuged at 17000g for 45min. at 4°C. The supernatant was collected for subsequent experiment.

4.4.2 Sodium-dodecyl sulfate polyacrylamide gel electrophoresis (SDS-PAGE)

To identify the different protein expression based on molecular weight, the SDS-PAGE was adopted to separate the protein[287]. SDS Gel is composed of two different layers which are stacking gel to line up all the protein samples loaded on the gel, and separating gel. The stacking gel was produced under the final acrylamide concentration of 5%. For separating gel, the final acrylamide concentration was determined according to the proteins to be evaluated ranging from 8% to 12% of resolving gel or 4-20% gradient gels. The samples running in SDS running buffer were analyzed using a BIORAD system supplemented with 6X SDS loading dye, and denatured for 5 min. at 95°C. Protein marker was used for the detection of the mass of the protein, and a constant voltage of 85V was applied to the stacking gel, and that of 200V was applied to the separating gel.

4.4.3 Protein Concentration Determination (Bradford Assay)

Bradford assay was adopted to determine the protein concentration. To generate a standard curve, the concentration of BSA solution ranges from 1-30μg/ml with diluted Bradford (1:5) in PBS. Prior to measuring the OD value using a spectrophotometer at 595nm, the samples

were mixed with diluted Bradford in PBS (total 1m), and incubated for 5 min. in the cuvettes at room temperature.

4.4.4 Western Blot Analysis

Western blot analysis was performed with wet-blot method. Filter papers, membrane, methanol (for PVDF (polyvinylidene difluoride) membrane only), and Blot Buffer were required for the assembly of a sandwich system. From negative to positive, the electrode of the system was sponge, four filter papers, SDS gel, membrane, respectively, and again four filter papers and sponge. After the equilibration of filter papers and the membrane in blot buffer (PVDF membrane activation in methanol), proteins were transferred onto PVDF (0.45µm pore size) or nitrocellulose membranes (0.45µm pore size) from SDS-PAGE gels at the constant voltage of 100 V for 1 h with blotting transfer buffer. After that, membranes were incubated with 5 % (w/v) milk powder in PBS for 1h at room temperature for blocking. Subsequently, the membranes were subjected to the primary antibody directly either for overnight at 4-8°C or 2h at room temperature. Before being incubated with the secondary antibody for 1h at room temperature in the darkness, the membranes were washed with PBST for three times (5-10 min each time). After that, two washes with PBST twice and once using PBS, the membranes were scanned by the LI-COR Odyssey System (LI-COR) for the detection of the specific fluorophore positive targets.

4.4.5 Chemical modification of streptavidin-sepharose beads for trypsin resistance

To reduce the contamination of samples by streptavidin-derived peptides, Streptavidin-sepharose beads were chemically modified for the resistance against digestion of streptavidin by trypsin. The series of steps performed were exactly the same as what were presented by Rafiee et al. [2020][225] The modified beads were stored at 4 °C in PBST for the subsequent experiment.

4.4.6 Preparation of protein lysates for MS

To prepare protein lysates for MS, two dishes (15cm) of cells were collected once they reached 80% confluency. After being washed for 3 times by PBS, the cells were pelleted by centrifuging at 1200g for 5min., and frozen in liquid N_2. After that, the pellets were stored at -

80°C for the subsequent experiment. Each frozen cell pellet was resuspended in 1 mL MS lysis buffer. To disrupt protein tangle, Lysates were passed through a G25 needle for 10 times, and sonicated using the Dianogene sonicator (four cycles at high intensity, 30 s per cycle (Fischer group)). After that, triton X-100 concentration was adjusted to 2%, and that of sodium chloride was adjusted to 150 mM. The samples were then transferred to 1.5 ml keratin free tubes, and centrifuged at 16000g for 10min. at 4°C. Using Bradford method, 3 mg of protein was adjusted for the subsequent experiment[195]. The detailed information of the lysis buffer was list in **Material 4.1.7**.

4.4.7 Streptavidin affinity pulldowns

After equilibrating with equilibration buffer for 5min., 40µl modified beads in 80µl bead slurry was incubated with adjusted protein sample at 4 °C overnight. Beads were washed on a rotating wheel at RT for 5min. with four different washing buffers. Besides, the wash was repeated twice for each buffer. For the removal of the waste buffer, the centrifugation parameter was 400g in the washing procedure.[195,225] All the components of washing buffer were listed in **Material 4.1.7**.

4.4.8 Mass spectrometry data acquisition and analysis

The tryptic peptides were analyzed by LC-MS at Protein Analytics Core Facility of Georg August University Göttingen. The raw data was processed with the software of MaxQuant[207] following the R packages, including EnhancedVolcano[288], proDA[208] and VennDiagram[289] for the subsequent analysis.

Supplementary Tables

Supplementary Table 1: Restriction digest protocols

Digest protocol of pJB354 vector-1	
Component	**Amount**
pJB354	2.5µg
AvrII (NEB)	1µl
FseI (NEB)	1µl
CutSmart buffer (NEB)	2µl
water	up to 20µl
37°C 2h	
Product for Gel extraction:11059bp	

Digest protocol of pY109 (lenti-LbCpf1) vector	
Component	**Amount**
pY109	2.5µg
BsmbI (NEB)	2µl
3.1 buffer (NEB)	2µl
water	up to 20µl
55°C 2h	
Product for Gel extraction:12606bp	

Digest protocol of pY109-crRNAs array vector	
Component	**Amount**
pY109-crRNAs array	2.5μg
PmeI (NEB)	1μl
BamHI HF (NEB)	1μl
CutSmart buffer (NEB)	2μl
water	up to 20μl
37°C 2h	
Product for Gel extraction:11014bp	

Digest protocol of pMB1610 vector	
Component	**Amount**
pMB1610	2.5μg
AatII (NEB)	1μl
SacI (NEB)	1μl
CutSmart buffer (NEB)	2μl
water	up to 20μl
37°C 2h	
Product for Gel extraction:3575bp	

Digest protocol of pJB354 vector-2	
Component	**Amount**
pJB354	2.5μg
PmeI (NEB)	1μl
BsrGI HF (NEB)	1μl
CutSmart buffer (NEB)	2μl
water	up to 20μl
37°C 2h	
Product for Gel extraction:13747bp	

Digest protocol of pJB357 vector-2	
Component	**Amount**
pJB357	2.5μg
PmeI (NEB)	1μl
BsrGI HF (NEB)	1μl
CutSmart buffer (NEB)	2μl
water	up to 20μl
37°C 2h	
Product for Gel extraction:13734bp	

Supplementary Table 2: Oligo annealing protocols

Oligo crRNAs array annealing	
Component	**Amount (μl)**
Sense oligo of crRNAs assay (100μM)	1
Antisense oligo of crRNAs assay (100μM)	1
Quick ligation buffer	5
water	3
Total	10

Oligo crRNA2 targets annealing	
Component	**Amount (μl)**
Sense oligo of crRNA2 targets (10μM)	10
Antisense oligo of crRNA2 targets (10μM)	10
Elution buffer	80
Total	100

Oligo AatII-SacI annealing	
Component	**Amount (μl)**
Sense oligo of AatII-SacI (10μM)	10
Antisense oligo of AatII-SacI (10μM)	10
Elution buffer	80
Total	100

Supplementary Table 3: PCR protocols

PCR protocol to produce inserts for the formation of pJB354-left HA-γ1-COP-GFP-right HA plasmids:

Fragment-C1: HA-1 left PCR protocol	
Component	**Amount (μl)**
P19 WT genomic DNA	7 (100ng)
XY11 forward	1.25 (10 μM)
XY12 reverse	1.25 (10 μM)
2xQ5 master mix	12.5
water	3
Total	25
Ta=72 °C Extension time=7s Product=123bp	

Fragment-C2: Copg1-GFP PCR protocol	
Component	**Amount (μl)**
pJB354	2 (100ng)
XY12 forward	1.25 (10 μM)
XY13 reverse	1.25 (10 μM)
2xQ5 master mix	12.5
water	8
Total	25
Ta=64 °C Extension time=2min Product=3425bp	

Fragment-C3: HA right PCR protocol	
Component	**Amount (μl)**
P19 WT genomic DNA	7 (100ng)
XY13 forward	1.25 (10 μM)
XY11 reverse	1.25 (10 μM)
2xQ5 master mix	12.5
water	3
Total	25
Ta=67 °C Extension time=7s Product=165bp	

PCR protocol to produce inserts for the formation of pJB354-left HA-γ2-COP-GFP-right HA plasmids:

Fragment-C1: HA-2 left PCR protocol	
Component	**Amount (μl)**
P19 WT genomic DNA	7 (100ng)
XY11 forward	1.25 (10 μM)
XY14 reverse	1.25 (10 μM)
2xQ5 master mix	12.5
water	3
Total	25
Ta=72 °C Extension time=7s Product=120bp	

Fragment-C2: Copg2-GFP PCR protocol	
Component	**Amount (μl)**
pJB357	2 (100ng)
XY14 forward	1.25 (10 μM)
XY13 reverse	1.25 (10 μM)
2xQ5 master mix	12.5
water	8
Total	25
Ta=64 °C Extension time=2min Product=3416bp	

Fragment-C3: HA right PCR protocol	
Component	**Amount (μl)**
P19 WT genomic DNA	7 (100ng)
XY13 forward	1.25 (10 μM)
XY11 reverse	1.25 (10 μM)
2xQ5 master mix	12.5
water	3
Total	25
Ta=67 °C Extension time=7s Product=165bp	

PCR protocol to produce inserts for the formation of pJB354-left HA-GFP-right HA plasmids:

Fragment-C1: HA-G left PCR protocol	
Component	**Amount (μl)**
P19 WT genomic DNA	7 (100ng)
XY11 forward	1.25 (10 μM)
XY18 reverse	1.25 (10 μM)
2xQ5 master mix	12.5
water	3
Total	25
Ta=72 °C Extension time=7s Product=120bp	

Fragment-C2: GFP-HA right PCR protocol	
Component	**Amount (μl)**
pJB354pJB354-left HA-γ1-COP-GFP-right HA	2 (100ng)
XY18 forward	1.25 (10 μM)
XY11 reverse	1.25 (10 μM)
2xQ5 master mix	12.5
water	8
Total	25
Ta=72 °C Extension time=30s Product=918bp	

PCR protocol to produce inserts for the formation of pJB354-left HA-γ1-2-COP-GFP-right HA plasmids:

Fragment-C1: HA-1 left PCR protocol	
Component	**Amount (μl)**
P19 WT genomic DNA	7 (100ng)
XY11 forward	1.25 (10 μM)
XY12 reverse	1.25 (10 μM)
2xQ5 master mix	12.5
water	3
Total	25
Ta=72 °C Extension time=7s Product=123bp	

Fragment-C2: Copg1 trunk PCR protocol	
Component	**Amount (μl)**
pJB354	2 (100ng)
XY12 forward	1.25 (10 μM)
XY15 reverse	1.25 (10 μM)
2xQ5 master mix	12.5
water	8
Total	25
Ta=64 °C Extension time=1min Product=1829bp	

Fragment-C3: Copg2 appendage PCR protocol	
Component	**Amount (μl)**
pJB357	2 (100ng)
XY15 forward	1.25 (10 μM)
XY13 reverse	1.25 (10 μM)
2xQ5 master mix	12.5
water	8
Total	25
Ta=67 °C Extension time=1min Product=1613bp	

Fragment-C4: HA right PCR protocol	
Component	**Amount (μl)**
P19 WT genomic DNA	7 (100ng)
XY13 forward	1.25 (10 μM)
XY11 reverse	1.25 (10 μM)
2xQ5 master mix	12.5
water	3
Total	25
Ta=67 °C Extension time=7s Product=165bp	

PCR protocol to produce inserts for the formation of pJB354-left HA-γ2-1-COP-GFP-right HA plasmids:

Fragment-C1: HA-2 left PCR protocol	
Component	**Amount (μl)**
P19 WT genomic DNA	7 (100ng)
XY11 forward	1.25 (10 μM)
XY14 reverse	1.25 (10 μM)
2xQ5 master mix	12.5
water	3
Total	25
Ta=72 °C Extension time=7s Product=120bp	

Fragment-C2: Copg2 trunk PCR protocol	
Component	**Amount (μl)**
pJB357	2 (100ng)
XY14 forward	1.25 (10 μM)
XY16 reverse	1.25 (10 μM)
2xQ5 master mix	12.5
water	8
Total	25
Ta=63 °C Extension time=1min Product=1823bp	

Fragment-C3: Copg1 appendage PCR protocol	
Component	**Amount (μl)**
pJB354	2 (100ng)
XY16 forward	1.25 (10 μM)
XY13 reverse	1.25 (10 μM)
2xQ5 master mix	12.5
water	8
Total	25
Ta=67 °C Extension time=1min Product=1616bp	

Fragment-C4: HA right PCR protocol	
Component	**Amount (μl)**
P19 WT genomic DNA	7 (100ng)
XY13 forward	1.25 (10 μM)
XY11 reverse	1.25 (10 μM)
2xQ5 master mix	12.5
water	3
Total	25
Ta=67 °C Extension time=7s Product=165bp	

PCR protocol to produce cassettes for the generation of CRISPR cell lines:

Cassette: left HA-γ1-COP-GFP-right HA PCR protocol	
Component	**Amount (μl)**
pJB354-left HA-γ1-COP-GFP-right HA	2 (100ng)
P-XY 01 forward	1.25 (10 μM)
P-XY 01 reverse	1.25 (10 μM)
2xQ5 master mix	12.5
water	8
Total	25
Ta=72 °C Extension time=2min Product=3629bp	

Cassette: left HA-γ2-COP-GFP-right HA PCR protocol	
Component	**Amount (μl)**
pJB354-left HA-γ2-COP-GFP-right HA	2 (100ng)
P-XY 01 forward	1.25 (10 μM)
P-XY 01 reverse	1.25 (10 μM)
2xQ5 master mix	12.5
water	8
Total	25
Ta=72 °C Extension time=2min Product=3620bp	

Cassette: left HA-GFP-right HA PCR protocol	
Component	**Amount (μl)**
pJB354-left HA-GFP-right HA	2 (100ng)
P-XY 01 forward	1.25 (10 μM)
P-XY 01 reverse	1.25 (10 μM)
2xQ5 master mix	12.5
water	8
Total	25
Ta=72 °C Extension time=30s Product=977bp	

Cassette: left HA-γ1-2-COP-GFP-right HA PCR protocol	
Component	**Amount (μl)**
pJB354-left HA-γ1-2-COP-GFP-right HA	2 (100ng)
P-XY 01 forward	1.25 (10 μM)
P-XY 01 reverse	1.25 (10 μM)
2xQ5 master mix	12.5
water	8
Total	25
Ta=72 °C Extension time=2min Product=3626bp	

Cassette: left HA-γ2-1-COP-GFP-right HA PCR protocol	
Component	**Amount (μl)**
pJB354-left HA-γ2-1-COP-GFP-right HA	2 (100ng)
P-XY 01 forward	1.25 (10 μM)
P-XY 01 reverse	1.25 (10 μM)
2xQ5 master mix	12.5
water	8
Total	25
Ta=72 °C Extension time=2min Product=3623bp	

PCR protocol to produce inserts for the formation of indPB4-γ1-COP-ultraID plasmids:

Fragment-u1: left HA-γ1-COP-GFP-right HA PCR protocol	
Component	**Amount (μl)**
pJB441	2 (100ng)
XY 35 forward	1.25 (10 μM)
XY 35 reverse	1.25 (10 μM)
2xQ5 master mix	12.5
water	8
Total	25
Ta=63 °C Extension time=30s Product=604bp	

PCR protocol to produce inserts for the formation of indPB4-γ2-COP-ultraID plasmids:

Fragment-u1: left HA-γ2-COP-GFP-right HA PCR protocol	
Component	**Amount (μl)**
pJB441	2 (100ng)
XY 36 forward	1.25 (10 μM)
XY 35 reverse	1.25 (10 μM)
2xQ5 master mix	12.5
water	8
Total	25
Ta=63 °C Extension time=30s Product=604bp	

PCR protocol to produce inserts for the formation of indPB4-ultraID-Ago2 plasmids:

Fragment-u1: left HA-GFP-right HA PCR protocol	
Component	**Amount (μl)**
pJB441	2 (100ng)
XY 39 forward	1.25 (10 μM)
XY 37 reverse	1.25 (10 μM)
2xQ5 master mix	12.5
water	8
Total	25
Ta=64 °C Extension time=30s Product=546bp	

Fragment-u2: left HA-GFP-right HA PCR protocol	
Component	**Amount (μl)**
pSF3-BirA R118G-hAgo-2	2 (100ng)
XY 38 forward	1.25 (10 μM)
XY 38 reverse	1.25 (10 μM)
2xQ5 master mix	12.5
water	8
Total	25
Ta=72 °C Extension time=90s Product=2685bp	

Reference

1. Farhan H, Rabouille C. Signalling to and from the secretory pathway. *J Cell Sci.* 2011;124(Pt 2):171-180.
2. Pulvirenti T, Giannotta M, Capestrano M, et al. A traffic-activated Golgi-based signalling circuit coordinates the secretory pathway. *Nat Cell Biol.* 2008;10(8):912-922.
3. Barlowe CK, Miller EA. Secretory protein biogenesis and traffic in the early secretory pathway. *Genetics.* 2013;193(2):383-410.
4. Yeong FM. Multi-step down-regulation of the secretory pathway in mitosis: a fresh perspective on protein trafficking. *Bioessays.* 2013;35(5):462-471.
5. Aviram N, Schuldiner M. Targeting and translocation of proteins to the endoplasmic reticulum at a glance. *J Cell Sci.* 2017;130(24):4079-4085.
6. Ellgaard L, Ruddock LW. The human protein disulphide isomerase family: substrate interactions and functional properties. *EMBO Rep.* 2005;6(1):28-32.
7. Ellgaard L, Helenius A. Quality control in the endoplasmic reticulum. *Nat Rev Mol Cell Biol.* 2003;4(3):181-191.
8. Thor F, Gautschi M, Geiger R, Helenius A. Bulk flow revisited: transport of a soluble protein in the secretory pathway. *Traffic.* 2009;10(12):1819-1830.
9. Lopez S, Perez-Linero AM, Manzano-Lopez J, et al. Dual Independent Roles of the p24 Complex in Selectivity of Secretory Cargo Export from the Endoplasmic Reticulum. *Cells.* 2020;9(5).
10. Sicari D, Igbaria A, Chevet E. Control of Protein Homeostasis in the Early Secretory Pathway: Current Status and Challenges. *Cells.* 2019;8(11).
11. Bethune J, Wieland FT. Assembly of COPI and COPII Vesicular Coat Proteins on Membranes. *Annu Rev Biophys.* 2018;47:63-83.
12. Rothman JE, Wieland FT. Protein sorting by transport vesicles. *Science.* 1996;272(5259):227-234.
13. Stanley P. Golgi glycosylation. *Cold Spring Harb Perspect Biol.* 2011;3(4).
14. Glick BS, Luini A. Models for Golgi traffic: a critical assessment. *Cold Spring Harb Perspect Biol.* 2011;3(11):a005215.
15. Jackson CL. Mechanisms of transport through the Golgi complex. *J Cell Sci.* 2009;122(Pt 4):443-452.
16. Dunlop MH, Ernst AM, Schroeder LK, Toomre DK, Lavieu G, Rothman JE. Land-locked mammalian Golgi reveals cargo transport between stable cisternae. *Nat Commun.* 2017;8(1):432.
17. Pelham HR, Rothman JE. The debate about transport in the Golgi--two sides of the same coin? *Cell.* 2000;102(6):713-719.
18. Pfeffer SR. How the Golgi works: a cisternal progenitor model. *Proc Natl Acad Sci U S A.* 2010;107(46):19614-19618.
19. Spang A, Schekman R. Reconstitution of retrograde transport from the Golgi to the ER in vitro. *J Cell Biol.* 1998;143(3):589-599.
20. Spang A. Retrograde traffic from the Golgi to the endoplasmic reticulum. *Cold Spring Harb Perspect Biol.* 2013;5(6).
21. Lorente-Rodriguez A, Barlowe C. Entry and exit mechanisms at the cis-face of the Golgi complex. *Cold Spring Harb Perspect Biol.* 2011;3(7).
22. Palade G. Intracellular aspects of the process of protein synthesis. *Science.* 1975;189(4200):347-358.
23. Farquhar MG. Multiple pathways of exocytosis, endocytosis, and membrane recycling: validation of a Golgi route. *Fed Proc.* 1983;42(8):2407-2413.

24. Langemeyer L, Frohlich F, Ungermann C. Rab GTPase Function in Endosome and Lysosome Biogenesis. *Trends Cell Biol.* 2018;28(11):957-970.
25. Karatekin E, Rothman JE. FEBS Letters Special Issue on Exocytosis and Endocytosis. *FEBS Lett.* 2018;592(21):3477-3479.
26. Goyal MJ. Paralog specific role of COPI pathway in P19 neuronal differentiation. *Thesis.* 2019.
27. Braakman I, Bulleid NJ. Protein folding and modification in the mammalian endoplasmic reticulum. *Annu Rev Biochem.* 2011;80:71-99.
28. Zhu G, Lee AS. Role of the unfolded protein response, GRP78 and GRP94 in organ homeostasis. *J Cell Physiol.* 2015;230(7):1413-1420.
29. Christis C, Lubsen NH, Braakman I. Protein folding includes oligomerization - examples from the endoplasmic reticulum and cytosol. *FEBS J.* 2008;275(19):4700-4727.
30. Liu Y, Ye Y. Proteostasis regulation at the endoplasmic reticulum: a new perturbation site for targeted cancer therapy. *Cell Res.* 2011;21(6):867-883.
31. Brewer JW, Diehl JA. PERK mediates cell-cycle exit during the mammalian unfolded protein response. *Proc Natl Acad Sci U S A.* 2000;97(23):12625-12630.
32. Iwawaki T, Hosoda A, Okuda T, et al. Translational control by the ER transmembrane kinase/ribonuclease IRE1 under ER stress. *Nat Cell Biol.* 2001;3(2):158-164.
33. Almanza A, Carlesso A, Chintha C, et al. Endoplasmic reticulum stress signalling - from basic mechanisms to clinical applications. *FEBS J.* 2019;286(2):241-278.
34. Genereux JC, Wiseman RL. Regulating extracellular proteostasis capacity through the unfolded protein response. *Prion.* 2015;9(1):10-21.
35. Pehar M, Lehnus M, Karst A, Puglielli L. Proteomic assessment shows that many endoplasmic reticulum (ER)-resident proteins are targeted by N(epsilon)-lysine acetylation in the lumen of the organelle and predicts broad biological impact. *J Biol Chem.* 2012;287(27):22436-22440.
36. Kahali S, Sarcar B, Fang B, et al. Activation of the unfolded protein response contributes toward the antitumor activity of vorinostat. *Neoplasia.* 2010;12(1):80-86.
37. Oyadomari S, Mori M. Roles of CHOP/GADD153 in endoplasmic reticulum stress. *Cell Death Differ.* 2004;11(4):381-389.
38. Marciniak SJ, Yun CY, Oyadomari S, et al. CHOP induces death by promoting protein synthesis and oxidation in the stressed endoplasmic reticulum. *Genes Dev.* 2004;18(24):3066-3077.
39. Sano R, Reed JC. ER stress-induced cell death mechanisms. *Biochim Biophys Acta.* 2013;1833(12):3460-3470.
40. Yamaguchi H, Wang HG. CHOP is involved in endoplasmic reticulum stress-induced apoptosis by enhancing DR5 expression in human carcinoma cells. *J Biol Chem.* 2004;279(44):45495-45502.
41. Bonifacino JS, Glick BS. The mechanisms of vesicle budding and fusion. *Cell.* 2004;116(2):153-166.
42. Aderhold P. On the Structure and Function of the COPI coat protein complex Coatomer. *thesis.* 2016.
43. Robinson MS. Adaptable adaptors for coated vesicles. *Trends Cell Biol.* 2004;14(4):167-174.
44. Hughes H, Stephens DJ. Assembly, organization, and function of the COPII coat. *Histochem Cell Biol.* 2008;129(2):129-151.
45. Bethune J, Kol M, Hoffmann J, Reckmann I, Brugger B, Wieland F. Coatomer, the coat protein of COPI transport vesicles, discriminates endoplasmic reticulum residents from p24 proteins. *Mol Cell Biol.* 2006;26(21):8011-8021.

46. Orci L, Ravazzola M, Meda P, et al. Mammalian Sec23p homologue is restricted to the endoplasmic reticulum transitional cytoplasm. *Proc Natl Acad Sci U S A.* 1991;88(19):8611-8615.
47. Rossanese OW, Soderholm J, Bevis BJ, et al. Golgi structure correlates with transitional endoplasmic reticulum organization in Pichia pastoris and Saccharomyces cerevisiae. *J Cell Biol.* 1999;145(1):69-81.
48. Kurokawa K, Suda Y, Nakano A. Sar1 localizes at the rims of COPII-coated membranes in vivo. *J Cell Sci.* 2016;129(17):3231-3237.
49. Bi X, Corpina RA, Goldberg J. Structure of the Sec23/24-Sar1 pre-budding complex of the COPII vesicle coat. *Nature.* 2002;419(6904):271-277.
50. Hariri H, Bhattacharya N, Johnson K, Noble AJ, Stagg SM. Insights into the mechanisms of membrane curvature and vesicle scission by the small GTPase Sar1 in the early secretory pathway. *J Mol Biol.* 2014;426(22):3811-3826.
51. Lee MC, Orci L, Hamamoto S, Futai E, Ravazzola M, Schekman R. Sar1p N-terminal helix initiates membrane curvature and completes the fission of a COPII vesicle. *Cell.* 2005;122(4):605-617.
52. Aridor M, Bannykh SI, Rowe T, Balch WE. Sequential coupling between COPII and COPI vesicle coats in endoplasmic reticulum to Golgi transport. *J Cell Biol.* 1995;131(4):875-893.
53. Barlowe C, Orci L, Yeung T, et al. COPII: a membrane coat formed by Sec proteins that drive vesicle budding from the endoplasmic reticulum. *Cell.* 1994;77(6):895-907.
54. Oka T, Nakano A. Inhibition of GTP hydrolysis by Sar1p causes accumulation of vesicles that are a functional intermediate of the ER-to-Golgi transport in yeast. *J Cell Biol.* 1994;124(4):425-434.
55. Adolf F, Herrmann A, Hellwig A, Beck R, Brugger B, Wieland FT. Scission of COPI and COPII vesicles is independent of GTP hydrolysis. *Traffic.* 2013;14(8):922-932.
56. Rhiel M. Vesicular Proteomics: Isoforms of the COPI and COPII coats-Implications in Protein Sorting and Disease. 2018.
57. Miller E, Antonny B, Hamamoto S, Schekman R. Cargo selection into COPII vesicles is driven by the Sec24p subunit. *EMBO J.* 2002;21(22):6105-6113.
58. Adolf F, Rhiel M, Reckmann I, Wieland FT. Sec24C/D-isoform-specific sorting of the preassembled ER-Golgi Q-SNARE complex. *Mol Biol Cell.* 2016;27(17):2697-2707.
59. Herzig S, Raemy E, Montessuit S, et al. Identification and functional expression of the mitochondrial pyruvate carrier. *Science.* 2012;337(6090):93-96.
60. Springer S, Malkus P, Borchert B, Wellbrock U, Duden R, Schekman R. Regulated oligomerization induces uptake of a membrane protein into COPII vesicles independent of its cytosolic tail. *Traffic.* 2014;15(5):531-545.
61. Nie C, Wang H, Wang R, Ginsburg D, Chen XW. Dimeric sorting code for concentrative cargo selection by the COPII coat. *Proc Natl Acad Sci U S A.* 2018;115(14):E3155-E3162.
62. Barlowe C, Helenius A. Cargo Capture and Bulk Flow in the Early Secretory Pathway. *Annu Rev Cell Dev Biol.* 2016;32:197-222.
63. Hara-Kuge S, Kuge O, Orci L, et al. En bloc incorporation of coatomer subunits during the assembly of COP-coated vesicles. *J Cell Biol.* 1994;124(6):883-892.
64. Eugster A, Frigerio G, Dale M, Duden R. COP I domains required for coatomer integrity, and novel interactions with ARF and ARF-GAP. *EMBO J.* 2000;19(15):3905-3917.
65. Jackson LP, Lewis M, Kent HM, et al. Molecular basis for recognition of dilysine trafficking motifs by COPI. *Dev Cell.* 2012;23(6):1255-1262.
66. Devos D, Dokudovskaya S, Alber F, et al. Components of coated vesicles and nuclear pore complexes share a common molecular architecture. *PLoS Biol.* 2004;2(12):e380.

67. Faini M, Beck R, Wieland FT, Briggs JA. Vesicle coats: structure, function, and general principles of assembly. *Trends Cell Biol.* 2013;23(6):279-288.
68. Dodonova SO, Aderhold P, Kopp J, et al. 9A structure of the COPI coat reveals that the Arf1 GTPase occupies two contrasting molecular environments. *Elife.* 2017;6.
69. Arakel EC, Richter KP, Clancy A, Schwappach B. delta-COP contains a helix C-terminal to its longin domain key to COPI dynamics and function. *Proc Natl Acad Sci U S A.* 2016;113(25):6916-6921.
70. Lee C, Goldberg J. Structure of coatomer cage proteins and the relationship among COPI, COPII, and clathrin vesicle coats. *Cell.* 2010;142(1):123-132.
71. Dodonova SO, Diestelkoetter-Bachert P, von Appen A, et al. VESICULAR TRANSPORT. A structure of the COPI coat and the role of coat proteins in membrane vesicle assembly. *Science.* 2015;349(6244):195-198.
72. Bykov YS, Schaffer M, Dodonova SO, et al. The structure of the COPI coat determined within the cell. *Elife.* 2017;6.
73. Blagitko N, Schulz U, Schinzel AA, Ropers HH, Kalscheuer VM. gamma2-COP, a novel imprinted gene on chromosome 7q32, defines a new imprinting cluster in the human genome. *Hum Mol Genet.* 1999;8(13):2387-2396.
74. Futatsumori M, Kasai K, Takatsu H, Shin HW, Nakayama K. Identification and characterization of novel isoforms of COP I subunits. *J Biochem.* 2000;128(5):793-801.
75. Wegmann D, Hess P, Baier C, Wieland FT, Reinhard C. Novel isotypic gamma/zeta subunits reveal three coatomer complexes in mammals. *Mol Cell Biol.* 2004;24(3):1070-1080.
76. Nickel W, Sohn K, Bunning C, Wieland FT. p23, a major COPI-vesicle membrane protein, constitutively cycles through the early secretory pathway. *Proc Natl Acad Sci U S A.* 1997;94(21):11393-11398.
77. Sohn K, Orci L, Ravazzola M, et al. A major transmembrane protein of Golgi-derived COPI-coated vesicles involved in coatomer binding. *J Cell Biol.* 1996;135(5):1239-1248.
78. Stamnes MA, Craighead MW, Hoe MH, et al. An integral membrane component of coatomer-coated transport vesicles defines a family of proteins involved in budding. *Proc Natl Acad Sci U S A.* 1995;92(17):8011-8015.
79. Harter C, Wieland FT. A single binding site for dilysine retrieval motifs and p23 within the gamma subunit of coatomer. *Proc Natl Acad Sci U S A.* 1998;95(20):11649-11654.
80. Hoffman GR, Rahl PB, Collins RN, Cerione RA. Conserved structural motifs in intracellular trafficking pathways: structure of the gammaCOP appendage domain. *Mol Cell.* 2003;12(3):615-625.
81. Arakel EC, Schwappach B. Formation of COPI-coated vesicles at a glance. *J Cell Sci.* 2018;131(5).
82. Ge X, Gong H, Dumas K, et al. Missense-depleted regions in population exomes implicate ras superfamily nucleotide-binding protein alteration in patients with brain malformation. *NPJ Genom Med.* 2016;1.
83. Galindo A, Soler N, McLaughlin SH, Yu M, Williams RL, Munro S. Structural Insights into Arl1-Mediated Targeting of the Arf-GEF BIG1 to the trans-Golgi. *Cell Rep.* 2016;16(3):839-850.
84. Gustafson MA, Fromme JC. Regulation of Arf activation occurs via distinct mechanisms at early and late Golgi compartments. *Mol Biol Cell.* 2017;28(25):3660-3671.

85. Peyroche A, Courbeyrette R, Rambourg A, Jackson CL. The ARF exchange factors Gea1p and Gea2p regulate Golgi structure and function in yeast. *J Cell Sci.* 2001;114(Pt 12):2241-2253.
86. Peyroche A, Courbeyrette R, Rambourg A, Jackson CL. Correction: The ARF exchange factors Gea1p and Gea2p regulate Golgi structure and function in yeast. *J Cell Sci.* 2019;132(13).
87. Mossessova E, Gulbis JM, Goldberg J. Structure of the guanine nucleotide exchange factor Sec7 domain of human arno and analysis of the interaction with ARF GTPase. *Cell.* 1998;92(3):415-423.
88. Richardson BC, Halaby SL, Gustafson MA, Fromme JC. Correction: The Sec7 N-terminal regulatory domains facilitate membrane-proximal activation of the Arf1 GTPase. *Elife.* 2016;5.
89. Richardson BC, Halaby SL, Gustafson MA, Fromme JC. The Sec7 N-terminal regulatory domains facilitate membrane-proximal activation of the Arf1 GTPase. *Elife.* 2016;5.
90. Deng Y, Golinelli-Cohen MP, Smirnova E, Jackson CL. A COPI coat subunit interacts directly with an early-Golgi localized Arf exchange factor. *EMBO Rep.* 2009;10(1):58-64.
91. Casanova JE. Regulation of Arf activation: the Sec7 family of guanine nucleotide exchange factors. *Traffic.* 2007;8(11):1476-1485.
92. Shin HW, Nakayama K. Guanine nucleotide-exchange factors for arf GTPases: their diverse functions in membrane traffic. *J Biochem.* 2004;136(6):761-767.
93. Gillingham AK, Munro S. The small G proteins of the Arf family and their regulators. *Annu Rev Cell Dev Biol.* 2007;23:579-611.
94. Weimer C, Beck R, Eckert P, et al. Differential roles of ArfGAP1, ArfGAP2, and ArfGAP3 in COPI trafficking. *J Cell Biol.* 2008;183(4):725-735.
95. Bigay J, Gounon P, Robineau S, Antonny B. Lipid packing sensed by ArfGAP1 couples COPI coat disassembly to membrane bilayer curvature. *Nature.* 2003;426(6966):563-566.
96. Bigay J, Antonny B. Real-time assays for the assembly-disassembly cycle of COP coats on liposomes of defined size. *Methods Enzymol.* 2005;404:95-107.
97. Mesmin B, Drin G, Levi S, et al. Two lipid-packing sensor motifs contribute to the sensitivity of ArfGAP1 to membrane curvature. *Biochemistry.* 2007;46(7):1779-1790.
98. Yahara N, Sato K, Nakano A. The Arf1p GTPase-activating protein Glo3p executes its regulatory function through a conserved repeat motif at its C-terminus. *J Cell Sci.* 2006;119(Pt 12):2604-2612.
99. Frigerio G, Grimsey N, Dale M, Majoul I, Duden R. Two human ARFGAPs associated with COP-I-coated vesicles. *Traffic.* 2007;8(11):1644-1655.
100. Watson PJ, Frigerio G, Collins BM, Duden R, Owen DJ. Gamma-COP appendage domain - structure and function. *Traffic.* 2004;5(2):79-88.
101. Bremser M, Nickel W, Schweikert M, et al. Coupling of coat assembly and vesicle budding to packaging of putative cargo receptors. *Cell.* 1999;96(4):495-506.
102. Spang A, Matsuoka K, Hamamoto S, Schekman R, Orci L. Coatomer, Arf1p, and nucleotide are required to bud coat protein complex I-coated vesicles from large synthetic liposomes. *Proc Natl Acad Sci U S A.* 1998;95(19):11199-11204.
103. Arakel EC, Schwappach B. Correction: Formation of COPI-coated vesicles at a glance (doi:10.1242/jcs.209890). *J Cell Sci.* 2018;131(7).
104. Eugster A, Frigerio G, Dale M, Duden R. The alpha- and beta'-COP WD40 domains mediate cargo-selective interactions with distinct di-lysine motifs. *Mol Biol Cell.* 2004;15(3):1011-1023.

105. Ma W, Goldberg J. Rules for the recognition of dilysine retrieval motifs by coatomer. *EMBO J.* 2013;32(7):926-937.
106. Schroder-Kohne S, Letourneur F, Riezman H. Alpha-COP can discriminate between distinct, functional di-lysine signals in vitro and regulates access into retrograde transport. *J Cell Sci.* 1998;111 (Pt 23):3459-3470.
107. Zerangue N, Malan MJ, Fried SR, et al. Analysis of endoplasmic reticulum trafficking signals by combinatorial screening in mammalian cells. *Proc Natl Acad Sci U S A.* 2001;98(5):2431-2436.
108. Zerangue N, Schwappach B, Jan YN, Jan LY. A new ER trafficking signal regulates the subunit stoichiometry of plasma membrane K(ATP) channels. *Neuron.* 1999;22(3):537-548.
109. Arakel EC, Brandenburg S, Uchida K, et al. Tuning the electrical properties of the heart by differential trafficking of KATP ion channel complexes. *J Cell Sci.* 2014;127(Pt 9):2106-2119.
110. Kilisch M, Lytovchenko O, Arakel EC, Bertinetti D, Schwappach B. A dual phosphorylation switch controls 14-3-3-dependent cell surface expression of TASK-1. *J Cell Sci.* 2016;129(4):831-842.
111. Schwappach B, Zerangue N, Jan YN, Jan LY. Molecular basis for K(ATP) assembly: transmembrane interactions mediate association of a K+ channel with an ABC transporter. *Neuron.* 2000;26(1):155-167.
112. Yuan H, Michelsen K, Schwappach B. 14-3-3 dimers probe the assembly status of multimeric membrane proteins. *Curr Biol.* 2003;13(8):638-646.
113. Xu P, Hankins HM, MacDonald C, et al. COPI mediates recycling of an exocytic SNARE by recognition of a ubiquitin sorting signal. *Elife.* 2017;6.
114. Denzel A, Otto F, Girod A, et al. The p24 family member p23 is required for early embryonic development. *Curr Biol.* 2000;10(1):55-58.
115. Aguilera-Romero A, Kaminska J, Spang A, Riezman H, Muniz M. The yeast p24 complex is required for the formation of COPI retrograde transport vesicles from the Golgi apparatus. *J Cell Biol.* 2008;180(4):713-720.
116. Bonnon C, Wendeler MW, Paccaud JP, Hauri HP. Selective export of human GPI-anchored proteins from the endoplasmic reticulum. *J Cell Sci.* 2010;123(Pt 10):1705-1715.
117. Fiedler K, Veit M, Stamnes MA, Rothman JE. Bimodal interaction of coatomer with the p24 family of putative cargo receptors. *Science.* 1996;273(5280):1396-1399.
118. Gommel DU, Memon AR, Heiss A, et al. Recruitment to Golgi membranes of ADP-ribosylation factor 1 is mediated by the cytoplasmic domain of p23. *EMBO J.* 2001;20(23):6751-6760.
119. Lanoix J, Ouwendijk J, Stark A, et al. Sorting of Golgi resident proteins into different subpopulations of COPI vesicles: a role for ArfGAP1. *J Cell Biol.* 2001;155(7):1199-1212.
120. Muniz M, Nuoffer C, Hauri HP, Riezman H. The Emp24 complex recruits a specific cargo molecule into endoplasmic reticulum-derived vesicles. *J Cell Biol.* 2000;148(5):925-930.
121. Shibuya A, Margulis N, Christiano R, Walther TC, Barlowe C. The Erv41-Erv46 complex serves as a retrograde receptor to retrieve escaped ER proteins. *J Cell Biol.* 2015;208(2):197-209.
122. Munro S, Pelham HR. A C-terminal signal prevents secretion of luminal ER proteins. *Cell.* 1987;48(5):899-907.
123. Semenza JC, Hardwick KG, Dean N, Pelham HR. ERD2, a yeast gene required for the receptor-mediated retrieval of luminal ER proteins from the secretory pathway. *Cell.* 1990;61(7):1349-1357.

124. Cabrera M, Muniz M, Hidalgo J, Vega L, Martin ME, Velasco A. The retrieval function of the KDEL receptor requires PKA phosphorylation of its C-terminus. *Mol Biol Cell.* 2003;14(10):4114-4125.
125. Dominguez M, Dejgaard K, Fullekrug J, et al. gp25L/emp24/p24 protein family members of the cis-Golgi network bind both COP I and II coatomer. *J Cell Biol.* 1998;140(4):751-765.
126. Lee SY, Yang JS, Hong W, Premont RT, Hsu VW. ARFGAP1 plays a central role in coupling COPI cargo sorting with vesicle formation. *J Cell Biol.* 2005;168(2):281-290.
127. Townsley FM, Wilson DW, Pelham HR. Mutational analysis of the human KDEL receptor: distinct structural requirements for Golgi retention, ligand binding and retrograde transport. *EMBO J.* 1993;12(7):2821-2829.
128. Schmitz KR, Liu J, Li S, et al. Golgi localization of glycosyltransferases requires a Vps74p oligomer. *Dev Cell.* 2008;14(4):523-534.
129. Eckert ES, Reckmann I, Hellwig A, et al. Golgi phosphoprotein 3 triggers signal-mediated incorporation of glycosyltransferases into coatomer-coated (COPI) vesicles. *J Biol Chem.* 2014;289(45):31319-31329.
130. Sato K, Sato M, Nakano A. Rer1p, a retrieval receptor for endoplasmic reticulum membrane proteins, is dynamically localized to the Golgi apparatus by coatomer. *J Cell Biol.* 2001;152(5):935-944.
131. Tu L, Tai WC, Chen L, Banfield DK. Signal-mediated dynamic retention of glycosyltransferases in the Golgi. *Science.* 2008;321(5887):404-407.
132. Tu L, Chen L, Banfield DK. A conserved N-terminal arginine-motif in GOLPH3-family proteins mediates binding to coatomer. *Traffic.* 2012;13(11):1496-1507.
133. Aoe T, Cukierman E, Lee A, Cassel D, Peters PJ, Hsu VW. The KDEL receptor, ERD2, regulates intracellular traffic by recruiting a GTPase-activating protein for ARF1. *EMBO J.* 1997;16(24):7305-7316.
134. Rein U, Andag U, Duden R, Schmitt HD, Spang A. ARF-GAP-mediated interaction between the ER-Golgi v-SNAREs and the COPI coat. *J Cell Biol.* 2002;157(3):395-404.
135. Schindler C, Rodriguez F, Poon PP, Singer RA, Johnston GC, Spang A. The GAP domain and the SNARE, coatomer and cargo interaction region of the ArfGAP2/3 Glo3 are sufficient for Glo3 function. *Traffic.* 2009;10(9):1362-1375.
136. Fernandez-Ulibarri I, Vilella M, Lazaro-Dieguez F, et al. Diacylglycerol is required for the formation of COPI vesicles in the Golgi-to-ER transport pathway. *Mol Biol Cell.* 2007;18(9):3250-3263.
137. Beck R, Sun Z, Adolf F, et al. Membrane curvature induced by Arf1-GTP is essential for vesicle formation. *Proc Natl Acad Sci U S A.* 2008;105(33):11731-11736.
138. Beck R, Prinz S, Diestelkotter-Bachert P, et al. Coatomer and dimeric ADP ribosylation factor 1 promote distinct steps in membrane scission. *J Cell Biol.* 2011;194(5):765-777.
139. Popoff V, Adolf F, Brugger B, Wieland F. COPI budding within the Golgi stack. *Cold Spring Harb Perspect Biol.* 2011;3(11):a005231.
140. Ostermann J, Orci L, Tani K, et al. Stepwise assembly of functionally active transport vesicles. *Cell.* 1993;75(5):1015-1025.
141. Yang JS, Lee SY, Spano S, et al. A role for BARS at the fission step of COPI vesicle formation from Golgi membrane. *EMBO J.* 2005;24(23):4133-4143.
142. Yang JS, Gad H, Lee SY, et al. A role for phosphatidic acid in COPI vesicle fission yields insights into Golgi maintenance. *Nat Cell Biol.* 2008;10(10):1146-1153.

143. Presley JF, Ward TH, Pfeifer AC, Siggia ED, Phair RD, Lippincott-Schwartz J. Dissection of COPI and Arf1 dynamics in vivo and role in Golgi membrane transport. *Nature.* 2002;417(6885):187-193.
144. Tanigawa G, Orci L, Amherdt M, Ravazzola M, Helms JB, Rothman JE. Hydrolysis of bound GTP by ARF protein triggers uncoating of Golgi-derived COP-coated vesicles. *J Cell Biol.* 1993;123(6 Pt 1):1365-1371.
145. Liu W, Duden R, Phair RD, Lippincott-Schwartz J. ArfGAP1 dynamics and its role in COPI coat assembly on Golgi membranes of living cells. *J Cell Biol.* 2005;168(7):1053-1063.
146. Yang JS, Lee SY, Gao M, et al. ARFGAP1 promotes the formation of COPI vesicles, suggesting function as a component of the coat. *J Cell Biol.* 2002;159(1):69-78.
147. Kartberg F, Asp L, Dejgaard SY, et al. ARFGAP2 and ARFGAP3 are essential for COPI coat assembly on the Golgi membrane of living cells. *J Biol Chem.* 2010;285(47):36709-36720.
148. Poon PP, Cassel D, Spang A, et al. Retrograde transport from the yeast Golgi is mediated by two ARF GAP proteins with overlapping function. *EMBO J.* 1999;18(3):555-564.
149. Cai H, Reinisch K, Ferro-Novick S. Coats, tethers, Rabs, and SNAREs work together to mediate the intracellular destination of a transport vesicle. *Dev Cell.* 2007;12(5):671-682.
150. Yamasaki A, Menon S, Yu S, et al. mTrs130 is a component of a mammalian TRAPPII complex, a Rab1 GEF that binds to COPI-coated vesicles. *Mol Biol Cell.* 2009;20(19):4205-4215.
151. Miller VJ, Sharma P, Kudlyk TA, et al. Molecular insights into vesicle tethering at the Golgi by the conserved oligomeric Golgi (COG) complex and the golgin TATA element modulatory factor (TMF). *J Biol Chem.* 2013;288(6):4229-4240.
152. Guo Y, Punj V, Sengupta D, Linstedt AD. Coat-tether interaction in Golgi organization. *Mol Biol Cell.* 2008;19(7):2830-2843.
153. Malsam J, Satoh A, Pelletier L, Warren G. Golgin tethers define subpopulations of COPI vesicles. *Science.* 2005;307(5712):1095-1098.
154. Andag U, Schmitt HD. Dsl1p, an essential component of the Golgi-endoplasmic reticulum retrieval system in yeast, uses the same sequence motif to interact with different subunits of the COPI vesicle coat. *J Biol Chem.* 2003;278(51):51722-51734.
155. Ren Y, Yip CK, Tripathi A, et al. A structure-based mechanism for vesicle capture by the multisubunit tethering complex Dsl1. *Cell.* 2009;139(6):1119-1129.
156. Suckling RJ, Poon PP, Travis SM, et al. Structural basis for the binding of tryptophan-based motifs by delta-COP. *Proc Natl Acad Sci U S A.* 2015;112(46):14242-14247.
157. Zink S, Wenzel D, Wurm CA, Schmitt HD. A link between ER tethering and COP-I vesicle uncoating. *Dev Cell.* 2009;17(3):403-416.
158. Diao A, Frost L, Morohashi Y, Lowe M. Coordination of golgin tethering and SNARE assembly: GM130 binds syntaxin 5 in a p115-regulated manner. *J Biol Chem.* 2008;283(11):6957-6967.
159. Shestakova A, Suvorova E, Pavliv O, Khaidakova G, Lupashin V. Interaction of the conserved oligomeric Golgi complex with t-SNARE Syntaxin5a/Sed5 enhances intra-Golgi SNARE complex stability. *J Cell Biol.* 2007;179(6):1179-1192.
160. Shorter J, Beard MB, Seemann J, Dirac-Svejstrup AB, Warren G. Sequential tethering of Golgins and catalysis of SNAREpin assembly by the vesicle-tethering protein p115. *J Cell Biol.* 2002;157(1):45-62.
161. Brunger AT. Structure and function of SNARE and SNARE-interacting proteins. *Q Rev Biophys.* 2005;38(1):1-47.

162. Fasshauer D. Structural insights into the SNARE mechanism. *Biochim Biophys Acta.* 2003;1641(2-3):87-97.
163. Hong W. SNAREs and traffic. *Biochim Biophys Acta.* 2005;1744(3):493-517.
164. Nichols BJ, Pelham HR. SNAREs and membrane fusion in the Golgi apparatus. *Biochim Biophys Acta.* 1998;1404(1-2):9-31.
165. Muller JM, Rabouille C, Newman R, et al. An NSF function distinct from ATPase-dependent SNARE disassembly is essential for Golgi membrane fusion. *Nat Cell Biol.* 1999;1(6):335-340.
166. Muller JM, Shorter J, Newman R, et al. Sequential SNARE disassembly and GATE-16-GOS-28 complex assembly mediated by distinct NSF activities drives Golgi membrane fusion. *J Cell Biol.* 2002;157(7):1161-1173.
167. Otto H, Hanson PI, Jahn R. Assembly and disassembly of a ternary complex of synaptobrevin, syntaxin, and SNAP-25 in the membrane of synaptic vesicles. *Proc Natl Acad Sci U S A.* 1997;94(12):6197-6201.
168. Whiteheart SW, Matveeva EA. Multiple binding proteins suggest diverse functions for the N-ethylmaleimide sensitive factor. *J Struct Biol.* 2004;146(1-2):32-43.
169. Yu RC, Jahn R, Brunger AT. NSF N-terminal domain crystal structure: models of NSF function. *Mol Cell.* 1999;4(1):97-107.
170. Szul T, Sztul E. COPII and COPI traffic at the ER-Golgi interface. *Physiology (Bethesda).* 2011;26(5):348-364.
171. Ungewickell E, Branton D. Assembly units of clathrin coats. *Nature.* 1981;289(5796):420-422.
172. Kirchhausen T, Harrison SC. Protein organization in clathrin trimers. *Cell.* 1981;23(3):755-761.
173. Crowther RA, Pearse BM. Assembly and packing of clathrin into coats. *J Cell Biol.* 1981;91(3 Pt 1):790-797.
174. Owen DJ, Collins BM, Evans PR. Adaptors for clathrin coats: structure and function. *Annu Rev Cell Dev Biol.* 2004;20:153-191.
175. Park SY, Guo X. Adaptor protein complexes and intracellular transport. *Biosci Rep.* 2014;34(4).
176. Keen JH, Chestnut MH, Beck KA. The clathrin coat assembly polypeptide complex. Autophosphorylation and assembly activities. *J Biol Chem.* 1987;262(8):3864-3871.
177. Dell'Angelica EC, Mullins C, Bonifacino JS. AP-4, a novel protein complex related to clathrin adaptors. *J Biol Chem.* 1999;274(11):7278-7285.
178. Dell'Angelica EC, Ohno H, Ooi CE, Rabinovich E, Roche KW, Bonifacino JS. AP-3: an adaptor-like protein complex with ubiquitous expression. *EMBO J.* 1997;16(5):917-928.
179. Ahle S, Mann A, Eichelsbacher U, Ungewickell E. Structural relationships between clathrin assembly proteins from the Golgi and the plasma membrane. *EMBO J.* 1988;7(4):919-929.
180. Hirst J, Itzhak DN, Antrobus R, Borner GHH, Robinson MS. Role of the AP-5 adaptor protein complex in late endosome-to-Golgi retrieval. *PLoS Biol.* 2018;16(1):e2004411.
181. Boehm M, Aguilar RC, Bonifacino JS. Functional and physical interactions of the adaptor protein complex AP-4 with ADP-ribosylation factors (ARFs). *EMBO J.* 2001;20(22):6265-6276.
182. Ford MG, Pearse BM, Higgins MK, et al. Simultaneous binding of PtdIns(4,5)P2 and clathrin by AP180 in the nucleation of clathrin lattices on membranes. *Science.* 2001;291(5506):1051-1055.
183. Kaksonen M, Roux A. Mechanisms of clathrin-mediated endocytosis. *Nat Rev Mol Cell Biol.* 2018;19(5):313-326.

184. Rosnoblet C, Peanne R, Legrand D, Foulquier F. Glycosylation disorders of membrane trafficking. *Glycoconj J.* 2013;30(1):23-31.
185. Custer SK, Todd AG, Singh NN, Androphy EJ. Dilysine motifs in exon 2b of SMN protein mediate binding to the COPI vesicle protein alpha-COP and neurite outgrowth in a cell culture model of spinal muscular atrophy. *Hum Mol Genet.* 2013;22(20):4043-4052.
186. Peter CJ, Evans M, Thayanithy V, et al. The COPI vesicle complex binds and moves with survival motor neuron within axons. *Hum Mol Genet.* 2011;20(9):1701-1711.
187. Li H, Custer SK, Gilson T, Hao le T, Beattie CE, Androphy EJ. alpha-COP binding to the survival motor neuron protein SMN is required for neuronal process outgrowth. *Hum Mol Genet.* 2015;24(25):7295-7307.
188. Jain Goyal M, Zhao X, Bozhinova M, et al. A paralog-specific role of COPI vesicles in the neuronal differentiation of mouse pluripotent cells. *Life Sci Alliance.* 2020;3(9).
189. Moelleken J, Malsam J, Betts MJ, et al. Differential localization of coatomer complex isoforms within the Golgi apparatus. *Proc Natl Acad Sci U S A.* 2007;104(11):4425-4430.
190. Choi-Rhee E, Schulman H, Cronan JE. Promiscuous protein biotinylation by Escherichia coli biotin protein ligase. *Protein Sci.* 2004;13(11):3043-3050.
191. Tong L. Structure and function of biotin-dependent carboxylases. *Cell Mol Life Sci.* 2013;70(5):863-891.
192. Roux KJ, Kim DI, Burke B, May DG. BioID: A Screen for Protein-Protein Interactions. *Curr Protoc Protein Sci.* 2018;91:19 23 11-19 23 15.
193. Roux KJ, Kim DI, Raida M, Burke B. A promiscuous biotin ligase fusion protein identifies proximal and interacting proteins in mammalian cells. *J Cell Biol.* 2012;196(6):801-810.
194. Kim DI, Jensen SC, Noble KA, et al. An improved smaller biotin ligase for BioID proximity labeling. *Mol Biol Cell.* 2016;27(8):1188-1196.
195. Kubitz L. *Characterisation of µltraID as a novel biotin ligase for proximity-dependent biotinylation and its comparison to established BioID enzymes*. Heidelberg: Faculty for Chemistry and Earth Sciences & Faculty for Biosciences, Ruprecht Karls University Heidelberg; 2020.
196. McNicholas S, Potterton E, Wilson KS, Noble ME. Presenting your structures: the CCP4mg molecular-graphics software. *Acta Crystallogr D Biol Crystallogr.* 2011;67(Pt 4):386-394.
197. Packer MS, Liu DR. Methods for the directed evolution of proteins. *Nat Rev Genet.* 2015;16(7):379-394.
198. Dunham WH, Mullin M, Gingras AC. Affinity-purification coupled to mass spectrometry: basic principles and strategies. *Proteomics.* 2012;12(10):1576-1590.
199. Gingras AC, Gstaiger M, Raught B, Aebersold R. Analysis of protein complexes using mass spectrometry. *Nat Rev Mol Cell Biol.* 2007;8(8):645-654.
200. Kocher T, Superti-Furga G. Mass spectrometry-based functional proteomics: from molecular machines to protein networks. *Nat Methods.* 2007;4(10):807-815.
201. Schwanhausser B, Busse D, Li N, et al. Global quantification of mammalian gene expression control. *Nature.* 2011;473(7347):337-342.
202. Nagaraj N, Wisniewski JR, Geiger T, et al. Deep proteome and transcriptome mapping of a human cancer cell line. *Mol Syst Biol.* 2011;7:548.
203. Arike L, Valgepea K, Peil L, Nahku R, Adamberg K, Vilu R. Comparison and applications of label-free absolute proteome quantification methods on Escherichia coli. *J Proteomics.* 2012;75(17):5437-5448.

204. Wittig S, Ganzella M, Barth M, et al. Cross-linking mass spectrometry uncovers protein interactions and functional assemblies in synaptic vesicle membranes. *Nat Commun.* 2021;12(1):858.
205. Krey JF, Wilmarth PA, Shin JB, et al. Accurate label-free protein quantitation with high- and low-resolution mass spectrometers. *J Proteome Res.* 2014;13(2):1034-1044.
206. Cox J, Hein MY, Luber CA, Paron I, Nagaraj N, Mann M. Accurate proteome-wide label-free quantification by delayed normalization and maximal peptide ratio extraction, termed MaxLFQ. *Mol Cell Proteomics.* 2014;13(9):2513-2526.
207. Cox J, Mann M. MaxQuant enables high peptide identification rates, individualized p.p.b.-range mass accuracies and proteome-wide protein quantification. *Nat Biotechnol.* 2008;26(12):1367-1372.
208. Constantin Ahlmann-Eltze SA. proDA: Probabilistic Dropout Analysis for Identifying Differentially Abundant Proteins in Label-Free Mass Spectrometry. *Nature Portfolio.* 2019.
209. Ahlmann-Eltze C, Anders S. proDA: Probabilistic Dropout Analysis for Identifying Differentially Abundant Proteins in Label-Free Mass Spectrometry. *bioRxiv.* 2020:661496.
210. Ahn HK, Kang YW, Lim HM, Hwang I, Pai HS. Physiological Functions of the COPI Complex in Higher Plants. *Mol Cells.* 2015;38(10):866-875.
211. Claerhout S, Dutta B, Bossuyt W, et al. Abortive autophagy induces endoplasmic reticulum stress and cell death in cancer cells. *PLoS One.* 2012;7(6):e39400.
212. De Genaro P, Simon MV, Rotstein NP, Politi LE. Retinoic acid promotes apoptosis and differentiation in photoreceptors by activating the P38 MAP kinase pathway. *Invest Ophthalmol Vis Sci.* 2013;54(5):3143-3156.
213. Nijhawan D, Honarpour N, Wang X. Apoptosis in neural development and disease. *Annu Rev Neurosci.* 2000;23:73-87.
214. Hollville E, Romero SE, Deshmukh M. Apoptotic cell death regulation in neurons. *FEBS J.* 2019;286(17):3276-3298.
215. Bedner E, Smolewski P, Amstad P, Darzynkiewicz Z. Activation of caspases measured in situ by binding of fluorochrome-labeled inhibitors of caspases (FLICA): correlation with DNA fragmentation. *Exp Cell Res.* 2000;259(1):308-313.
216. Chae HJ, Kang JS, Byun JO, et al. Molecular mechanism of staurosporine-induced apoptosis in osteoblasts. *Pharmacol Res.* 2000;42(4):373-381.
217. Watkin LB, Jessen B, Wiszniewski W, et al. COPA mutations impair ER-Golgi transport and cause hereditary autoimmune-mediated lung disease and arthritis. *Nat Genet.* 2015;47(6):654-660.
218. Izumi K, Brett M, Nishi E, et al. ARCN1 Mutations Cause a Recognizable Craniofacial Syndrome Due to COPI-Mediated Transport Defects. *Am J Hum Genet.* 2016;99(2):451-459.
219. Kawada K, Iekumo T, Saito R, et al. Aberrant neuronal differentiation and inhibition of dendrite outgrowth resulting from endoplasmic reticulum stress. *J Neurosci Res.* 2014;92(9):1122-1133.
220. Oslowski CM, Urano F. Measuring ER stress and the unfolded protein response using mammalian tissue culture system. *Methods Enzymol.* 2011;490:71-92.
221. Jin H, Komita M, Aoe T. The Role of BiP Retrieval by the KDEL Receptor in the Early Secretory Pathway and its Effect on Protein Quality Control and Neurodegeneration. *Front Mol Neurosci.* 2017;10:222.
222. Jones-Villeneuve EM, McBurney MW, Rogers KA, Kalnins VI. Retinoic acid induces embryonal carcinoma cells to differentiate into neurons and glial cells. *J Cell Biol.* 1982;94(2):253-262.

223. Pachernik J, Bryja V, Esner M, Kubala L, Dvorak P, Hampl A. Neural differentiation of pluripotent mouse embryonal carcinoma cells by retinoic acid: inhibitory effect of serum. *Physiol Res.* 2005;54(1):115-122.
224. Beck R, Rawet M, Wieland FT, Cassel D. The COPI system: molecular mechanisms and function. *FEBS Lett.* 2009;583(17):2701-2709.
225. Rafiee MR, Sigismondo G, Kalxdorf M, et al. Protease-resistant streptavidin for interaction proteomics. *Mol Syst Biol.* 2020;16(5):e9370.
226. Sears RM, May DG, Roux KJ. BioID as a Tool for Protein-Proximity Labeling in Living Cells. *Methods Mol Biol.* 2019;2012:299-313.
227. Qi HH, Ongusaha PP, Myllyharju J, et al. Prolyl 4-hydroxylation regulates Argonaute 2 stability. *Nature.* 2008;455(7211):421-424.
228. Cikaluk DE, Tahbaz N, Hendricks LC, et al. GERp95, a membrane-associated protein that belongs to a family of proteins involved in stem cell differentiation. *Mol Biol Cell.* 1999;10(10):3357-3372.
229. Tahbaz N, Carmichael JB, Hobman TC. GERp95 belongs to a family of signal-transducing proteins and requires Hsp90 activity for stability and Golgi localization. *J Biol Chem.* 2001;276(46):43294-43299.
230. Donaldson JG, Finazzi D, Klausner RD. Brefeldin A inhibits Golgi membrane-catalysed exchange of guanine nucleotide onto ARF protein. *Nature.* 1992;360(6402):350-352.
231. Helms JB, Rothman JE. Inhibition by brefeldin A of a Golgi membrane enzyme that catalyses exchange of guanine nucleotide bound to ARF. *Nature.* 1992;360(6402):352-354.
232. Lowe M. The Physiological Functions of the Golgin Vesicle Tethering Proteins. *Front Cell Dev Biol.* 2019;7:94.
233. Sonnichsen B, Lowe M, Levine T, Jamsa E, Dirac-Svejstrup B, Warren G. A role for giantin in docking COPI vesicles to Golgi membranes. *J Cell Biol.* 1998;140(5):1013-1021.
234. Munro S. The golgin coiled-coil proteins of the Golgi apparatus. *Cold Spring Harb Perspect Biol.* 2011;3(6).
235. Sohda M, Misumi Y, Yamamoto A, et al. Interaction of Golgin-84 with the COG complex mediates the intra-Golgi retrograde transport. *Traffic.* 2010;11(12):1552-1566.
236. Gillingham AK. At the ends of their tethers! How coiled-coil proteins capture vesicles at the Golgi. *Biochem Soc Trans.* 2018;46(1):43-50.
237. Miyazaki K, Wakana Y, Noda C, Arasaki K, Furuno A, Tagaya M. Contribution of the long form of syntaxin 5 to the organization of the endoplasmic reticulum. *J Cell Sci.* 2012;125(Pt 23):5658-5666.
238. Linders PT, Horst CV, Beest MT, van den Bogaart G. Stx5-Mediated ER-Golgi Transport in Mammals and Yeast. *Cells.* 2019;8(8).
239. Buchwalter A, Schulte R, Tsai H, Capitanio J, Hetzer M. Selective clearance of the inner nuclear membrane protein emerin by vesicular transport during ER stress. *Elife.* 2019;8.
240. Witkos TM, Chan WL, Joensuu M, et al. GORAB scaffolds COPI at the trans-Golgi for efficient enzyme recycling and correct protein glycosylation. *Nat Commun.* 2019;10(1):127.
241. Kuliyev E, Gingras S, Guy CS, Howell S, Vogel P, Pelletier S. Overlapping Role of SCYL1 and SCYL3 in Maintaining Motor Neuron Viability. *J Neurosci.* 2018;38(10):2615-2630.

242. Hamlin JN, Schroeder LK, Fotouhi M, et al. Scyl1 scaffolds class II Arfs to specific subcomplexes of coatomer through the gamma-COP appendage domain. *J Cell Sci.* 2014;127(Pt 7):1454-1463.
243. Ludes-Meyers JH, Bednarek AK, Popescu NC, Bedford M, Aldaz CM. WWOX, the common chromosomal fragile site, FRA16D, cancer gene. *Cytogenetic and genome research.* 2003;100(1-4):101-110.
244. Mahmud MAA, Noguchi M, Domon A, Tochigi Y, Katayama K, Suzuki H. Cellular Expression and Subcellular Localization of Wwox Protein During Testicular Development and Spermatogenesis in Rats. *J Histochem Cytochem.* 2021:22155421991629.
245. Bednarek AK, Keck-Waggoner CL, Daniel RL, et al. WWOX, the FRA16D gene, behaves as a suppressor of tumor growth. *Cancer Res.* 2001;61(22):8068-8073.
246. Liu SY, Chiang MF, Chen YJ. Role of WW domain proteins WWOX in development, prognosis, and treatment response of glioma. *Exp Biol Med (Maywood).* 2015;240(3):315-323.
247. Hartwig C, Zlatic SA, Wallin M, Vrailas-Mortimer A, Fahrni CJ, Faundez V. Trafficking mechanisms of P-type ATPase copper transporters. *Curr Opin Cell Biol.* 2019;59:24-33.
248. Mellman I, Simons K. The Golgi complex: in vitro veritas? *Cell.* 1992;68(5):829-840.
249. Aligianis IA, Morgan NV, Mione M, et al. Mutation in Rab3 GTPase-activating protein (RAB3GAP) noncatalytic subunit in a kindred with Martsolf syndrome. *Am J Hum Genet.* 2006;78(4):702-707.
250. Diao A, Rahman D, Pappin DJ, Lucocq J, Lowe M. The coiled-coil membrane protein golgin-84 is a novel rab effector required for Golgi ribbon formation. *J Cell Biol.* 2003;160(2):201-212.
251. Luo L, Hannemann M, Koenig S, et al. The Caenorhabditis elegans GARP complex contains the conserved Vps51 subunit and is required to maintain lysosomal morphology. *Mol Biol Cell.* 2011;22(14):2564-2578.
252. Govek EE, Newey SE, Akerman CJ, Cross JR, Van der Veken L, Van Aelst L. The X-linked mental retardation protein oligophrenin-1 is required for dendritic spine morphogenesis. *Nat Neurosci.* 2004;7(4):364-372.
253. Guo D, Yang X, Shi L. Rho GTPase Regulators and Effectors in Autism Spectrum Disorders: Animal Models and Insights for Therapeutics. *Cells.* 2020;9(4).
254. Bleijerveld OB, van Holten TC, Preisinger C, et al. Targeted phosphotyrosine profiling of glycoprotein VI signaling implicates oligophrenin-1 in platelet filopodia formation. *Arterioscler Thromb Vasc Biol.* 2013;33(7):1538-1543.
255. Rosenthal CK. Sorting Vangl2 at the Golgi. *Nature Cell Biology volume.* 2013;15(2).
256. Alexandra Walton DR. A novel Golgi-associated Vangl2 translational variant required for PCP regulation in vertebrates. *preprint server for biology bioRxiv.org.* 2020.
257. Luo PM, Boyce M. Directing Traffic: Regulation of COPI Transport by Post-translational Modifications. *Front Cell Dev Biol.* 2019;7:190.
258. Adolf F, Rhiel M, Hessling B, et al. Proteomic Profiling of Mammalian COPII and COPI Vesicles. *Cell Rep.* 2019;26(1):250-265 e255.
259. Sahlmuller MC, Strating JR, Beck R, et al. Recombinant heptameric coatomer complexes: novel tools to study isoform-specific functions. *Traffic.* 2011;12(6):682-692.
260. Hu T, Kao CY, Hudson RT, Chen A, Draper RK. Inhibition of secretion by 1,3-Cyclohexanebis(methylamine), a dibasic compound that interferes with coatomer function. *Mol Biol Cell.* 1999;10(4):921-933.

261. Horton AC, Racz B, Monson EE, Lin AL, Weinberg RJ, Ehlers MD. Polarized secretory trafficking directs cargo for asymmetric dendrite growth and morphogenesis. *Neuron.* 2005;48(5):757-771.
262. Ye B, Zhang Y, Song W, Younger SH, Jan LY, Jan YN. Growing dendrites and axons differ in their reliance on the secretory pathway. *Cell.* 2007;130(4):717-729.
263. Aniento F, Gu F, Parton RG, Gruenberg J. An endosomal beta COP is involved in the pH-dependent formation of transport vesicles destined for late endosomes. *J Cell Biol.* 1996;133(1):29-41.
264. Whitney JA, Gomez M, Sheff D, Kreis TE, Mellman I. Cytoplasmic coat proteins involved in endosome function. *Cell.* 1995;83(5):703-713.
265. Appenzeller-Herzog C, Hauri HP. The ER-Golgi intermediate compartment (ERGIC): in search of its identity and function. *J Cell Sci.* 2006;119(Pt 11):2173-2183.
266. Kennedy MJ, Hanus C. Architecture and Dynamics of the Neuronal Secretory Network. *Annu Rev Cell Dev Biol.* 2019;35:543-566.
267. Bowen AB, Bourke AM, Hiester BG, Hanus C, Kennedy MJ. Golgi-independent secretory trafficking through recycling endosomes in neuronal dendrites and spines. *Elife.* 2017;6.
268. Saraste J, Marie M. Intermediate compartment (IC): from pre-Golgi vacuoles to a semi-autonomous membrane system. *Histochem Cell Biol.* 2018;150(5):407-430.
269. Merianda TT, Lin AC, Lam JS, et al. A functional equivalent of endoplasmic reticulum and Golgi in axons for secretion of locally synthesized proteins. *Mol Cell Neurosci.* 2009;40(2):128-142.
270. Fu X, Brown KJ, Yap CC, Winckler B, Jaiswal JK, Liu JS. Doublecortin (Dcx) family proteins regulate filamentous actin structure in developing neurons. *J Neurosci.* 2013;33(2):709-721.
271. Comstra HS, McArthy J, Rudin-Rush S, et al. The interactome of the copper transporter ATP7A belongs to a network of neurodevelopmental and neurodegeneration factors. *Elife.* 2017;6.
272. Wozniak MJ, Melzer M, Dorner C, Haring HU, Lammers R. The novel protein KBP regulates mitochondria localization by interaction with a kinesin-like protein. *BMC Cell Biol.* 2005;6:35.
273. Dorner C, Ciossek T, Muller S, Moller PH, Ullrich A, Lammers R. Characterization of KIF1C, a new kinesin-like protein involved in vesicle transport from the Golgi apparatus to the endoplasmic reticulum. *J Biol Chem.* 1998;273(32):20267-20275.
274. Niwa S, Tanaka Y, Hirokawa N. KIF1Bbeta- and KIF1A-mediated axonal transport of presynaptic regulator Rab3 occurs in a GTP-dependent manner through DENN/MADD. *Nat Cell Biol.* 2008;10(11):1269-1279.
275. Fukui K, Sasaki T, Imazumi K, Matsuura Y, Nakanishi H, Takai Y. Isolation and characterization of a GTPase activating protein specific for the Rab3 subfamily of small G proteins. *J Biol Chem.* 1997;272(8):4655-4658.
276. Wada M, Nakanishi H, Satoh A, et al. Isolation and characterization of a GDP/GTP exchange protein specific for the Rab3 subfamily small G proteins. *J Biol Chem.* 1997;272(7):3875-3878.
277. Nagano F, Sasaki T, Fukui K, Asakura T, Imazumi K, Takai Y. Molecular cloning and characterization of the noncatalytic subunit of the Rab3 subfamily-specific GTPase-activating protein. *J Biol Chem.* 1998;273(38):24781-24785.
278. Hirokawa N, Niwa S, Tanaka Y. Molecular motors in neurons: transport mechanisms and roles in brain function, development, and disease. *Neuron.* 2010;68(4):610-638.
279. Chauvin S, Sobel A. Neuronal stathmins: a family of phosphoproteins cooperating for neuronal development, plasticity and regeneration. *Prog Neurobiol.* 2015;126:1-18.

280. Jaglin XH, Poirier K, Saillour Y, et al. Mutations in the beta-tubulin gene TUBB2B result in asymmetrical polymicrogyria. *Nat Genet.* 2009;41(6):746-752.
281. Jimenez-Mateos EM, Gonzalez-Billault C, Dawson HN, Vitek MP, Avila J. Role of MAP1B in axonal retrograde transport of mitochondria. *Biochem J.* 2006;397(1):53-59.
282. Avila J, Dominguez J, Diaz-Nido J. Regulation of microtubule dynamics by microtubule-associated protein expression and phosphorylation during neuronal development. *Int J Dev Biol.* 1994;38(1):13-25.
283. Hirokawa N. Kinesin and dynein superfamily proteins and the mechanism of organelle transport. *Science.* 1998;279(5350):519-526.
284. Flemr M, Buhler M. Single-Step Generation of Conditional Knockout Mouse Embryonic Stem Cells. *Cell Rep.* 2015;12(4):709-716.
285. Labun K, Montague TG, Gagnon JA, Thyme SB, Valen E. CHOPCHOP v2: a web tool for the next generation of CRISPR genome engineering. *Nucleic Acids Res.* 2016;44(W1):W272-276.
286. Zetsche B, Heidenreich M, Mohanraju P, et al. Multiplex gene editing by CRISPR-Cpf1 using a single crRNA array. *Nat Biotechnol.* 2017;35(1):31-34.
287. Laemmli UK, Molbert E, Showe M, Kellenberger E. Form-determining function of the genes required for the assembly of the head of bacteriophage T4. *J Mol Biol.* 1970;49(1):99-113.
288. Blighe K, Rana, S., and Lewis, M. EnhancedVolcano: Publication-ready volcano plots with enhanced colouring and labeling. 2018.
289. Chen H, Boutros PC. VennDiagram: a package for the generation of highly-customizable Venn and Euler diagrams in R. *BMC Bioinformatics.* 2011;12:35.

Abbreviations

% percentage
°C degree Celsius
bp base pairs
kDa kilodalton
g gram
h hour
k kilo
L litre
m milli
min minute
n nano
s second
V volt
µ micro
µg microgram
µl microlitre
ADP adenosine di-phosphate
AP adaptor protein
AP-MS combination proximity-dependent biotinylation with affinity purification and mass spectrometry
Ara-C arabinosylcytosine C
Arf1 ADP-ribosylation factor 1
ATP adenosine triphosphate

BACs bacterial artificial chromosome
BFA brefeldin A
BioID method to analyze interactome
BPL biotin protein ligase
ultraID method to analyze interactome
CCVs Clathrin coated vesicles
COPI Coat protein complex I
COPII Coat protein complex II
DAPI 4',6-diamidino-2-phenylindole
α–MEM Eagle's minimum essential medium alpha modified
DMSO dimethyl sulfoxide
DNA deoxyribonucleic acid
DTT dithiothreitol
EBs embryoid bodies
EDTA ethylenediaminetetraacetic acid
ER endoplasmic reticulum
ERAD ER-associated degradation
ERESs ER exit sites
ERGIC ER-to-Golgi intermediate compartment
GAP GTPase-activating protein
GBF1 Golgi-specific brefeldin-A-resistant factor 1
GEF guanine nucleotide exchange factor
GM130 130 kDa cis-Golgi matrix protein
GO gene ontology
GTP guanosine-5'-triphosphate
IP immunoprecipitation
KO knock out
LC-MS/MS liquid chromatography-mass spectrometry
LFQ label-free quantitative
mES mouse embryonic stem cells
mRNA messenger RNA
MS mass spectrometry
PAGE polyacrylamide gel electrophoresis
PBS phosphate buffered sialine
PCR polymerase chain reaction
RA retinoic acid
RNA ribonucleic acid
RT room temperature
SDS sodium dodecyl sulfate
SMN survival motor neuron
SNARE soluble NSF Attachment Protein receptor
SRP signal recognition particle
TEMED tetramethylethylenediamine
TGN trans-Golgi network
ultraID-MS ultraID coupled to mass spectrometry
UPR unfolded protein response
UV ultraviolet